

## The semiclassical tool in mesoscopic physics

RODOLFO A. JALABERT

*Université Louis Pasteur, 3-5 rue de l'Université, 67084 Strasbourg Cedex, France*

*Institut de Physique et Chimie des Matériaux de Strasbourg, 23 rue du Loess, 67037 Strasbourg Cedex, France*

**Summary.** — Semiclassical methods are extremely valuable in the study of transport and thermodynamical properties of ballistic microstructures. By expressing the conductance in terms of classical trajectories, we demonstrate that quantum interference phenomena depend on the underlying classical dynamics of non-interacting electrons. In particular, we are able to calculate the characteristic length of the ballistic conductance fluctuations and the weak localization peak in the case of chaotic dynamics. Integrable cavities are not governed by single scales, but their non-generic behavior can also be obtained from semiclassical expansions (over isolated trajectories or families of trajectories, depending on the system). The magnetic response of a microstructure is enhanced with respect to the bulk (Landau) susceptibility, and the semiclassical approach shows that this enhancement is the largest for integrable geometries, due to the existence of families of periodic orbits. We show how the semiclassical tool can be adapted to describe weak residual disorder, as well as the effects of electron-electron interactions. The interaction contribution to the magnetic susceptibility also depends on the nature of the classical dynamics of non-interacting electrons, and is parametrically larger in the case of integrable systems.

## 1. – Introduction

The field of Quantum Chaos, whose recent developments are reviewed in this volume, deals with general and fundamental questions, like the dependence of quantum properties on the underlying classical dynamics of a physical system [1, 2, 3, 4]. Traditionally, there have been few experimental systems (Rydberg atoms [5] and microwave cavities [6] among them) where to perform measurements and test the theoretical ideas of Quantum Chaos. In the last decade, low-temperature transport in mesoscopic semiconductor structures was proposed and used as a new laboratory for studying Quantum Chaos [7, 8] and many interesting concepts have been developed from such a connection [9, 10, 11, 12, 13, 14, 15].

The mesoscopic regime is attained in small condensed matter systems at sufficiently low temperatures for the electrons to propagate coherently across the sample [16, 17, 18, 19]. The phase coherence of the electron wave-function is broken by an inelastic event (coupling to an external environment, electron-phonon or electron-electron scattering, etc) over a distance  $L_\Phi$  larger than the size of the system ( $a$ ). In a more precise language, we should not talk of electrons, which are strongly interacting, but of Landau quasiparticles, which are the weakly interacting carriers (at low energies and small temperatures) moving in a self consistent field. The quasiparticle lifetime gives the limitation on  $L_\Phi$  arising from electron-electron interactions. Following the standard practice, we will refer to the carriers as “electrons” and we will not distinguish between the electrostatically imposed external potential and the self consistent field.

The view of a mesoscopic system as a single phase-coherent unit allows us to deal with a one-particle problem, where the theoretical concepts of Quantum Chaos are more simply applied. However, this simplistic approach does not describe the physical reality completely since in real life  $L_\Phi$  is larger than  $a$  but never strictly infinite. The fact that Mesoscopic Physics is not such an ideal laboratory for Quantum Chaos makes the richness of their relationship. Mesoscopic systems are extremely useful to study the interplay between quantum and classical mechanics, and at the same time, we can use this interplay to test fundamental questions of Condensed Matter Physics, like decoherence, dissipation and many-body effects.

Mesoscopic Physics was initially focused on disordered metals, where the classical motion of electrons is a random walk between the impurities. The phase-coherence in the multiple scattering of electrons gives rise to corrections to the classical (Drude) conductance. The most studied quantum interference phenomena in disordered metals are the *Aharonov-Bohm oscillations* of the conductance in multiply connected geometries, the *weak localization* effect (a decrease in the average conductance around zero magnetic field), and the *universal conductance fluctuations* (reproducible fluctuations in the conductance versus magnetic field or Fermi energy with *rms* of size of the order  $e^2/h$ , independent of the average conductance) [20]. A perturbative treatment of disorder, followed by an average over impurity configurations, has provided the calculational tool leading to the understanding of those phenomena [21]. The small parameter is  $k_F l$ , with  $k_F = 2\pi/\lambda_F$  the Fermi wave-vector and  $l$  the elastic mean-free-path (*i.e.* the typical distance traveled by the electron between successive collision with the impurities).

Mesoscopic disordered conductors are then characterized by  $\lambda_F \ll l \ll a \ll L_\Phi$ .

It is in a “second generation” of mesoscopic systems, semiconductor microstructures, that the connection with Quantum Chaos has been more successfully developed. Extremely pure semiconductor (*GaAs/AlGaAs*) heterostructures make it possible to create a two-dimensional electron gas (2DEG) by quantizing the motion perpendicular to the interphase [22]. Given the crystalline perfection and the fact that the dopants are away from the plane of the carriers, an electron can travel a long distance before its initial momentum is randomized. This typical distance, the transport mean-free-path  $l_T$ , is generally larger than the elastic mean-free-path (due to small-angle scattering [23]) and it can achieve values of  $5 - 15\mu m$ .

Various techniques have been developed to produce a lateral confinement in the 2DEG and define one-dimensional (quantum wires) and zero-dimensional (quantum boxes or cavities) structures. Spatial resolutions of the order of a *micron* allow to define, at the level of the 2DEG, mesoscopic structures smaller than the elastic mean-free-path, paving the way to the *ballistic* regime [24, 25]. When  $a \ll l_T$  the classical motion of the two-dimensional electrons is given by the collisions with the walls defining the cavity, with a very small drift due to the weak impurity potential. We reserve the term of *clean* system for the ideal case in which  $l_T$  is strictly infinite, allowing us to completely ignore the effects of disorder. In usual ballistic transport the disorder effects are very small, and the distinction between ballistic and clean regimes is often skipped. On the other hand, thermodynamical properties are more sensitive to the residual disorder, and we will show in this work how to include such effects within a semiclassical approach. Changing the shape of a clean cavity we can go from integrable to chaotic dynamics and study the consequences at the quantum level.

It is important to realize that the constraints arising from the measurement limit the type of problems to study. For instance, we cannot address one of the central questions of Quantum Chaos, the relationship between the (short range) statistical properties of the spectrum of a quantum system and the nature of the underlying classical dynamics [26], since in the mesoscopic regime we do not have access to single-particle energies. We do not deal with microscopic systems where the level spacing  $\Delta$  can become larger than the temperature broadening  $k_B T$ . The fruitful connection between Quantum Chaos and Mesoscopic Physics has to be established from the observables that are accessible in the laboratory.

The broad (long range) features of the density of states of a ballistic cavity can be tested by the measurement of its magnetic susceptibility, which is a thermodynamical property. This is a considerably difficult experiment due to the smallness of the orbital response, thus only a few experimental results exist up to now [27, 28]. The physical property of ballistic microstructures which is most easily measured is their electrical resistance, and as a consequence, an important wealth of experimental results on ballistic transport has been obtained in the last decade [8, 29, 30, 31, 32, 33, 34, 36, 37, 38, 39, 40]. In order to measure the electrical resistance we have to open the cavities, connecting them to measuring devices that are necessarily macroscopic and can be thought as electron reservoirs (Fig. 1). In the case of magnetization measurements we are dealing with a

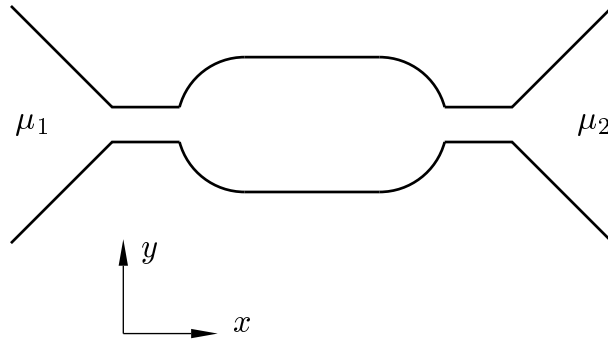


Fig. 1. – Typical ballistic cavity coupled to reservoirs characterized by chemical potentials  $\mu_1$  and  $\mu_2$ .

closed system. In the transport experiments we have an open system with a continuous spectrum. The experimental situation concerning the existing results is to be contrasted with the theoretical one, since closed systems have traditionally captured most of the attention in Quantum Chaos.

In this work we review the theory of both, open and closed ballistic microstructures, in connection with the two types of cited experiments concerning transport and thermodynamical properties. The unifying concept in our presentation is the use of semiclassical approximations for the calculation of the quantum observables. The restriction to the semiclassical tool is made in order to provide a pedagogical and consistent approach to Mesoscopic Physics. Other techniques, like supersymmetry or random matrix theory (reviewed in this volume [41, 42]) have also proven to be very helpful for understanding mesoscopic systems.

Our aim is to present the semiclassical approach as a tool, showing its principles and illustrating how it works in a few examples. It is expected that this introduction can provide an entry point towards other applications of semiclassics in Mesoscopic Physics.

Semiclassical approaches were essential at the advent of Quantum Mechanics and have ever since remained a privileged tool for developing our intuition on new problems and for performing analytical calculations as well [4, 43]. The semiclassical approximation in one-dimension is referred in standard textbooks as the WKB (Wentzel-Kramers-Brillouin) method and allows to obtain closed expressions for eigenenergies and eigenfunctions. The extension to higher dimensions is built from the Van Vleck approximation to the propagator, expressed as a sum over classical trajectories, each of them associated with a weight given by a stability prefactor and a phase depending on the classical action. The consistent use of the stationary-phase method whenever an integral has to be evaluated allows us to link classical mechanics with other quantum protagonists, like the Green

function, the density of states, matrix elements, scattering amplitudes, etc. The dependence of the properties of a quantum system on the underlying classical mechanics can then be established, and this is why the semiclassical approach is so widely used in the studies of Quantum Chaos.

For the usual densities of the 2DEG ( $3 \times 10^{11} \text{ cm}^{-2}$ ) the Fermi wave-lengths are of the order of  $40 \text{ nm}$ . The semiclassical approximation is therefore justified in the study of mesoscopic ballistic cavities since  $\lambda_F \ll a \ll l_T \ll L_\Phi$ .

The semiclassical expansions are well suited to study the nontrivial effect of small perturbations. In this work we will often use the fact that a weak magnetic field can be accounted for by attaching an extra phase to the action associated with each unperturbed trajectory. Other perturbations, like a smooth disordered potential or a change in the Fermi energy can also be treated by this combination of semiclassics and classical perturbation theory.

We remark that the use of semiclassical expansions that we do in the theory of mesoscopic systems differs from that of Quantum Chaos. The finite values of  $L_\Phi$  and  $l$ , that we emphasized above, and the thermal broadening due to the Fermi distribution of electrons account for the fact that our semiclassical expansions are always cut off after a certain typical trajectory length. This observation considerably simplifies our calculations and keeps us away from the convergence problems that plague semiclassical expansions. Moreover, in certain cases, like in the orbital magnetism of an integrable structure, we arrive to a good physical understanding by only considering a few orbits.

As mentioned before, the first generation of mesoscopic systems, the disordered metals, have mainly been analyzed within diagrammatic perturbation theory. There has also been semiclassical descriptions as a way of representing specific diagrams and providing intuitive interpretations [44, 45]. For instance, it can be shown that the weak localization effect arises from the constructive interference of time-reversed backscattering trajectories. Since the scattering centers of disorder metals (defects, impurities, interstitials, etc) are of atomic dimensions the single scattering events have to be treated quantum mechanically. Therefore the semiclassical description of disordered systems is a mixed one, built from a classical propagation between quantum scatterings. Assuming that the classical single scattering events have a random outcome and invoking an ensemble average, we are lead to a diffusive motion of electrons. The situation is then quite different from that of ballistic systems, were the classical trajectories are completely determined by the geometry and the dynamics can be chaotic or integrable depending on the shape of the cavity. Also, the notion of impurity average, so crucial in disordered systems, is usually replaced in the ballistic regime by averages over energy or over samples.

At this point it is useful to establish a further clarification concerning our use of the term “semiclassics”. In Condensed Matter Physics the semiclassical model usually describes the evolution of a wave-packet of Bloch electron levels by classical equations of motion that take into account the band structure effects through the dispersion relations [46]. Such a description allows the study of classical transport from the Boltzmann equation and the determination of Fermi surfaces in metals. The periodic potential of the crystal is included quantum mechanically, while the externally applied field is

treated classically. The band structure effects in the 2DEG are extremely simple since we are always restricted to the bottom of the conduction band, which can be taken as parabolic with an effective mass  $m = 0.067m_e$ . For the usual Fermi wave-lengths of the order of  $40nm$  the electrons are distributed over many atomic sites, and as in standard condensed matter textbooks we include the periodic potential through the dispersion relation. However, we go beyond the classical description of electron propagation in the applied field in order to incorporate the quantum interference effects.

This review article is organized as follows. In Sec. **2** we present the scattering approach to coherent transport and develop a semiclassical theory for conductance. The conductance fluctuations [7, 47] and the weak localization effect [48] are studied with the semiclassical tool and differences according to the nature of the underlying classical dynamics are predicted. Sec. **3** deals with integrable cavities: the square, for which the semiclassical expansions are organized in terms of families of trajectories [49] and the circle, where the effects of diffraction and tunneling can be easily incorporated into the semiclassical description [50]. Sec. **4** describes a few experimental results related with the theories previously developed and discusses the relation of complementarity between semiclassics and random matrix theory. In that section we also refer to the case of cavities with mixed dynamics and the semiclassical approach to bulk conductivity.

The second part of this work is devoted to orbital magnetism. The magnetic susceptibility of clean dots [51, 52] is calculated in Sec. **5**. Sec. **6** studies weak-disorder effects in ballistic cavities, and applies such a study to the magnetic response of semiconductor microstructures [53]. In Sec. **7** we include the effects of electron-electron interaction in the orbital response of quantum dots [54] summarizing the various contributions in different regimes and establishing a comparison with the existing experimental results. In Sec. **8** we conclude with a summary of the strenghts and weakness of the semiclassical approach in Mesoscopic Physics and we point at some open problems.

## 2. – Quantum transport through classically chaotic cavities

Our understanding of quantum transport greatly owes to the Landauer-Büttiker approach of viewing conductance as a scattering problem [55, 56, 18, 19]. The interpretation of conductance measurements in the ballistic regime from a Quantum Chaos point of view will therefore involve the study of the quantum and classical mechanics of open systems. In this section we describe some features of classical scattering relevant for quantum conductance, we give a simple presentation of the Landauer-Büttiker formalism, and we use semiclassical methods to relate classical and quantum properties of ballistic cavities.

**2.1. Chaotic scattering.** – The study of a physical system from the Quantum Chaos point of view usually starts with its classical dynamics. In open systems, we have to consider a classical scattering problem. The concept of chaos [57], developed for closed systems, and related to the long-time properties of the trajectories, has to be re-examined in open systems since the trajectories exit the scattering region after a finite amount of time. We will not review the field of Chaotic Scattering [58, 59, 60], but only present the minimal information needed to understand the quantum properties of ballistic cavities. In this section we will mainly deal with chaotic dynamics, but not exclusively; some of the results are general and independent of the dynamics. In addition, we will stress the differences between chaotic and integrable cases.

The “transient chaos” of a scattering problem is characterized by the infinite set of trajectories which stay in the scattering region forever. This set is constituted by the periodic unstable orbits of the scattering region (the “strange repeller”) and their stable manifold (the trajectories that converge to the previous ones in the infinite-time limit). Chaotic scattering is obtained when the dynamics in the neighborhood of the repeller is chaotic in the usual sense, and this set has a fractal dimension in the space of classical trajectories. When an incoming particle enters the scattering region, it approaches the strange repeller, bounces around close to this set for a while and it is eventually ejected from the scattering region (if it did not have the right initial conditions to be trapped).

If we scan a set of scattering trajectories (say, we fix the initial position  $y$  at the left entrance of the cavity of Fig. 1 and we vary the injection angle  $\theta$ ) studying the time  $\tau$  that the particle spends in the interaction region, we obtain a fractal curve for  $\tau(\theta)$ . The infinitely trapped trajectories give the divergences of  $\tau(\theta)$  and determine its self-similar structure. The study of  $\tau(\theta)$  is a quick way to determine if our scattering is chaotic.

The rate at which particles escape from the scattering region ( $\gamma$ ) results from a balance between the rate in which nearby trajectories diverge away from the repeller (characterized by its largest Lyapunov exponent  $\lambda$ ) and the rate at which the chaotic escaping trajectories are folded back into the scattering region (depending on the density of the repeller, that is measured by its fractal dimension  $d$ ). More precisely, if we start (or inject) particles in the scattering region, the survival probability at time  $\tau$  will be  $P(\tau) = e^{-\gamma\tau}$ , with  $\gamma = \lambda(1 - d)$  [59, 60, 61]. The *escape rate* may be interpreted as the inverse of the typical time spent by the particles in the scattering region.

In Fig. 2.a we show the length distribution (which in billiards is equivalent to the

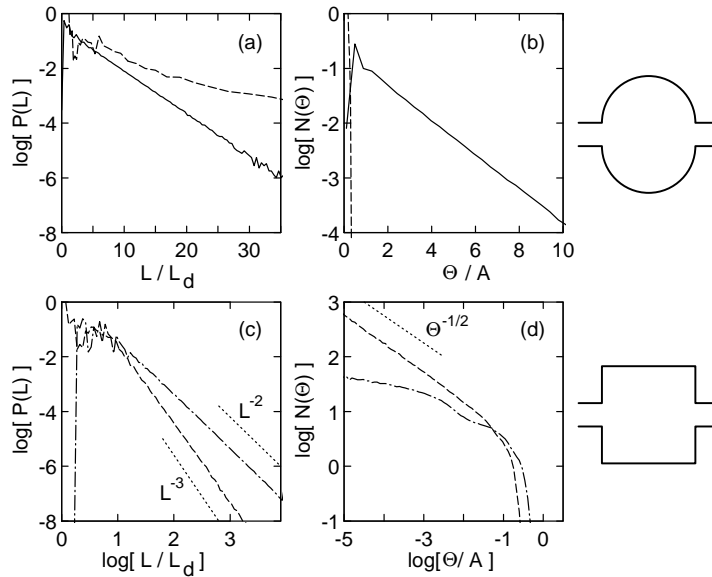


Fig. 2. – Classical distributions of length [(a),(c)] and effective area [(b),(d)] for the stadium (solid line) and rectangular (dashed line) billiards. In the stadium both distributions are close to exponential after a short transient region and are very different from the distributions for the rectangle, which show the power-law behavior characteristic of non-chaotic systems. Different power laws are indicated by dotted lines. In panel (c), the dash-dotted line is the two-particle distribution of length differences (Eq. (2.42)). In (d) the dash-dotted line is the two-particle distribution of area differences for transmitted particles (Eq. (2.43)). ( $A$  is the area of the cavity,  $L_d$  is the direct length between the leads. From Ref. [10].)

length distribution) for a cavity with the shape of a stadium, and verify the exponential law (solid line),  $P(L) = e^{-\gamma_{cl}L}$  (with  $\gamma_{cl} = \gamma/v$  and  $v$  the constant velocity of the scattering particles). Our curve becomes ragged for large lengths due to the finite number of particles that we are able to simulate. The exponential law sets in very fast, after a length corresponding to a few bounces.

The appearance of a single scale is not surprising since in chaotic scattering the particle moves ergodically over the whole energy surface while in the scattering region. The value of the escape rate can be estimated from general arguments of ergodicity in the case of chaotic cavities with small openings, where the typical trajectory bounces around many times before it escapes [62]. Assuming that the instantaneous distribution of trajectories is uniform on the energy surface, the escape rate is simply given by  $\gamma = F/A$ , where  $F$  is the flux through the holes (equal to the size of the holes times  $v/\pi$ , the factor of  $\pi$  comes from integration over the departing angles),  $A$  is the area of



the two-dimensional scattering domain. In the case of small holes this simple estimate reproduces remarkably well the escape rates obtained from the numerical determination of the survival probability using classical trajectories.

Our interest in the escape rate is due to the fact that, as we will show in the sequel, the energy scale of the conductance fluctuations is given by this classical quantity. In addition, we will show that the conductance fluctuations as a function of magnetic field are governed by the area distribution. Scattering trajectories are open, and therefore do not have a well defined enclosed area. Instead, we define the “effective area” of a trajectory  $s$  from the circulation of the vector potential along the path  $\mathcal{C}_s$ . We assume a perpendicular magnetic field  $\mathbf{B} = B\hat{\mathbf{z}}$  generated by a vector potential  $\mathbf{A}$ , and define the effective area by

$$(2.1) \quad \Theta_s = \frac{2\pi}{B} \int_{\mathcal{C}_s} \mathbf{A} \cdot d\mathbf{r} ,$$

If  $s$  were a closed trajectory,  $\Theta_s$  would be equal to  $2\pi$  times the enclosed area. Unlike the scattering time,  $\Theta$  can be positive or negative. In the chaotic case the distribution of effective areas, like the distribution of lengths, is expected to depend on a single scale. Numerical calculations and analytical arguments [7, 62, 63, 64, 65, 66] yield a distribution

$$(2.2) \quad N(\Theta) \propto \exp(-\alpha_{cl}|\Theta|) ,$$

where the parameter  $\alpha_{cl}$  can be interpreted as the inverse of the typical area enclosed by a scattering trajectory. In Fig. 2.b we present the distribution  $N(\Theta)$  (only for positive  $\Theta$ , solid line) obtained from simulating classical trajectories in a stadium cavity, showing good agreement with the proposed distribution. Scattering trajectories yield an effective area which is not gauge-invariant. However, the large (in absolute value) effective areas are associated with long trajectories that bounce many times, which are constituted by many loops and two extreme “legs” in and out of the cavity. The dominant contribution comes from the loops and therefore it is gauge-invariant. Changing the choice of the gauge in our numerical simulations modifies the distribution for small  $\Theta$ , but not the exponent  $\alpha_{cl}$  governing the distribution of large  $\Theta$ .

Exploiting the ergodic properties of the chaotic dynamics in the scattering domain and assuming that the area is accumulated in a random-walk fashion, the parameter  $\alpha_{cl}$  can be related to the escape rate and the typical length scale of the cavity [62, 66]. As in the case of the escape rate, these estimations compare very favorably with the values extracted from numerical simulations.

In the integrable case the particle moves over only that part of the energy surface consistent with the conserved quantity. Therefore, we no longer have a single scale. In situations with multiple scales we expect to observe power-law distributions [67, 63, 68, 69]. For the case of a rectangular cavity we obtain the results of Fig. 2c and d with an approximate  $L^{-3}$  dependence for the length distribution (dashed) and  $\Theta^{-1/2}$  for the

area distribution (dashed). However, for integrable cavities the concept of distributions is not completely rigorous since the survival probabilities depend on the initial conditions chosen for the trajectories. For our simulations we have used a uniform distribution of  $y$  along the entrance lead and a  $\cos\theta$  weighted angular distribution as initial conditions (consistently with the classical limit of the quantum problem).

It is important to recall our discussion about the differences between the traditional Quantum Chaos approach and our view of Mesoscopic Physics describing condensed matter systems. For instance, the only features of the length and area distributions that will be experimentally relevant are those happening at scales just a few times larger than the typical size and area of the cavity (trajectories shorter than our physical cut-offs). Therefore, we will not be concerned about the tails of such distributions [70, 69].

**2.2. The scattering approach to the conductance.** – Within the Landauer-Büttiker approach, in the phase-coherent regime the resistance is not related to an intensive resistivity of the type defined in standard condensed matter books [46] (like, for instance, electron-phonon interaction), but arises from the elastic scattering that electrons suffer while traversing mesoscopic sample between the measuring devices. The measuring devices are macroscopic and behave as electron reservoirs. They are characterized by an electrochemical potential  $\mu$ , which does not vary while giving and accepting electrons. The role of the reservoirs is crucial as they render the total system infinite, and the spectrum continuous. It is only in the reservoirs that the randomization of electron phases is assumed to take place.

The simplest experimental set up is the two-probe measurement (Fig. 1), where the sample is attached between two reservoirs whose electrochemical potentials differ by the value of the applied voltage  $V$ , which is supposed to be very small ( $\mu_1 - \mu_2 = eV \ll \mu_1$ ). In this work we will concentrate exclusively in ideal two-probe experiments. The multiprobe case [56] does not pose new fundamental problems but the theoretical description becomes more complicated since a matrix of conductance coefficients must be introduced. These conductances are also expressed in terms of transmission coefficients, which can be treated with the semiclassical approach [71, 7, 72, 11, 12] in the same way as in the two-probe case that we discuss here.

The scattering description necessitates a set of asymptotic states. In our case such a set is provided by the propagating channels of the leads connecting the sample with the reservoirs. Sample, reservoirs and leads are the three key elements of ballistic transport.

Assuming the leads to be disorder-free, with hard walls (of width  $W$ ) in the  $y$ -direction and infinite in the  $x$ -direction, their eigenstates with energy  $\varepsilon$  are products particle-in-a-box wave-functions

$$(2.3) \quad \phi_a(y) = \sqrt{\frac{2}{W}} \sin\left(\frac{\pi a y}{W}\right),$$

( $a$  integer) in the transverse direction and plane-waves propagating in the longitudinal direction, with wave-vectors  $k_a$  such that  $\varepsilon = \hbar^2/(2m)((a\pi/W)^2 + k_a^2)$ . The  $N$  transverse

momenta which satisfy this relationship with  $k_a^2 > 0$  define the  $2N$  propagating channels of the leads with energy  $\varepsilon$ . The incoming lead-states are

$$(2.4) \quad \varphi_{1(2),\varepsilon,a}^{(-)}(\mathbf{r}) = \frac{1}{v_a^{1/2}} e^{\pm i k_a x} \phi_a(y), \quad \mathbf{r} = (x, y), \quad a = 1, \dots, N.$$

The normalization factor  $v_a^{-1/2} = (m/\hbar k_a)^{1/2}$  is chosen in order to have a unit of incoming flux in each channel. The subindex 1 (2) corresponds to channels propagating from the left (right) reservoir with longitudinal momenta  $k_a$  ( $-k_a$ ), and  $k_a$  explicitly positive. The outgoing lead-states  $\varphi_{1(2),\varepsilon,a}^{(+)}$  are defined as in (2.4), but with the  $\pm$  of the exponent inverted. The time order of outgoing and incoming lead-states is obtained by giving an infinitesimal positive (negative) imaginary part to  $k_a$ .

The scattering states corresponding to an electron incoming from lead 1 (2) with energy  $\varepsilon$ , in the mode  $a$  are given, in the asymptotic regions, by

$$(2.5a) \quad \Psi(\mathbf{r})_{1,\varepsilon,a}^{(+)} = \begin{cases} \varphi_{1,\varepsilon,a}^{(-)}(\mathbf{r}) + \sum_{b=1}^N r_{ba} \varphi_{1,\varepsilon,b}^{(+)}(\mathbf{r}), & x < 0 \\ \sum_{b=1}^N t_{ba} \varphi_{2,\varepsilon,b}^{(+)}(\mathbf{r}), & x > 0 \end{cases}.$$

$$(2.5b) \quad \Psi(\mathbf{r})_{2,\varepsilon,a}^{(+)} = \begin{cases} \sum_{b=1}^N t'_{ba} \varphi_{1,\varepsilon,b}^{(+)}(\mathbf{r}), & x < 0 \\ \varphi_{2,\varepsilon,a}^{(-)}(\mathbf{r}) + \sum_{b=1}^N r'_{ba} \varphi_{2,\varepsilon,b}^{(+)}(\mathbf{r}), & x > 0 \end{cases}.$$

The  $2N \times 2N$  scattering matrix  $S$ , relating incoming flux and outgoing fluxes, can be written in terms of the  $N \times N$  reflection and transmission matrices  $r$  and  $t$  ( $r'$  and  $t'$ ) from the left (right) as

$$(2.6) \quad S = \begin{pmatrix} r & t' \\ t & r' \end{pmatrix}.$$

Current conservation implies that the incoming flux should be equal to the outgoing flux, and therefore  $S$  is unitary ( $SS^\dagger = I$ ). In terms of the total transmission ( $T = \sum_{a,b} |t_{ba}|^2$ ) and reflection ( $R = \sum_{a,b} |r_{ba}|^2$ ) coefficients, the unitarity condition is expressed as  $T + R = N$ . Also, unitarity dictates that  $T = T'$  and  $R = R'$ . Furthermore, in the absence of magnetic field, time reversal invariance dictates that  $S$  is symmetric ( $S = S^T$ ). Cavities with geometrical symmetries (up-down or right-left) are described by scattering matrices with a block structure [73].

The set  $\{\Psi_{1(2)\varepsilon,a}^{(+)}\}$  constitutes an orthogonal (but not orthonormal) basis, [74, 75],

$$(2.7) \quad \int d\mathbf{r} \Psi_{l,\varepsilon,a}^{(+)*}(\mathbf{r}) \Psi_{l',\varepsilon',a'}^{(+)}(\mathbf{r}) = \frac{2\pi}{v_a} \delta_{aa'} \delta(k_a - k_{a'}) \delta_{ll'}.$$

Using the spectral decomposition of the retarded Green function in this basis and taking into account the analytical properties of the transmission amplitudes in the complex

$k$ -plane, we can relate the Green function to the scattering amplitudes. Alternatively, the formal theory of scattering (Lippmann-Schinger) can be adapted to wave-guides and obtain [76]

$$(2.8a) \quad t_{ba} = i\hbar(v_a v_b)^{1/2} \exp[-i(k_b x' - k_a x)] \int_{\mathcal{S}_{x'}} dy' \int_{\mathcal{S}_x} dy \phi_b^*(y') \phi_a(y) G(\mathbf{r}', \mathbf{r}; E)$$

$$(2.8b) \quad r_{ba} = -\delta_{ab} \exp[2ik_b x'] + i\hbar(v_a v_b)^{1/2} \exp[-i(k_b x' + k_a x)] \int_{\mathcal{S}_{x'}} dy' \int_{\mathcal{S}_x} dy \phi_b^*(y') \phi_a(y) G(\mathbf{r}', \mathbf{r}; E),$$

where the integrations take place at the transverse cross sections  $\mathcal{S}_x$  on the left lead and  $\mathcal{S}_{x'}$  on the right (left) lead for the transmission (reflection) amplitudes. The physical observables are obtained from the transmission and reflection coefficients ( $T_{ba} = |t_{ba}|^2$  and  $R_{ba} = |r_{ba}|^2$ ) between modes, which, by current conservation, do not depend on the choice of the transverse cross sections. We will use this freedom to take  $\mathcal{S}_x$  and  $\mathcal{S}_{x'}$  at the entrance and exit of the cavity (or both at the entrance for (2.8b)), and we will omit the  $x$  and  $x'$  dependences henceforth.

The intuitive interpretation of the above equations as a particle arriving at the cavity in mode  $a$ , propagating inside (through the Green function), and exiting in mode  $b$  is quite straightforward. Expressing the scattering amplitudes in terms of Green functions is extremely useful for analytical and numerical computations. Diagrammatic perturbation theory, as well as semiclassical expansions, are built on Green functions.

So far, we have presented the scattering theory for samples connected to wave-guides. Now, we reproduce the standard counting argument to relate conductance with scattering [55, 56, 18, 19]. As stated at the beginning of this section, we assume that the left reservoir has an electrochemical potential  $\mu_1$  slightly higher than the one of the right reservoir ( $\mu_1 - \mu_2 = eV$ ).

In the energy interval  $eV$  between  $\mu_2$  and  $\mu_1$  electrons are injected into right-going states emerging from reservoir 1, but none are injected into left-going states emerging from reservoir 2. Consequently, there is a net right-going current proportional to the number of states in the interval  $\mu_1 - \mu_2$ , given by

$$(2.9) \quad I = g_s e \sum_{a=1}^N v_a \frac{dn_a}{d\varepsilon} eV \sum_{b=1}^N T_{ba} = g_s \frac{e^2}{h} \left( \sum_{a,b=1}^N T_{ba} \right) V.$$

$N$  is the number of propagating channels at the energy  $\mu_1$ , the factor  $g_s = 2$  takes into account spin degeneracy,  $\sum_{b=1}^N T_{ba}$  is the probability for an electron coming in the mode  $a$  to traverse the system,  $dn_a/d\varepsilon$  quasi-one-dimensional density of states (which for non-interacting particles satisfies that  $dn_a/d\varepsilon = 1/hv_a$ ). Then, the two-probe conductance is just proportional to the total transmission coefficient of the microstructure,

$$(2.10) \quad G = \frac{I}{V} = g_s \frac{e^2}{h} \quad T = g_s \frac{e^2}{h} \text{Tr}\{tt^\dagger\}.$$

A more rigorous alternative to the counting argument presented above can be obtained from linear response (Kubo formula) for the conductivity, within a wave-guide geometry [76, 77]. The extension to finite magnetic fields [75, 80, 81] presents some subtleties, but the final form is still the simple looking Eq. (2.10). The magnetic fields that we consider will always be very weak, and therefore the zero-field formulation of the conductance that we presented is sufficient for our purposes.

**2.3. Quantum interference in ballistic cavities.** – The scattering formalism presented in the last chapter is the base for the semiclassical theory of ballistic transport that we develop in this work. It is also at the origin of the numerical studies of elastic scattering due to impurities or transport through phase-coherent cavities. In this chapter we describe the results of numerical calculations as a way to introduce the quantum interference effects that we are interested in. These exact computations will later be used to test the applicability of our analytical results.

In a tight-binding model representing the cavity and the leads, the Green function can be calculated recursively, starting from its exact expression in the leads, by matrix multiplications and inversions [78, 79, 72]. The discrete version of Eq. (2.2), together with (2.10), allow us to obtain the transmission coefficient through the cavity.

We can simulate any potential in the cavity by choosing the in-site energies of the tight-binding Hamiltonian. In this work we will concentrate in cavities that are billiards (defined by hard-walls and with zero potential in the classically allowed region). This choice is the simplest for numerical and analytical calculations, and allows us to treat the case of a classical dynamics that exhibits hard chaos. It is clearly a rough approximation to the experimentally achievable micro-cavities, and its applicability depends on the fabrication details [9, 40].

In Fig. 3 we show the transmission coefficient of an asymmetric cavity as a function of the incoming flux  $kW/\pi$  ( $\mu_1 = \hbar^2 k^2/2m$ , the integer part of  $kW/\pi$  is the number of propagating channels). The overall behavior of the transmitted flux is a linear increase with  $k$ . In the next chapters we will show that the classical limit of the semiclassical approximation, corresponding to the neglect of quantum interference, reproduces the slope of this secular behavior, which is noted as “classical”. The term “classical” should be taken with some caution, since the incoming flux is still quantized in the modes of the leads.

Superimposed to the secular behavior, we observe fine-structure fluctuations characteristic of the cavity under study. These conductance fluctuations, analogous to those of disordered metals, also appear if we fix the Fermi energy and use the magnetic field as a tuning parameter. The conductance fluctuations are characterized by their magnitude,  $\langle(\delta T)^2\rangle$ , and the correlation scale as a function of wave-vector  $\Delta k_c$  (or magnetic field  $\Delta B_c$ ). Our numerical results seem to indicate that these characteristic scales do

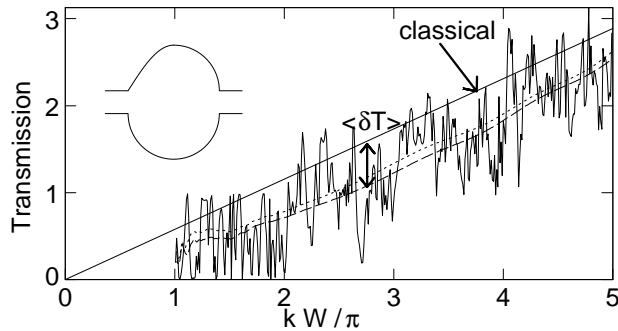


Fig. 3. – Transmission coefficient for the cavity of the inset as a function of wave-vector ( $W$  is the width of the leads). The straight solid line is the classical transmission, the fluctuating solid line is the full quantum transmission  $T_{qm}$ , and the dashed (dotted) line is the smoothed  $T_{qm}$  at  $B=0$  ( $BA/\Phi_0=0.25$ ). (From Ref. [10].)

not change as we go into the semiclassical limit of large  $k$ . However, these results are necessarily limited by the maximum wave-vector that we are able to treat (scaling with the size of our tight-binding model). In the following chapters we will show how semiclassicals can be used to extract energy-independent values of  $\Delta k_c$  and  $\Delta B_c$  in chaotic billiards. The independence of  $\langle(\delta T)^2\rangle$  on the incident energy is a necessary condition if the ballistic conductance fluctuations are to share some of the universal properties of those of disordered systems. Semiclassical arguments will be used to support such scale invariance for chaotic billiards, and we will point out the difficulties concerning the calculation of  $\langle(\delta T)^2\rangle$ .

The secular behavior (dashed line) lies below the classical value of the transmission coefficient, due to mode effects from confinement in the leads. The above defined classical limit only reproduces the slope of the large- $k$  smoothed transmission coefficient, but the shift  $\langle\delta T\rangle$  (as well as the fluctuations) does not disappear in the large- $k$  limit. The presence of a weak magnetic field tends to decrease the offset, yielding a secular behavior (dotted line) that runs higher than in the  $B=0$  case. This is the weak localization effect for ballistic cavities [48]. The reason why we chose an asymmetric cavity is that the ballistic weak localization effect is strongly dependent on the spatial symmetries of the cavity [73].

Our numerical results show that the conductance fluctuations and the weak localization effect, first discussed in the context of disordered mesoscopic conductors, are also present in ballistic mesoscopic cavities. The distinctions concerning these two types

of mesoscopic systems, that we discussed in the introduction, force us to rethink the appropriate definition of averages, as well as the concept of universality.

**2.4. Semiclassical transmission amplitudes.** – Our goal is to calculate the conductance through a cavity (like the ones in Figs. 1 and 3) by using Eqs. (2.10) and (2.2) within a semiclassical approach. The Green function is the Laplace transform of the propagator. The Van Vleck expression for the latter, together with a stationary-phase integration on the time variable, leads to the semiclassical approximation for the Green function [4]

$$(2.11) \quad G(\mathbf{r}', \mathbf{r}; E) = \frac{2\pi}{(2\pi i \hbar)^{(d+1)/2}} \sum_{s(\mathbf{r}, \mathbf{r}')} \sqrt{D_s} \exp \left[ \frac{i}{\hbar} S_s(\mathbf{r}', \mathbf{r}; E) - i \frac{\pi}{2} \nu_s \right].$$

The sum is over classical trajectories  $s$ , with energy  $E$ , going between the initial and final points  $\mathbf{r} = (x, y)$  and  $\mathbf{r}' = (x', y')$ . As in the previous chapter, we will take  $x$  and  $x'$  at the junctions between the leads and the cavity, and therefore we will not write any  $x$  dependence.  $S_s = \int_{C_s} \mathbf{p} \cdot d\mathbf{q}$  is the action integral along the path  $C_s$ . In the case of billiards without magnetic field  $S_s/\hbar = kL_s$ , where  $L_s$  is the trajectory length. The factor  $D_s$  describing the evolution of the classical probability can be expressed as a determinant of second derivatives of the action [4, 43]. In our geometry, if we denote by  $\theta$  and  $\theta'$  the incoming and outgoing angles of the trajectory with the  $x$ -axis,  $D_s = (v|\cos\theta'|/m)^{-1} |(\partial\theta/\partial y')_y|$ . We include in the phase  $\nu_s$  the Maslov index counting the number of constant-energy conjugate points and the phase acquired at the bounces with the walls when those are given by an infinite potential (hard walls). In our calculations we will always take the spatial dimensionality  $d=2$ .

In the case of hard-wall leads, the transverse wave-functions have the sinusoidal form of Eq. (2.3). Using the semiclassical expression (2.11) of the Green function in Eq. (2.2) we see that, for large integers  $a$ , the integral over  $y$  will be dominated by the stationary-phase contribution occurring for trajectories starting at points  $y_0$  defined by

$$(2.12) \quad \left( \frac{\partial S}{\partial y} \right)_{y'} = -p_y = -\frac{\bar{a}\hbar\pi}{W}, \quad \bar{a} = \pm a,$$

The dominant trajectories are those entering the cavity with the angles  $\theta_{\bar{a}}$  such that  $\sin\theta_{\bar{a}} = \bar{a}\pi/kW$ . Thus, the initial transverse momentum of the trajectories equals the momentum of the transverse wave-function. As always in this type of reasoning, we have assumed that we could interchange the order of the integration and the sum over trajectories. Integrating the gaussian fluctuations we have

$$(2.13) \quad t_{ba} = i \sqrt{\frac{v_b}{2W}} \int dy' \phi_b(y') \sum_{\bar{a}=\pm a} \sum_{s(\theta_{\bar{a}}, y')} \text{sgn}(\bar{a}) \sqrt{\hat{D}_s} \exp \left[ \frac{i}{\hbar} \hat{S}_s(y', \theta_{\bar{a}}; E) - i \frac{\pi}{2} \hat{\nu}_s \right].$$

The reduced action is

$$(2.14) \quad \hat{S}(y', \theta_a; E) = S(y', y_0(\theta_a, y'); E) + \frac{\hbar\pi\bar{a}}{W} y_0(\theta_a, y') ,$$

The prefactor is now given by  $\hat{D} = (v \cos \theta')^{-1} |(\partial y / \partial y')_\theta|$ , and the new index  $\hat{\nu}$  (that we still call Maslov index) is increased by one if  $(\partial \theta / \partial y)_{y'}$  is positive. At this intermediate stage we have a mixed representation, with trajectories starting with fixed angles ( $\pm \theta_a$ ) and finishing at points  $y'$ . A new stationary-phase over  $y'$  calls for. However, this is not possible in the case where families of trajectories with degenerate action exist and the reduced action  $\hat{S}$  is a linear function of  $y'$ . This is the case of trajectories directly crossing the cavity without suffering collisions or the case in which the cavity has rectangular shape. In the next section we analyze these two cases in detail. Here we will assume that trajectories are isolated and we can perform the  $y'$  integration by stationary phase. The final points  $y'_0$  are selected according to

$$(2.15) \quad \left( \frac{\partial \hat{S}}{\partial y'} \right)_{\bar{a}} = \left( \frac{\partial S}{\partial y'} \right)_y = p_{y'} = -\frac{\bar{b}\hbar\pi}{W} , \quad \bar{b} = \pm b ,$$

implying that the trajectories have an outgoing angle  $\theta_{\bar{b}}$  such that  $\sin \theta_{\bar{b}} = \bar{b}\pi/kW$ . The semiclassical expression for the transmission amplitude can then be casted as [7]

$$(2.16) \quad t_{ba} = -\frac{\sqrt{2\pi i\hbar}}{2W} \sum_{\bar{a}=\pm a} \sum_{\bar{b}=\pm b} \sum_{s(\bar{b}, \bar{a})} \text{sgn}(\bar{a}\bar{b}) \sqrt{\tilde{D}_s} \exp\left(\frac{i}{\hbar} \tilde{S}_s(\bar{b}, \bar{a}; E) - i\frac{\pi}{2} \tilde{\nu}_s\right)$$

The reduced action is

$$(2.17) \quad \tilde{S}(\bar{b}, \bar{a}; E) = S(y'_0, y_0; E) + \frac{\hbar\pi\bar{a}}{W} y_0 - \frac{\hbar\pi\bar{b}}{W} y'_0 .$$

For billiards it can be written as  $\tilde{S} = \hbar k \tilde{L}$ , with  $\tilde{L} = L + ky_0 \sin \theta_a - ky'_0 \sin \theta_{\bar{b}}$ . The prefactor is now given by

$$(2.18) \quad \tilde{D}_s = \frac{1}{mv \cos \theta'} \left| \left( \frac{\partial y}{\partial \theta'} \right)_\theta \right| ,$$

and the Maslov index is

$$(2.19) \quad \tilde{\nu} = \nu + H \left( \left( \frac{\partial \theta}{\partial y} \right)_{y'} \right) + H \left( \left( \frac{\partial \theta'}{\partial y'} \right)_\theta \right) ,$$

where  $H$  is the Heaviside step function [82].



Similar arguments can be used to write the semiclassical reflection amplitude in terms of trajectories leaving and returning to the cross section at the left entrance with appropriate quantized angles. Note that there are two kinds of trajectories contributing to  $G(y', y; E)$  in the case of reflected paths: those which penetrate into the cavity and those which go directly from  $y$  to  $y'$  staying on the cross section of the lead. It is only trajectories of the first kind which contribute to the semiclassical reflection amplitude, as trajectories of the second kind merely cancel the  $\delta_{ba}$  of Eq. (2.8b).

The semiclassical transmission amplitude (2.16) is, for an open system, the analogous of the Gutzwiller trace formula for the density of states in a closed system [4]. Both are expressed as a sum over isolated classical trajectories, making the connection between classical and quantum properties transparent. The main difference between the scattering and energy-level problems, at the semiclassical level, is that the trace formula involves the sum over periodic orbits while the transmission amplitude is given by open trajectories that go across the scattering region. In chaotic systems the number of trajectories connecting two given points grows exponentially with the trajectory length. In open systems the trajectories can escape the scattering region, therefore their proliferation is much weaker than in the close case (although still exponential). Therefore, the convergence of semiclassical propagators in chaotic scattering (even if we ignore the physical cutoffs discussed in the introduction) will not encounter the difficulties of the trace formula. From the quantum point of view, since the Gutzwiller trace formula must reproduce a delta-function spectrum, it can be conditionally convergent at most, while the quantum transmission amplitude is a smooth function of the Fermi energy (away from the thresholds at the opening of new modes) and so the semiclassical sum can be absolutely convergent (depending on the value of the fractal dimension  $d$  of the strange repeller governing the chaotic scattering [83]).

Chaotic scattering problems have been studied by Miller [84] in the context of molecular collisions in terms of the semiclassical propagator in the momentum representation. In this case the relevant sum in this case is over classical trajectories with fixed incident and outgoing momenta, similar but not identical to what we find for the transmission amplitude in our waveguide geometry. Our procedure furnishes a more explicit semiclassical expression to use in the Landauer-Büttiker conductance formulas and allows one to handle more complicated situations like finite magnetic field and soft walls in the leads [72], tunneling in the cavities [50], or the presence of families of trajectories [49]. The last case, discussed in detail in the next section, leads to an expression of the semiclassical transmission amplitudes as a sum over *families of trajectories* (in analogy with the Berry-Tabor formula for the density of states of integrable systems [85]). The simple prescription for the Maslov indices makes possible the numerical evaluation of the semiclassical transmission amplitude. In this section we will not pursue section the explicit summation of Eq. (2.16) over classical trajectories, but in (3.6) we discuss the work of Lin and Jensen [86] addressing such a problem for a circular scattering domain.

**2.5. Transmission coefficients and average values.** – Transmission coefficients are obtained from the magnitude squared of the transmission amplitudes. In a semiclassical

approach they are given by sums over *pairs* of trajectories. Since we will be focusing on billiards, it is convenient to scale out the energy (or momentum) dependence and write

$$(2.20) \quad T(k) = \sum_{a,b=1}^N T_{ba}(k) = \frac{1}{2} \left( \frac{\pi}{kW} \right) \sum_{a,b=1}^N \sum_{\bar{a}=\pm a} \sum_{\bar{b}=\pm b} \sum_{s(\bar{a},\bar{b})} \sum_{u(\bar{a},\bar{b})} F_{\bar{b},\bar{a}}^{s,u}(k) ,$$

$$(2.21) \quad F_{\bar{b},\bar{a}}^{s,u}(k) = \sqrt{\tilde{A}_s \tilde{A}_u} \exp [ik(\tilde{L}_s - \tilde{L}_u) + i\pi\phi_{s,u}] .$$

Where  $s$  and  $u$  label the paths with extreme angles  $\theta_{\bar{a}}$  and  $\theta_{\bar{b}}$ ,  $\tilde{A}_s = (\hbar k/W)\tilde{D}_s$ , and  $\phi_{s,u} = (\tilde{\nu}_u - \tilde{\nu}_s)/2 + \bar{a} + \bar{b}$ . Note that  $\tilde{A}$  is independent of energy, therefore the only energy-dependence is in the selection of the injection angles and in the explicit  $k$ -dependence of the actions.

We would like to understand in which sense the semiclassical transmission coefficients, given by (2.20) and (2.21), are able to account for the highly structured curve of Fig. 3. We do not attempt a detailed description or an identification of classical trajectories (like in Refs. [87, 88]), but a characterization of the overall features, like the secular behavior or the statistical properties of the fluctuations. For this purpose we need to define an average procedure. Since we dispose of a single cavity, our averages must be over energy (or wave-vector). Our semiclassical approximations are supposed to be valid in the large- $k$  limit, thus for an observable  $O(k)$  we define

$$(2.22) \quad \langle O \rangle = \lim_{q \rightarrow \infty} \frac{1}{q} \int_{q_c}^{q_c+q} dk O(k) , \quad \frac{q_c W}{\pi} \gg 1 .$$

This average is particularly suited for analytical calculations, but not for dealing with experimental or numerical results, where we only dispose of a finite  $k$ -range (and the averages are necessarily local). However, if we average over many oscillations, we expect to get the same results as with (2.22). An average over a finite energy-range is precisely the effect of finite temperature on the conductance.

The secular behavior is linearly increasing with  $k$  (outgoing flux proportional to the incoming flux). The slope is given by the average of  $T(k)/k$ , that is,

$$(2.23) \quad \mathcal{T} = \left\langle \frac{\pi}{kW} T(k) \right\rangle = \frac{1}{2} \left\langle \left( \frac{\pi}{kW} \right)^2 \sum_{a,b=1}^N \sum_{\bar{a}=\pm a} \sum_{\bar{b}=\pm b} \sum_{s,u} F_{\bar{b},\bar{a}}^{s,u}(k) \right\rangle .$$

In the large  $k$ -limit the modes are closely spaced in angle, and the sums over modes can be converted into integrals over angles:  $\sum_a^N \sum_{\bar{a}=\pm a} \rightarrow (kW)/\pi \int_{-1}^1 d(\sin \theta)$ . After this conversion, the only  $k$ -dependence remains in the phase factors, and we can interchange the angle-integral with the  $k$ -average obtaining

$$(2.24) \quad \mathcal{T} = \frac{1}{2} \int_{-1}^1 d(\sin \theta) \int_{-1}^1 d(\sin \theta') \sum_{s(\theta, \theta')} \sqrt{\tilde{A}_s \tilde{A}_u} \langle \exp [ik(\tilde{L}_s - \tilde{L}_u) + i\pi\phi_{s,u}] \rangle .$$

Our definition of averages immediately yields that  $k(\tilde{L}_s - \tilde{L}_u) + \pi\phi_{s,u} = 0$ . In the absence of symmetries, such a relation is only possible if  $s = u$ . Quantum interference is therefore absent in the resulting diagonal term. Using the definition of  $\tilde{A}$  and changing variables, from the outgoing angle  $\theta'$  to the initial position  $y$ , we have

$$(2.25) \quad \mathcal{T} = \frac{1}{2} \int_{-1}^1 d(\sin \theta) \int_0^W \frac{dy}{W} f(y, \theta) ,$$

where  $f(y, \theta) = 1$  if the trajectory with initial conditions  $(y, \theta)$  is transmitted and  $f(y, \theta) = 0$  otherwise. The above expression is purely classical and has the intuitive interpretation of a probability of transmission. It can also be easily obtained from a Boltzmann equation approach [72]. The classical form of the transmission coefficient is relevant when the temperature is high enough to kill the interference effects, and it has been used to understand the early experiments on transport in ballistic junctions at Helium temperatures [24, 25, 71, 22].

Unlike (2.16), Eq. (2.25) is very easy to implement numerically, if we have the information of the classical dynamics. We simply have to sample the space of classical trajectories with random choices of the initial position and initial angles (with a weight of  $\cos \theta$ ). Following this procedure yields a value of  $\mathcal{T}$  consistent with the slope of the quantum numerical results (within the statistical errors with which we can determine them).

The secular behavior of the conductance (dashed line in Fig. 3) is given by the straight line that best fits  $T(k)$ , defined by its slope (equal to the classical transmission probability  $\mathcal{T}$ ) and the shift,

$$(2.26) \quad \langle \delta T \rangle = \left\langle \left( T - \left( \frac{\pi}{kW} \right) \mathcal{T} \right) \right\rangle$$

Operationally,  $\delta T$  is well defined. However, it is not possible to give a simple semiclassical prescription for its calculation. In (2.7) we will address the problem of its magnetic field dependence, which determines the weak localization effect.

**2.6. Conductance fluctuations.** – The most striking feature of the data in Fig. 3 are the conductance fluctuations around the mean value. The shape of these fluctuations is characterized by their power spectrum. The semiclassical treatment of the power spectrum [7, 10] was based on the semiclassical approach to  $S$ -matrix fluctuations as a function of energy, introduced by Gutzwiller [90] and extensively developed by Blümel

and Smilansky [47] and Gaspard and Rice [61]. The main conclusion is that the power spectrum is directly related to properties of the classical phase space.

In order to characterize the fluctuations, we introduce the  $k$ -correlation function

$$(2.27) \quad C_k(\Delta k) = \langle \delta T(k + \Delta k) \delta T(k) \rangle ,$$

with

$$(2.28) \quad \delta T = T - \left( \frac{kW}{\pi} \mathcal{T} + \langle \delta T \rangle \right) .$$

The semiclassical calculation of the correlation function involves a sum over four trajectories,

$$(2.29) \quad C_k(\Delta k) = \frac{1}{4} \left\langle \left( \frac{\pi}{kW} \right)^2 \sum_{a,b} \sum_{a',b'} \sum_{\bar{a}=\pm a} \sum_{\bar{b}=\pm b} \sum_{\bar{a}'=\pm a'} \sum_{\bar{b}'=\pm b'} \sum_{s,u} \sum'_{s',u'} \sum'_{\bar{s},\bar{a}} F_{\bar{b},\bar{a}}^{s,u}(k + \Delta k) F_{\bar{b}',\bar{a}'}^{s',u'}(k) \right\rangle .$$

The ‘‘prime’’ in the summations over trajectories indicates that the completely diagonal terms  $s = u$  (and  $s' = u'$ ) are excluded, since they contribute to  $\mathcal{T}$ . The semiclassical expression for  $C_k(\Delta k)$  is fairly complicated since four trajectories contribute to each summand. We will restrict ourselves to the diagonal (in modes) component  $C_k^D(\Delta k)$ , obtained from (2.29) by taking  $a = a'$  and  $b = b'$ .

In taking the  $k$ -average, we consider the limit when the modes are very dense and therefore we replace the sums over modes by integrals over angles (as we did in the previous chapter). The only  $k$ -dependence is in  $\langle \exp[ik(\tilde{L}_s - \tilde{L}_u + \tilde{L}_t - \tilde{L}_v)] \rangle$ . The infinite  $k$ -average implies that the only contribution is for  $\tilde{L}_s - \tilde{L}_u + \tilde{L}_t - \tilde{L}_v = 0$ . Because of the definition of  $C_k^D$ , all four paths satisfy the same boundary conditions on angles, and hence they are all chosen from the same discrete set of paths. In the absence of symmetry, the only contribution (excluding  $s = u$  and  $s' = u'$ ) is  $s = u'$  and  $u = s'$ . Thus we find

$$(2.30) \quad C_k^D(\Delta k) = \frac{1}{4} \int_{-1}^1 d(\sin \theta) \int_{-1}^1 d(\sin \theta') \sum_{s(\theta,\theta')} \sum'_{u(\theta,\theta')} \tilde{A}_s \tilde{A}_u \exp \left[ i\Delta k(\tilde{L}_s - \tilde{L}_u) \right] ,$$

which is independent of  $k$ . As previously stated, we characterize the conductance fluctuations from the Fourier power spectrum

$$(2.31) \quad \hat{C}_k(x) = \int d(\Delta k) C_k(\Delta k) e^{ix\Delta k} .$$

The semiclassical approximation to the diagonal term reads

$$(2.32) \quad \widehat{C}_k^D(x) = \frac{\pi}{2} \int_{-1}^1 d(\sin \theta) \int_{-1}^1 d(\sin \theta') \sum_{s(\theta, \theta')} \sum_{u(\theta, \theta')} ' \tilde{A}_s \tilde{A}_u \delta(\tilde{L}_s + x - \tilde{L}_u)$$

In the chaotic case, we can make progress analytically by assuming that (1) the trajectories are uniformly distributed in the sine of the angle, (2) the angular constraints linking trajectories  $u$  and  $s$  can be ignored, and (3) the constraint  $u \neq s$  can be ignored because of the proliferation of long paths. Introducing angular integrations over  $\tilde{\theta}$  and  $\tilde{\theta}'$  we write

$$(2.33) \quad \widehat{C}_k^D(x) = \frac{\pi}{8} \int_{-1}^1 d(\sin \theta) \int_{-1}^1 d(\sin \theta') \sum_{s(\theta, \theta')} \tilde{A}_s \int_{-1}^1 d(\sin \tilde{\theta}) \int_{-1}^1 d(\sin \tilde{\theta}') \\ \times \sum_{u(\tilde{\theta}, \tilde{\theta}')} \tilde{A}_u \delta(\tilde{L}_s + x - \tilde{L}_u) \propto \int_0^\infty dL P(L+x)P(L) ,$$

$$(2.34) \quad P(L) = \frac{1}{4} \int_{-1}^1 d(\sin \theta) \int_{-1}^1 d(\sin \theta') \sum_{u(\theta, \theta')} \tilde{A}_u \delta(L - \tilde{L}_u) ,$$

is the classical distribution of lengths ( $x$  is taken positive). As previously discussed, the distribution of lengths is exponential for chaotic billiards for large  $L$  ( $P(L) \propto e^{-\gamma_{cl}L}$ ), while there may be deviations at small  $L$ . Using the exponential form for all lengths, we find that

$$(2.35) \quad \widehat{C}_k^D(x) \propto e^{-\gamma_{cl}|x|} ,$$

which is valid for all  $x$  since  $\widehat{C}_D(x)$  must be real and symmetric. This form for the power spectrum implies that the wave-vector correlation function is Lorentzian [47].

$$(2.36) \quad C_k^D(\Delta k) = \frac{C_k^D(0)}{1 + (\Delta k/\gamma_{cl})^2} .$$

We have treated the case of billiards, where the energy-dependence is easily scaled out, and we are lead to the distribution of lengths. But the result of Ref. [47] is general for energy-correlation functions. A semiclassical analysis and an energy-average over intervals small in the classical scale (unchanged trajectories) but large in the quantum scale (many oscillations) yields  $C_E^D(\Delta E) = C_E^D(0)/[1 + (\Delta E/(\hbar\gamma))^2]$ .

The conductance fluctuations are on a scale  $\Delta E_c = \hbar\gamma$  much larger than the level spacing  $\Delta$ , since the openings of the cavity put us in the regime of overlapping resonances. This regime has been extensively studied in Nuclear Physics, in the context of compound

nuclei, and the fluctuations we have discussed are known as Ericson fluctuations [91]. The same physics has also been studied in one-dimensional models of chaotic scattering obtained as a variant of the kicked rotator [92], where the quantum correlation lengths have been shown to be well described by the numerically computed escape rates.

The derivation of the magnetic field correlation function [7] follows the same lines as the case treated above. The correlation function defined as an average over  $k$

$$(2.37) \quad C_B(\Delta B) = \langle \delta T(k, B + \Delta B) \delta T(k, B) \rangle .$$

Again, our definition of averages will facilitate the analytical calculations. In analyzing experimental or numerical results, averages over finite  $k$  or  $B$  intervals (small enough not to modify the classical dynamics) are generally used.

Treating the diagonal (in modes) component  $C_B^D(\Delta B)$ , assuming  $\Delta B$  small enough not to change the classical trajectories significantly, and using the pairing  $s = u'$ ,  $u = s'$ , we are lead to the action differences  $[S_s(B + \Delta B) - S_u(B + \Delta B) + S_u(B) - S_s(B)]/\hbar = (\Theta_s - \Theta_u)\Delta B/\Phi_0$ . In analogy with the previous case, we have

$$(2.38) \quad C_B^D(\Delta B) = \frac{1}{4} \int_{-1}^1 d(\sin \theta) \int_{-1}^1 d(\sin \theta') \sum_{s(\theta, \theta')} \sum_{u(\theta, \theta')} ' \tilde{A}_s \tilde{A}_u \exp \left[ i \frac{\Delta B}{\Phi_0} (\Theta_s - \Theta_u) \right],$$

$$(2.39) \quad \begin{aligned} \hat{C}_B^D(\eta) &= \frac{\Phi_0 \pi}{2} \int_{-1}^1 d(\sin \theta) \int_{-1}^1 d(\sin \theta') \sum_{s(\theta, \theta')} \sum_{u(\theta, \theta')} ' \tilde{A}_s \tilde{A}_u \delta(\Theta_s + \eta - \Theta_u) \\ &\propto \int_{-\infty}^{\infty} d\Theta N(\Theta + \eta) N(\Theta). \end{aligned}$$

Using the exponential form (2.2) of the distribution of effective areas  $N(\Theta)$ , for all values of  $\Theta$  yields the power spectrum [7]

$$(2.40) \quad \hat{C}_B^D(\eta) \propto e^{-\alpha_{cl} |\eta|} (1 + \alpha_{cl} |\eta|)$$

and the correlation function

$$(2.41) \quad C_B^D(\Delta B) = \frac{C_B^D(0)}{[1 + (\Delta B/\alpha_{cl}\Phi_0)^2]^2}$$

We have only been able to calculate semiclassically the line-shapes of the diagonal parts of  $C_k(\Delta k)$  and  $C_B(\Delta B)$ , which are  $k$ -independent. On the other hand, for a chaotic cavity we expect only one characteristic scale for each correlation function. We then conjecture that (2.35) and (2.40) also represent the full power spectra, and that

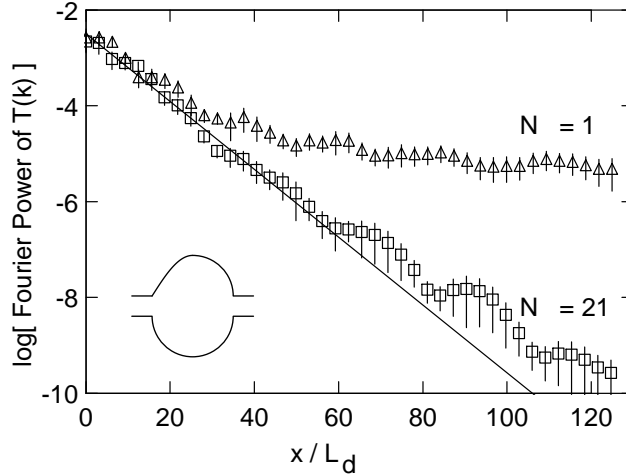


Fig. 4. – Power spectrum of  $T(k)$  for the chaotic structure shown for two fillings:  $N = 21$  (squares) and  $N=1$  (triangles). In the former case, the agreement with the semiclassical theory is excellent, in the extreme quantum limit when only one mode is propagating in the leads, there is more high-frequency power and the agreement with the semiclassical theory is poorer. (From Ref. [10].)

$C_k$  and  $C_B$  are  $k$ -independent (like  $C_k^D$  and  $C_B^D$ ). Thus, we expect the conductance fluctuations to persist (and remain invariant) in the large- $k$  limit.

We need to perform a systematic study of the conductance fluctuations in order to test the semiclassical predictions. Since there is some arbitrariness in determining the averages of the numerical data, we directly calculate the power spectra  $\hat{C}_k(x)$  and  $\hat{C}_B(\eta)$  from the Fourier power of the raw data. Once we smooth them, we verify that they are well represented by Eqs. (2.35) and (2.40) over large ranges of  $x$  and  $\eta$ . In Fig. 4 we see (for  $\hat{C}_k$ ) deviations for small lengths ( $x \simeq L_d$ ) and for large  $x$ . Similar agreement is obtained for  $\hat{C}_B$  [7, 10]. The deviations for small lengths (or areas) are understandable since the chaotic nature of the dynamics (and the statistical treatment of the trajectories that we used) cannot give an appropriate description for short trajectories. The deviations for large lengths arise from the limitations of semiclassics and of the diagonal approximation, and they become less important as we go in the large  $k$ -limit.

The analysis of the power spectra has the advantage of separating the fluctuations according to their length (or area) scales. This is important when we want to make the connection with the experimental world of Mesoscopic Physics. Only the features associated with scales smaller than our physical cut-offs will be relevant.

If we fit the power spectra obtained from the *quantum numerical calculations* in an interval where the forms (2.35) and (2.40) are respected we can extract quantum correlation lengths  $\gamma_{qm}$  and  $\alpha_{qm}$ , that can be compared with the rates  $\gamma_{cl}$  and  $\alpha_{cl}$  obtained

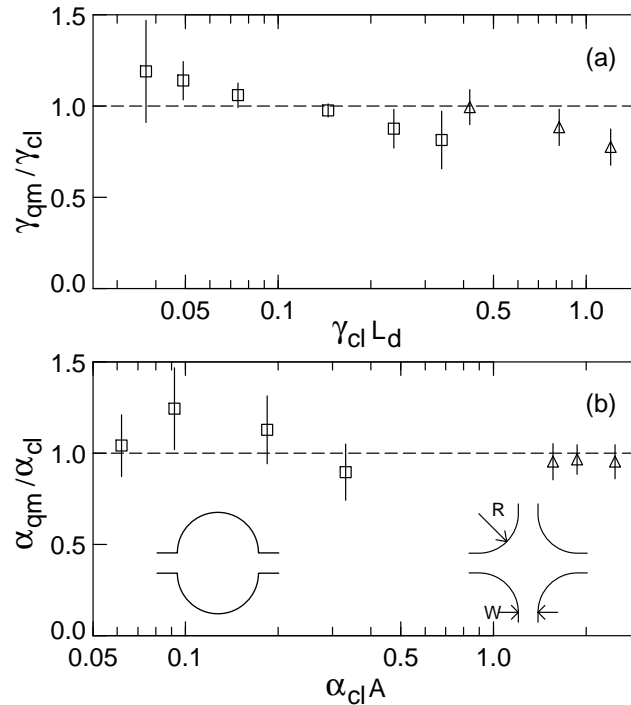


Fig. 5. – (a) Ratio of the wave-vector correlation length to the classical escape rate  $\gamma_{cl}$  as a function of  $\gamma_{cl}$  for both types of structures shown. 4-disc structure (triangles) with  $R/W = 1, 2, 4$ , and stadium (squares) with  $R/W = 0.5, 1, 2, 4, 6, 8$ . (b) Ratio of magnetic field correlation length to  $\alpha_{cl}$ , the exponent of the distribution of effective areas, as a function of  $\alpha_{cl}$ . 4-disc structure with  $R/W = 1, 2, 4$ , and open stadium with  $R/W = 1, 2, 4, 6$ . (From Ref. [7].)

from the simulation of the *classical dynamics*. Semiclassics provides the link, through Eqs. (2.35) and (2.40), between quantum and classical parameters. Fig. 5 shows that  $\gamma_{qm}, \alpha_{qm}$  are indeed given by the classical quantities  $\gamma_{cl}, \alpha_{cl}$  to high accuracy while they are varied over roughly two orders of magnitude by changing the size of the structures considered (for the four-probe structure, we considered the fluctuations of the Hall resistance, which is a function of the transmission coefficient between leads [56, 71, 72], for which the previous semiclassical analysis is applicable). The  $k$ -independence of  $\gamma_{qm}, C_k(0), \alpha_{qm}$  and  $C_B(0)$  is approximately respected in our numerical simulations away of the quantum limit of small  $N$  [10].

In an integrable cavity each trajectory belongs to a torus defined by two constants of motion. Moreover, if the conserved quantities in the cavity and in the leads are the same, the scattering trajectories are organized in families, and as we will see in the next section,



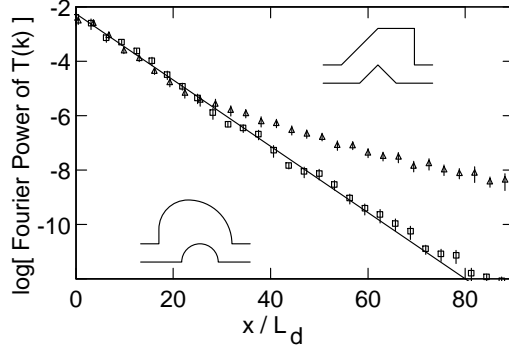


Fig. 6. – Power spectra of  $T(k)$  for the chaotic (squares) and regular (triangles) structures shown ( $N = 33$ ). The regular structure has more power at large frequencies because of more trajectories with large enclosed areas. The line is a fit to Eq. (2.35). (From Ref. [10].)

we need to modify the form of the semiclassical transmission amplitudes. Leaving aside this last case, there are at least three assumptions leading to Eqs. (2.35) and (2.40) that break down in the case of integrable dynamics: the length and area distributions are not characterized by a single scale (exhibiting, as we saw in (2.1), power-laws), there are angular correlations between incident and outgoing angles, and the constraint of two trajectories to satisfy the same boundary conditions on angles cannot be ignored. From Eq. (2.32), the power spectrum  $\widehat{C}_k^D(x)$  is evidently related to the distribution of two distinct paths with a difference in length of  $x$ . Thus we conjecture that

$$(2.42) \quad \widehat{C}_D(x) \propto \int_0^\infty dL \int_0^1 d(\sin \theta) P_2(L+x, L, \theta)$$

where  $P_2(L+x, L, \theta)$  is the classical distribution for two distinct trajectories at angle  $\theta$ , one with length  $L$  and the other with length  $L+x$ . Numerical simulations for  $P_2$  in rectangular a cavity (Fig. 2c) show that it does not factorize. It is characterized by a decay  $1/x^2$  for large  $x$ , while  $P(L)$  follows a  $1/L^3$  law.

In the case of the power spectrum of  $T(B)$ , we assume that a similar expression holds in terms of the classical distribution for two trajectories at angle  $\theta$  with effective areas  $\Theta$  and  $\Theta + \eta$

$$(2.43) \quad \widehat{C}_D(\eta) \propto \int_{-\infty}^\infty d\Theta \int_0^1 d(\sin \theta) N_2(\Theta + \eta, \Theta, \theta).$$

The result of classical simulation in Fig. 2 shows that this distribution is roughly constant up to a cutoff which is less than the area of the rectangle.

Numerical calculations of integrable cavities yield a more ragged conductance, as compared with the chaotic case [63, 10]. This is reflected by more power strength at large

lengths (Fig. 6) and areas, consistently with our conjecture for linking conductance fluctuations and  $P_2$ . Lai and collaborators [68] showed that the fine scale energy fluctuations of the  $S$  matrix are greatly enhanced for non-hyperbolic dynamics, as compared with the hyperbolic case, and predicted for  $C_E(\Delta E)$  a cusp-shaped peak at  $\Delta E = 0$ .

**2.7. Weak localization in the ballistic regime.** – In our discussion of the secular behavior of the conductance through a ballistic cavity (Fig. 3), we pointed that the shift  $\langle \delta T \rangle$  is sensitive to the magnetic field. The presence of a small field increases the average conductance. By analogy with the disordered case, we call this effect the ballistic weak localization [48, 10]. It is important to realize that it is an average effect. Only after removing the (large) conductance fluctuations by the  $k$ -average, we obtain the (small) difference between the secular behaviors with and without magnetic field. The two-probe conductance is an even function of the magnetic field, therefore in a given sample,  $g(B)$  may have a *maximum or a minimum* at  $B = 0$ . The two possible cases are observed, experimentally [30] and in the numerical simulations.

In our calculation of the slope of the secular behavior (2.25) we neglected the possibility that unlike paths may have the same effective action and only considered the diagonal approximation of pairing each trajectory with itself. Ignoring degeneracies among actions is correct in the absence of symmetries, but time-reversal or spatial symmetries force us to consider non-diagonal (in trajectories) terms. Obtaining exact spatial symmetries of the confining potential in actual microstructures is quite difficult due to the limitations in the fabrication procedure, but the time-reversal symmetry is exactly fulfilled by simply turning off the external magnetic field.

It is easy to identify a set of degenerate trajectories that yields quantum interference. Let us consider the reflection coefficient and separate it on its diagonal (in modes) and off diagonal components

$$(2.44) \quad R = R^D + R^{OD} = \sum_{a=1}^N R_{aa} + \sum_{b \neq a}^N R_{ba} ,$$

$$(2.45) \quad R_{aa} = \frac{1}{2} \left( \frac{\pi}{kW} \right) \sum_{\bar{a}=\pm a} \sum_{\bar{b}=\pm a} \sum_{s(\bar{a},\bar{b})} \sum_{u(\bar{a},\bar{b})} F_{\bar{b},\bar{a}}^{s,u}(k) .$$

The factors  $F$  have the same meaning as in Eq. (2.21), but now they refer to reflecting trajectories. Averaging  $R(k)/k$  and doing the diagonal (in trajectories) approximation yields the classical reflection probability  $\mathcal{R}$  (analogous to Eq. (2.25)) verifying  $\mathcal{T} + \mathcal{R} = 1$ . In the absence of magnetic field there are symmetry related trajectories in  $R^D$  and in  $R^{OD}$ . The time-reversed of a trajectory  $s(\bar{a}, \bar{b})$  is  $s^T(\bar{b}, \bar{a})$ , starting with the angle  $\theta_{\bar{b}}$  and coming back to the lead with angle  $\theta_{\bar{a}}$ , therefore it contributes to  $R_{ab}$ . If  $b \neq a$  there is no interference between  $s$  and  $s^T$ , thus the only diagonal (in trajectories) terms to be considered are in  $R^D$  (trajectories leaving with an angle  $\theta$  and returning with  $\theta$  or  $-\theta$ ).

The contribution of such trajectories can be treated in a similar way as in the case of  $\mathcal{R}$  and  $\mathcal{T}$  (except that we only have *one* sum over modes),

$$(2.46) \quad \langle \delta R^D(B=0) \rangle = \frac{1}{2} \int_{-1}^1 d(\sin \theta) \sum_{s(\theta, \pm\theta)} \tilde{A}_s .$$

If we now turn on a magnetic field  $B$  weak enough not to modify appreciably the geometry of the paths, we only need to consider the phase difference between  $s$  and  $s^T$ , that is given by the effective area  $\Theta_s$  according to  $(S_s - S_u)/\hbar = 2\Theta_s B/\Phi_0$ . Thus, we obtain

$$(2.47) \quad \langle \delta R^D(B) \rangle = \frac{1}{2} \int_{-1}^1 d(\sin \theta) \sum_{s(\theta, \pm\theta)} \tilde{A}_s \exp \left[ i \frac{2B}{\Phi_0} \Theta_s \right] ,$$

which yields an order unity ( $k$ -independent) contribution to the average conductance containing only classical parameters (and  $\Phi_0$ ).

In a chaotic system it is reasonable to assume that there is a uniform distribution of exiting angles, and that the distribution (2.2) of effective areas is valid even if we constraint the initial and final angles of the trajectories to fixed values of  $\theta$  and  $\theta'$ . Therefore we can write [48]

$$(2.48) \quad \langle \delta R^D(B) \rangle = \frac{1}{4} \int_{-1}^1 d(\sin \theta) \int_{-1}^1 d(\sin \theta') \sum_{s(\theta, \theta')} \tilde{A}_s \int_{-\infty}^{\infty} d\Theta N(\Theta) \exp \left[ i \frac{2B}{\Phi_0} \Theta_s \right] \\ = \frac{\mathcal{R}}{1 + (2B/\alpha_{cl}\Phi_0)^2} .$$

The Lorentzian line-shape is governed by the same parameter  $\alpha_{cl}$  of the conductance fluctuations (up to a factor of 2). Notice that  $\langle R^D(B=0) \rangle = 2\mathcal{R}$ , and the diagonal reflection coefficients  $R_{aa}$  are on average twice as large as the typical off diagonal term ( $\mathcal{R}/N$ ). This factor of two enhancement, known as “coherent backscattering”, is called “elastic enhancement” in Nuclear Physics [93, 94].

We have shown that by the application of a magnetic field larger than  $\alpha_{cl}\Phi_0/2$ , the diagonal reflection coefficient is reduced from  $2\mathcal{R}$  to  $\mathcal{R}$ . By unitarity, this means that  $R^{OD} + T$  must increase by  $\mathcal{R}$ . However, there are not time-symmetric pairs of trajectories producing interference effects in  $R^{OD}$  or  $T$ , and we are not able to evaluate semiclassically the corrections (or order 1) to their leading behavior (or order  $N$ ). The weak localization is the  $B$ -dependent part of the shift  $\langle \delta T(B) \rangle$  of Fig. 3, but we have been able to calculate semiclassically only one part of it, the coherent backscattering  $\langle \delta R^D(B) \rangle$ .

Our semiclassical result of Eq. (2.49), predicts two important parameters of the elastic backscattering: its magnitude and its magnetic field scale. Due to the off-diagonal

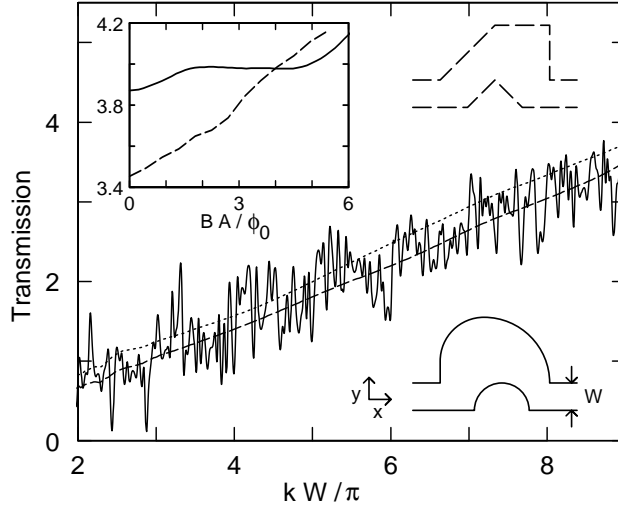


Fig. 7. – Transmission coefficient as a function of wave-vector for the half-stadium structure shown in the bottom right. The  $T = 0$  fluctuations (solid) are eliminated by smoothing using a temperature which corresponds to 20 correlation lengths. The offset of the resulting  $B = 2\Phi_0/A$  curve (dotted) from that for  $B = 0$  (dashed) demonstrates the average magnetoconductance effect. Inset: smoothed transmission coefficient as a function of the flux through the cavity ( $kW/\pi = 9.5$ ) showing the difference between the chaotic structure in the bottom right (solid) and the regular structure in the top right (dashed). (From Ref. [48].)

contribution, we expect the magnitude of the weak localization effect to be different than the coherent backscattering. On the other hand, as with the conductance fluctuations, we expect the weak localization of a chaotic cavity to be characterized by a single field scale, that should necessarily be the one of the coherent backscattering. We confirm such a conjecture with the numerical results of Fig 7, where the magnetoconductance of a chaotic cavity is shown to have a Lorentzian line-shape, with the width given by the classical parameter  $\alpha_{cl}$ .

Our numerical studies allow to address the problem of the off-diagonal contributions. For the two structures of Fig. 8 we split the field dependent part of the (smoothed) total reflection coefficient  $R(B = 0) - R(B)$  (solid) in its diagonal (dashed) and off-diagonal (dotted) parts. For the structure with the stopper  $\langle \delta R^D \rangle$  is approximately independent of  $k$ , its magnitude is within 30% of  $\mathcal{R}$ , and the elastic enhancement factor goes approximately from 2 to 1 when we turn on the field. But there is an important off-diagonal contribution, of opposite sign. Therefore, the weak localization effect is reduced respect to the coherent backscattering. The structure without stoppers exhibits similar features, but has a very reduced weak localization effect. Also, the magnitude of

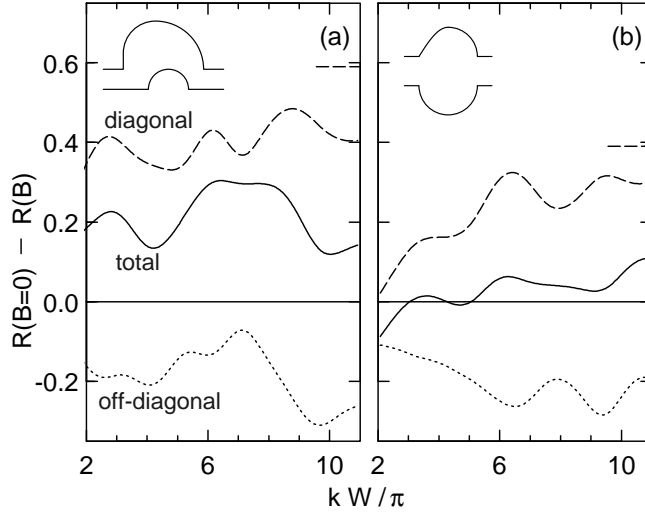


Fig. 8. – Change in the total (smoothed) reflection coefficient (solid), as well as the diagonal (dashed) and off-diagonal (dotted) parts, upon changing  $B$  from 0 to  $2\alpha_{cl}\Phi_0$ . The dashed ticks on the right mark the classical value of  $\mathcal{R}$ . (From Ref. [48].)

the coherent backscattering differs considerably from  $\mathcal{R}$  and there is an important net variation as a function of  $k$ . Such effects are probably due to the presence of short paths and the approximate nature of the uniformity assumption used to obtain Eq. (2.49).

In (4.2) we will discuss some proposals to cope with this limitation of the semiclassical approximation and the predictions of the theory of random matrices applied to ballistic transport. With the random matrix approach we are able to calculate averages of diagonal, as well as non-diagonal, coefficients.

In the case of integrable cavities similar considerations to those invoked in the discussion of conductance fluctuations are pertinent. Lacking a rigorous theory, we conjecture how to modify our formalism taking into account the assumptions that break down in the integrable case. For instance, the uniformity assumption leading to Eq. (2.49) is no longer valid, and we should work with an angle-dependent distribution function  $N(\Theta, \theta)$ . Evaluating (2.47) numerically for circular and polygonal shapes leads [approximately] to  $\langle \delta R^D(B) \rangle \propto |B|$  for small  $B$  [48, 11]. Such linear behavior can be obtained by taking the Fourier transform of a distribution  $N(\Theta) \propto 1/\Theta^2$ . In of Fig. 7 (inset) we see for the quantum mechanical calculations in a polygonal cavity the triangular shape of the weak localization peak, together with the Lorentzian one of the chaotic case. We thus verify that the difference in the area distributions of chaotic and integrable cavities leads to a qualitative difference in the shape of the weak localization peak.

### 3. – Scattering and integrability in quantum transport

In the previous section we analyzed quantum interference effects in ballistic cavities using a semiclassical approach. In the discussion leading to the semiclassical form of the transmission amplitude, we stressed the fact that the simple form of (2.16), expressed as a sum over classical trajectories, was only valid in the case in which trajectories were isolated, as typically happens for chaotic systems. In this chapter we treat the case of trajectories that appear in *families* and we obtain a different form of the semiclassical transmission amplitudes than in the previous case. This difference, arising from the classical dynamics, has important consequences at the level of the quantum observables. We first discuss in this section the example of the families of trajectories that directly cross a ballistic cavity [10, 86], and then the case of the scattering through a rectangular billiard by using a continuous fraction approach [49]. Transport through a square cavity has also been discussed by Wirtz and collaborators [95]; an alternative form of the transmission coefficients was proposed and the correspondence between quantum results and classical trajectories was established. At the end of the section we present another integrable case: circular cavities, for which the semiclassical form (2.16) is applicable, and can be adapted in order to incorporate effects of diffraction and tunneling.

**3.1. Direct trajectories.** – A typical structure, like that of Fig. 1 will have a family of trajectories that cross directly from one lead to the other, without suffering any collision. This is the simplest case to illustrate the modifications that we need to include in the semiclassical approach to transport due to the presence of families of trajectories. As discussed in (2.4), we can always do the first integration of (2.8a) by stationary-phase. The resulting Eq. (2.13) for the contribution of direct trajectories to the transmission amplitude  $t_{ba}$  writes as

$$(3.1) \quad t_{ba}^d = \frac{i}{W} \sqrt{\frac{\cos \theta_b}{\cos \theta}} \left\{ \int_{L_d \tan \theta}^W dy' \sin \left[ \frac{\pi b y'}{W} \right] \exp \left[ i \left( \frac{k}{\cos \theta} + \frac{\pi a y_0}{W} \right) \right] - \int_0^{W - L_d \tan \theta} dy' \sin \left[ \frac{\pi b y'}{W} \right] \exp \left[ i \left( \frac{k L_d}{\cos \theta} - \frac{\pi a y_0}{W} \right) \right] \right\} .$$

$W$  is the width of the leads and  $L_d$  the distance between them. The two terms correspond to the two families, with injection angles  $\pm\theta$ , verifying  $\sin \theta = a\pi/kW$ . The length of all the trajectories is  $L = L_d/\cos \theta$ , and  $y_0 = y' \mp L_d \tan \theta$  is the initial point of the trajectory reaching the exiting cross section at  $y'$  in the first (second) term. Of course, we cannot perform as before the integral over  $y'$  by stationary-phase as there is no quadratic term in the action. However we can calculate the integral in a closed form. For the diagonal term we obtain [10]

$$(3.2) \quad t_{aa}^d = -\exp[ikL] \left\{ (1 - \rho \tan \theta) \exp(-i\pi a \rho) + \frac{1}{\pi a} \sin(\pi a \rho) \right\} ,$$

with  $\rho = (L_d/W) \tan \theta$ . For large quantum numbers  $a$  we can neglect the last (small and rapidly oscillating) term. The off-diagonal terms ( $a \neq b$ ) vanish if  $a$  and  $b$  have different parity. For modes with the same parity we have

$$(3.3) \quad t_{ba}^d = -\frac{2}{\pi} \sqrt{\frac{\cos \theta_b}{\cos \theta_a}} \exp i [kL - \pi a \rho] \left\{ \frac{1}{b+a} \exp \left[ -i \frac{(b+a)\pi \rho}{2} \right] \sin \left[ \frac{(b+a)\pi \rho}{2} \right] - \frac{1}{b-a} \exp \left[ -i \frac{(b-a)\pi \rho}{2} \right] \sin \left[ \frac{(b-a)\pi \rho}{2} \right] \right\} .$$

As expected, the result is strongly peaked for  $b=a$  (where Eq. (3.2) should be used), but shows nevertheless an important off-diagonal contribution for close quantum numbers  $b$  and  $a$ . In Ref. [86], Lin generalized these results to the case in which the leads are not collinear.

It is important to notice the different dependence on  $\hbar$  (or  $k$ ) for the contribution from the family of direct trajectories and the isolated trajectories. The number of modes that support direct trajectories is  $N(W/L_d)$ , and therefore the effect of direct trajectories does not disappear in the semiclassical limit. The existence of direct trajectories complicates the comparison between experiment (both numerical and laboratory) and the semiclassical theory. Thus in many of our numerical simulations we have introduced “stoppers” in the billiards which eliminate this effect; the experimentalists have also tried to avoid this problem by displacing the leads [30], having an angle smaller than  $\pi$  between them [8, 39], or using stoppers inside the cavity [30, 37].

**3.2. Scattering through a rectangular cavity.** – The dynamics in a rectangular cavity is integrable, and the conserved quantities are the absolute value of the projections of the momentum of the particle along the two axis. The motion of the particle inside the cavity can be represented by a straight line in the extended (or unfolded) space where the cavity is periodically repeated in both directions (Fig. 9). In order to simplify the notation, we work in this section with a square cavity of length side 1 (without loss of generality since we can always scale the sides of a rectangular cavity to the square of unit length).

For a trajectory starting at the point  $y_0$  of the entrance lead with and angle  $\theta$ , we would like to know after how many bounces with the walls, the particle is going to leave the cavity. In the unfolded space, this problem translates into finding the first window (*i.e.* image of the lead connections) encountered by the straight line  $D(y_0)$  defined by  $y = y_0 + x \tan \theta$ . If we now change  $y_0$ , keeping  $\theta$  fixed, the nearby trajectories will exit by the same window until a certain critical value  $y_0^c$ , where we pass to another family of trajectories associated with a different window. Evaluating the families of trajectories with a given injection angle leads to a diophantic problem [49]. The coordinates  $(p, q)$  of the exiting windows are part of the intermediate fractions (or Farey series) appearing in the continued fraction representation of  $1/\tan \theta$ . Our interest in fixed injection angles stems from the semiclassical approximation to the transmission amplitude, that according

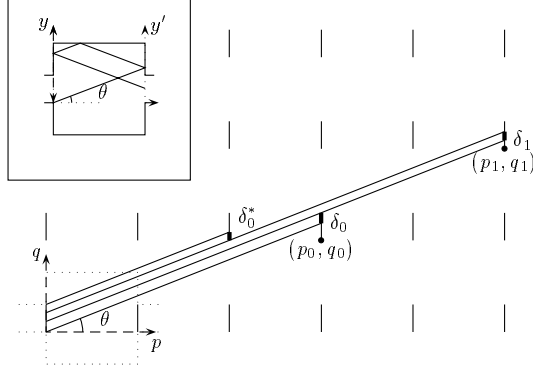


Fig. 9. – Unfolded space for the dynamics in a square cavity (inset). The trajectory entering at the lowest point ( $y=0$ ) of the left lead with an angle  $\theta$  is shown in the original and extended space. It belongs to the family that leaves the cavity through the exiting lead  $(p_0, q_0)$  and has a weight  $\delta_0$ . For this angle  $\theta$  there are two families contributing to the transmission amplitude (0 and 1) and one family contributing to the reflection amplitude ( $0^*$ ). (From Ref. [49].)

to Eq. (2.13) selects the angles  $\pm\theta$ , with  $\sin\theta = a\pi/kW$ .

Let us start with the trajectory entering the cavity at the lowest point ( $y_0=0$ ), whose exiting lead is defined by the segment  $[(p_0, q_0); (p_0, q_0 + W)]$  which intersects  $D(0)$  (see Fig. 9). As we increase  $y_0$ , we will remain within a family of degenerate trajectories (that we note by  $n=0$ ) until the exiting point  $y_0 + p_0 \tan\theta$  hits the uppermost point of the segment. The pair  $(p_0, q_0)$  must verify the conditions:

- a.  $0 < p_0 \tan\theta - q_0 < W$  ,
- b.  $\forall(p, q)$  such that  $0 < p \tan\theta - q < p_0 \tan\theta - q_0 \Rightarrow p > p_0$  .

According to a, the first  $y$ -interval is  $[0, \delta_0]$  (or equivalently, the first  $y'$ -interval is  $[W - \delta_0, W]$ ), while condition b means that  $(p_0, q_0)$  is the first lattice point verifying a. The uppermost family will be associated with an interval  $[(p_0^*, q_0^*); (p_0^*, q_0^* + W)]$ , where the pair  $(p_0^*, q_0^*)$  verifies similar conditions as  $(p_0, q_0)$ :

- c.  $0 < W + p_0^* \tan\theta - q_0^* < W$  ,
- d.  $\forall(p, q)$  such that  $W + p_0^* \tan\theta - q_0^* < W + p \tan\theta - q < W \Rightarrow p > p_0^*$  .

According to c, the first  $y$ -interval of the uppermost family is  $[W - \delta_0^*, W]$  (the first  $y'$ -interval is  $[0, \delta_0^*]$ ), while d implies that  $(p_0^*, q_0^*)$  is the first lattice point verifying c.

Now that we have determined the lowest and the uppermost families for the  $[0, W]$   $y$ -interval, the following sequences of families can be obtained by reducing ourselves to the  $y$ -interval  $[\delta_0, W - \delta_0^*]$ , and with the changes of  $(p_0, q_0)$ ,  $(p_0^*, q_0^*)$  by  $(p_1, q_1)$ ,  $(p_1^*, q_1^*)$



the conditions  $a - d$  define the next two families. Continuing this procedure until the two sequences of families begin to overlap each other, we obtain the sequence of lower families defined by their initial and final points,

$$(3.4a) \quad y'_i(p_l, q_l) = W + (p_l - p_{l-1}) \tan \theta - (q_l - q_{l-1}) ,$$

$$(3.4b) \quad y'_f(p_l, q_l) = W ,$$

The width (or “weight”) of the family is  $\delta_l = y'_f - y'_i = q_l - q_{l-1} - (p_l - p_{l-1}) \tan \theta$ . For the upper-families we have

$$(3.5a) \quad y'_i(p_u^*, q_u^*) = 0 ,$$

$$(3.5b) \quad y'_f(p_l^*, q_l^*) = (p_u^* - p_{u-1}^*) \tan \theta - (q_u^* - q_{u-1}^*) ,$$

and the width  $\delta_u^* = (p_u^* - p_{u-1}^*) \tan \theta - (q_u^* - q_{u-1}^*)$ . The very last family is simultaneously shadowed by lower and upper families, therefore has  $y'_i$  given by (3.4a) and  $y'_f$  by (3.5b).

We can now establish the relationship with the continued fraction representation of  $\Theta = 1/\tan \theta$ , that is defined by the sequences  $(\alpha_m)$  and  $(a_m)$  as follows [96]:

$$(3.6) \quad \alpha_0 = \Theta \quad a_0 = [\alpha_0] \\ \alpha_{m+1} = \frac{1}{\alpha_m - a_m} \quad a_{m+1} = [\alpha_{m+1}] .$$

$[\alpha]$  denotes the integer part of  $\alpha$ . The best rational approximations to  $\Theta$  are the fractions  $P_m/Q_m$ , called convergents, and obtained from the recurrence relations

$$(3.7) \quad \begin{cases} P_m = P_{m-2} + a_m P_{m-1} \\ Q_m = Q_{m-2} + a_m Q_{m-1} \end{cases} ,$$

with the initial choice of  $(P_{-1}, Q_{-1}) = (1, 0)$  and  $(P_0, Q_0) = ([\Theta], 1)$ . Since  $(P_m)$  and  $(Q_m)$  are sequences of integers, we can represent the convergents as lattice points  $(P_m, Q_m)$  that approach the straight line  $D(0)$  as  $m$  increases from above (even  $m$ ) and below (odd  $m$ ).

The  $m$ -th Farey sequence (or intermediate fractions) are the intermediate lattice points on the segment  $[(P_{m-2}, Q_{m-2}), (P_m, Q_m)]$  defined by

$$(3.8) \quad \begin{cases} p_m^k = P_{m-2} + kP_{m-1} \\ q_m^k = Q_{m-2} + kQ_{m-1} \end{cases} \quad 0 \leq k \leq a_m .$$

This sequence sequence of equally spaced lattice points  $(p_m^k, q_m^k)$  starts at the convergent  $(P_{m-2}, Q_{m-2})$  (for  $k=0$ ) and finishes at  $(P_m, Q_m)$  (for  $k=a_m$ ). The translation vector is given by the coordinates of the convergent  $(P_{m-1}, Q_{m-1})$ . The intermediate fractions with odd (even)  $m$  verify the properties the conditions  $b$  ( $d$ ), thus determining the lattice

points associated with the exiting leads. The two types of families are given by the Farey sequences of even and odd order convergents, with the additional requirements that the exiting points are closer than  $W$  to the straight line  $D(0)$ . Odd (even) values of  $p_n$  correspond to transmission (reflection) trajectories. The initialization  $(p_{-1}, q_{-1}) = (1, 0)$  and  $(p_0, q_0) = ([\Theta], 1)$  is an arbitrary choice, and some special care has to be taken in the case in which  $\tan \theta < 1/2$  where they may exist lattice points between the initial ones.

The continued fraction representation of a generic (irrational) real number results in an infinite sequence of convergents. However, the fact that we have defined a finite distance  $W$  to approach  $D(0)$  implies that once the lower and upper families begin to overlap we do not need to consider higher convergents. Therefore, each angle  $\theta_a$  is associated to a finite number of families. In addition, it can be shown that at most three sequences of intermediate fractions are relevant [49].

**3.3. Semiclassical transmission amplitudes for square cavities.** – In the extended space, the Green function between points at the entrance and exit leads equals to that of the free space taken between the initial point and the image of the final one (with the adjustment of the phases at the reflections on the hard walls).

As in the previously studied cases, the semiclassical approach for the transmission amplitudes  $t_{ba}$  selects the incoming angle  $\theta$  corresponding to the mode  $a$  (Eqs. (2.12)-(2.14)). Symmetry arguments for a rectangular cavity dictate that  $t_{ba} = 0$  if  $a+b$  is odd. For even  $a+b$  we perform the  $y'$ -integration for each family of trajectories  $n$ , obtaining a transmission amplitude

$$(3.9) \quad t_{ba} = -\frac{i}{W} \sqrt{\frac{\cos \theta_b}{\cos \theta_a}} \sum_n \varepsilon_n \exp[ik\tilde{L}_n] \{I_n(a+b) - I_n(a-b)\} ,$$

where

$$(3.10) \quad I_n(x) = \frac{W}{\pi x} \left( \exp \left[ i \frac{\pi x}{W} y_f'^{(n)} \right] - \exp \left[ i \frac{\pi x}{W} y_i'^{(n)} \right] \right) .$$

$(p_n, q_n)$  are the coordinates of the exiting lead in the extended space,  $y_i'^{(n)}$  and  $y_f'^{(n)}$  are the extreme points of the exiting interval. We have defined the phase  $\varepsilon_n = \exp[i\pi(a+1)\varepsilon(q_n)]$ , with  $\varepsilon(q_n) = 0$  (1) for even (odd)  $q_n$ . The parity of  $q_n$  appears in the phase due to mirror symmetries involved in going to the extended space. The phase gained at the hard-walls is given by the index  $\tilde{\nu}_n = 2(p_n + q_n - 1)$ . The trajectories of the  $n$ -th family have a length  $L_n = p_n / \cos \theta_a$  (all lengths are expressed in units of the side of the square), we have defined the reduced length  $\tilde{L}_n = p_n \cos \theta_a + q_n \sin \theta_a$ . The trajectories that contribute to the transmission amplitude are those going from the left to the right lead, therefore only the values  $n$  with odd  $p_n$  are considered. Similarly to the contribution of direct trajectories, the case  $\bar{a} + \bar{b} = 0$  has to be treated separately for the  $y'$ -integration. However, the corresponding result is included in Eq. (3.9) by taking

the limit  $x \rightarrow 0$ . Obviously,  $\bar{a} + \bar{b} = 0$  corresponds to the maximum transmission since this is the case where the classical trajectory arrives to the exiting lead with the quantized angle of mode  $b$ .

When the  $y'$ -intervals are of the form  $[W - \delta_l, W]$  or  $[0, \delta_u^*]$  (Eqs. (3.2)-(3.2)) we can separate the semiclassical sum into upper ( $u$ ) and lower ( $l$ ) families and write

$$(3.11) \quad t_{ba} = \frac{1}{W} \sqrt{\frac{\cos \theta_b}{\cos \theta_a}} \sum_{n=l,u} \varepsilon_n \varepsilon'_n \exp[ik\tilde{L}_n] \{ \Delta_n(a+b) - \Delta_n(a-b) \} \delta_n ,$$

with the family-dependent function  $\Delta_n$  defined by

$$(3.12) \quad \Delta_n(x) = \frac{2W}{\pi x \delta_n} \exp \left[ i \varepsilon'_n \frac{\pi x}{2W} \delta_n \right] \sin \left[ \frac{\pi x}{2W} \delta_n \right] ,$$

$\varepsilon'_n = 1$  if  $n = u$  and  $\varepsilon'_n = -1$  if  $n = l$  [97]. As previously stated, only odd  $p_n$  should be considered in the expansion for the transmission amplitude. The “last” family does not have a  $y'$ -interval with the simple form of the previous ones. Therefore, when this family contributes to the transmission amplitude, we cannot use for it the simple form (3.11) depending only on the weights  $\delta_n$ , but Eq. (3.9) together with the limits (3.4a) and (3.5b).

The forms (3.9) and (3.11) of the transmission amplitude provide a very powerful method to numerically compute the conductance through a rectangular cavity. For each  $a = 1 \dots N$ , we only need to calculate a finite number of convergents and intermediate fractions of the continued fraction representation of  $1/\tan \theta_a$  and recursively obtain the weighting intervals  $\delta_n$ . The advantage over quantum methods based on discretization (recursive Green function, wave function matching, etc) is that it can be used for large wave-vectors  $k$ . The method actually gets more exact with increasing  $k$  since it involves a semiclassical approximation.

In Fig. 10 we present the conductance of a square cavity calculated from Eq. (3.11) for an small opening ( $W = 0.05$ ) in a large  $k$ -interval. We remark two salient features: the linear increase of the mean conductance with  $N = kW/\pi$  and the fluctuations around the mean, which become larger as  $k$  increases. The linear increase of  $\langle T \rangle$  with a slope given by the classical transmission coefficient agrees with the classical behavior discussed in the previous section. The increase of the fluctuations obtained within the semiclassical approach is consistent with previous quantum computations [10]. The quantum mechanical calculations of Wirtz *et al.* [95] for a square cavity allowed to identified the peaks of the Fourier transform of the transmission amplitude with the families (or bundles) of classical trajectories contributing in the semiclassical expansion.

Unitarity, the mathematical translation of charge conservation, is a critical test for semiclassical approximations. Fig. 10 shows that it is relatively well respected, except at the opening of new modes, where we obtain diffraction peaks. The curve  $R+T$  has a slope of  $N$ , within an error of 5%. The departures from unitarity are smaller than

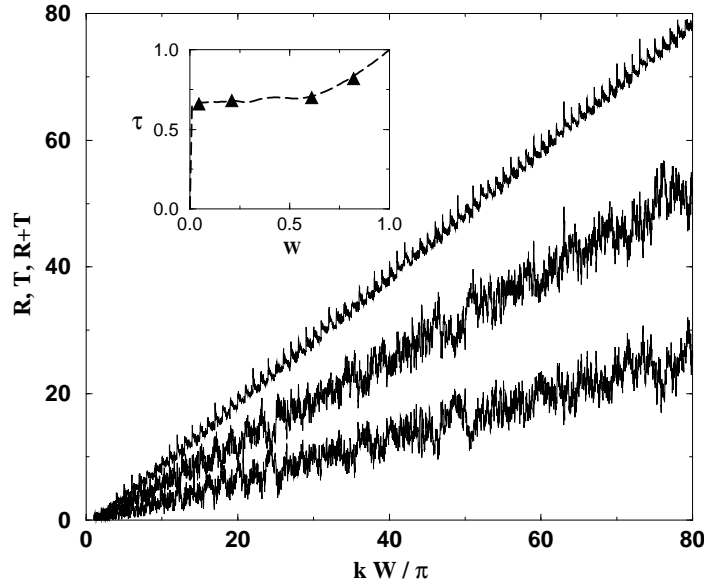


Fig. 10. – Reflection  $R$  (lower curve), transmission  $T$  (medium), and  $R+T$  (upper) for a square cavity as a function of wave-vector for an opening of  $W = 0.05$  (in units of the size of the square). Inset: classical transmission probability as a function of  $W$  from the slope of  $T(k)$  (triangles) and from Eq. (2.25) (dashed).

the fluctuations, therefore it is justified to approach the latter with our semiclassical methods.

**3.4. Mean conductance in a square cavity.** – Our semiclassical approach can be further simplified in order to render the calculations analytically tractable. The function  $\Delta_n(x)$  defined in Eq. (3.12) is peaked for  $x = 0$  (when the quantized angles of the incoming and outgoing modes coincide with the angle of the trajectory) and decays on the scale of  $W/\delta_n$ , therefore it can be approximated by the rectangular function

$$(3.13) \quad \Pi_n(x) = \begin{cases} \exp\left[i\varepsilon'_n \frac{\pi x}{2W} \delta_n\right], & \text{if } |x| < \frac{W}{2\delta_n}, \\ 0 & \text{otherwise.} \end{cases}$$

Thus, the semiclassical  $t_{ba}$  simplifies to:

$$(3.14) \quad t_{ba} = \frac{1}{W} \sqrt{\frac{\cos\theta_b}{\cos\theta_a}} \sum_n \Pi_n(a-b) \varepsilon_n \varepsilon'_n \delta_n \exp[ik\tilde{L}_n].$$

Within this approximation, the total transmission coefficient is expressed as a sum over pairs of families of trajectories (with odd  $p_n$  and  $p_{n'}$ ).

$$(3.15) \quad T = \frac{1}{W^2} \sum_{a,b=1}^N \frac{\cos \theta_b}{\cos \theta_a} \sum_{n,n'} \varepsilon_n \bar{\varepsilon}_{n'} \varepsilon'_n \varepsilon'_{n'} \delta_n \delta_{n'} \exp [ik(\tilde{L}_n - \tilde{L}_{n'})] \Pi_n(a-b) \bar{\Pi}_{n'}(a-b) .$$

The secular behavior of the transmission coefficient can be obtained from the  $k$ -average of  $T(k)/k$ , leading to the diagonal approximation between the families of trajectories ( $n = n'$ ). In the case of isolated trajectories, the diagonal approximation yielded the classical probability of transmission by pairing individual trajectories. In the present case, the concept of families of trajectories replaces the role of individual trajectories. Inserting the definition of the function  $\Pi$ , we find (to leading order in  $kW/\pi$ )

$$(3.16) \quad \langle T \rangle \simeq \frac{1}{W^2} \sum_{a=1}^N \sum_n \delta_n^2 \left( \sum_{b=b_{min}}^{b_{max}} \frac{\cos \theta_b}{\cos \theta_a} \right) ,$$

$b_{min} = \max \{a - W/2\delta_n, 1\}$  and  $b_{max} = \min \{a + W/2\delta_n, N\}$ . In the classical limit of  $N = kW/\pi \gg 1$  the sum over  $b$  can be approximated by an integral leading to

$$(3.17) \quad \langle T \rangle \simeq \sum_{a=1}^N \sum_n \frac{\delta_n}{W} .$$

For each mode  $a$  we have simply obtained the total weight of trajectories contributing to transmission. Converting also the sum over  $a$  into an integral we write

$$(3.18) \quad \langle T \rangle \simeq \frac{kW}{\pi} \mathcal{T} \quad , \quad \mathcal{T} = \int_0^{\pi/2} d\theta \cos \theta \sum_n \frac{\delta_n}{W} .$$

Thus, the total transmission coefficient is proportional to the number of modes, and the constant  $\mathcal{T}$  is a purely geometric factor. Breaking the contribution of families into that of individual trajectories we are left with the usual classical transmission probability (2.25).

In the inset of Fig. 10 we compare the mean slope in the numerical (semiclassical) results (triangles) with the classical transmission probability  $\mathcal{T}$  obtained from Eq. (2.25) by sampling the space of classical trajectories with random choices of initial conditions  $\theta$  and  $y$  (dashed). We verify the good agreement between the two approaches and we see that  $\mathcal{T}$  remains almost constant over a large interval of variation of the opening. A more efficient path to  $\mathcal{T}$  than Eq. (2.25) is to sample the angles  $\theta$  and to incorporate the weights  $\delta_n$  emerging from the intermediate fractions of  $1/\tan \theta$ , as suggested by Eq. (3.18). We then see that the continued fraction approach is not only useful for evaluating semiclassical effects, but also for classical properties like the transmission

coefficient (and also the length distribution). Random sampling of classical trajectories is an appropriate procedure for chaotic structures, where the ergodicity of phase space results in an exponential distribution of lengths. On the other hand, integrable cavities exhibit power-law distributions, which are more difficult to obtain by trajectory sampling. In this case, the continued fraction approach is very efficient since, for a given angle, only a finite number of terms are relevant, and the contributing families are incorporated at once according to their weight.

**3.5. Conductance fluctuations in a square cavity.** – As visible from Fig. 10, the oscillations around the mean transmission coefficient grow with larger  $N$ . We will now evaluate the local fluctuations  $\langle(\delta T)^2\rangle = \langle(T - [(kW/\pi)\mathcal{T} + \langle\delta T\rangle])^2\rangle$ . We begin with the simplified expression (3.15) of  $T$ , and write

$$(3.19) \quad T^2 = \frac{1}{W^4} \sum_{a,b,a',b'=1}^N \frac{\cos\theta_b \cos\theta_{b'}}{\cos\theta_a \cos\theta_{a'}} \sum_{n,n',n'',n'''} \varepsilon_n \bar{\varepsilon}_{n'} \varepsilon_{n''} \bar{\varepsilon}_{n'''} \varepsilon'_n \bar{\varepsilon}'_{n'} \varepsilon'_{n''} \bar{\varepsilon}'_{n'''} \delta_n \delta_{n'} \delta_{n''} \delta_{n'''} \\ \exp \left[ ik(\tilde{L}_n - \tilde{L}_{n'} + \tilde{L}_{n''} - \tilde{L}_{n'''}) \right] \Pi_n(a-b) \bar{\Pi}_{n'}(a-b) \Pi_{n''}(a'-b') \bar{\Pi}_{n'''}(a'-b') .$$

As before, we only consider the terms having a null phase, for which

$$(3.20) \quad \tilde{L}_n - \tilde{L}_{n'} + \tilde{L}_{n''} - \tilde{L}_{n'''} = 0 .$$

This condition is satisfied with the pairing  $\tilde{L}_n = \tilde{L}_{n'}$  and  $\tilde{L}_{n''} = \tilde{L}_{n'''}$ , but the resulting term cancels against the square of the average transmission coefficient. A non trivial pairing is obtained when  $\tilde{L}_n = \tilde{L}_{n'''}$  and  $\tilde{L}_{n'} = \tilde{L}_{n''}$  with  $\tilde{L}_n \neq \tilde{L}_{n'}$ , which implies  $a = a'$ . The contribution of this pairing to the local fluctuations is

$$(3.21) \quad \langle(\delta T)^2\rangle_I = \frac{1}{W^4} \sum_{a=1}^N \sum_{b,b'=1}^N \frac{\cos\theta_b \cos\theta_{b'}}{\cos^2\theta_a} \sum_{n,n'} \Pi_n(a-b) \bar{\Pi}_{n'}(a-b) \Pi_{n'}(a-b') \bar{\Pi}_n(a-b') \delta_n^2 \delta_{n'}^2 \\ = \frac{1}{W^4} \sum_{a=1}^N \sum_{n,n'} \left( \min \left\{ \frac{W}{\delta_n}, \frac{W}{\delta_{n'}} \right\} \right)^2 \delta_n^2 \delta_{n'}^2 .$$

In the semiclassical limit the sum over  $a$  can be converted into an integral dictating a linear behavior of  $\langle(\delta T)^2\rangle_I$  with respect to  $k$ .

The two pairings above described are those usually considered in dealing with chaotic cavities, except that in such cases we take individual trajectories instead families. In the integrable system we are studying there is another non trivial way of satisfying Eq. (3.20), that is,  $\tilde{L}_n - \tilde{L}_{n'} = \tilde{L}_{n''} - \tilde{L}_{n'''}$ , with  $\tilde{L}_n \neq \tilde{L}_{n'}$  and  $\tilde{L}_n \neq \tilde{L}_{n''}$ . This typically happens when  $n, n', n'',$  and  $n'''$  belong to the same ( $m$ -th) Farey sequence and they are respectively associated with the intermediate functions  $(p_m^{k+j}, q_m^{k+j}), (p_m^k, q_m^k), (p_m^{k'}, q_m^{k'}),$

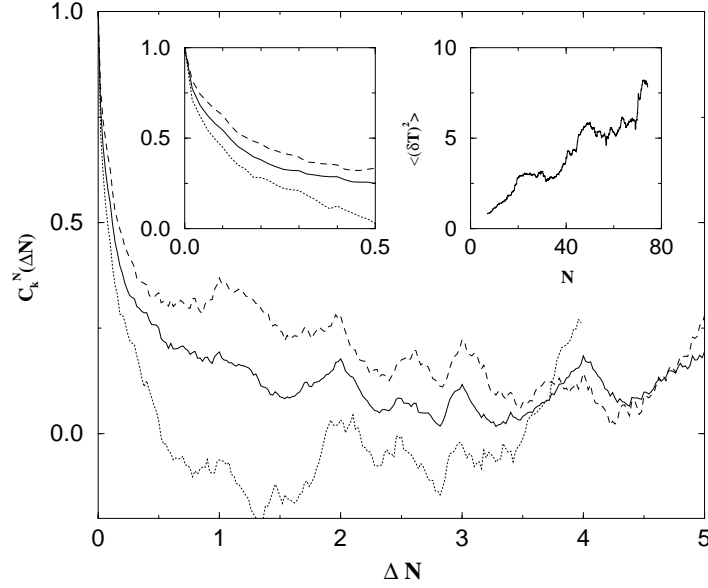


Fig. 11. – Correlation function locally normalized according to Eq. (3.23) for three  $N$ -intervals: 20-40 (dotted), 40-60 (solid), and 60-80 (dashed) with an opening  $W = 0.05$ . Left inset: blow up of the small  $\Delta N$  region showing a cusp at the origin. Right inset: local variance  $\langle(\delta T)^2(k)\rangle$  exhibiting a linear increase with  $N = kW/\pi$ .

and  $(p_m^{k'+j}, q_m^{k'+j})$ , with  $k \neq k'$ ,  $j \neq 0$  and  $k, k', k+j, k'+j \in (0, a_m)$ . Also, since we are dealing with transmission coefficients, we need  $p_m^k, p_m^{k'}, p_m^{k+j}$  and  $p_m^{k'+j}$  to be odd, which implies that if  $j$  is odd,  $P_{m-1}$  must be even. Under such conditions, we have  $\tilde{L}_n - \tilde{L}_{n'} = j(P_{m-1} \cos \theta_a + Q_{m-1} \sin \theta_a)$ . If neither  $n$  nor  $n'$  correspond to the first family of the sequence ( $k, k' \neq 0$ ) the four exiting intervals have the same length  $\delta_m = |P_{m-1} \tan \theta - Q_{m-1}|$ .

This last contribution to the local fluctuations can be expressed as a sum over the convergents

$$(3.22) \quad \langle(\delta T)^2\rangle_{II} = \sum_{a=1}^N \sum_m \sum_{k, k'=0}^{a_m} \sum_j \frac{\delta_m^2}{W^2},$$

with the above specified restrictions for  $k, k'$  and  $j$ . As in the previous case, converting the sum over  $a$  into an integral yields a contribution  $\langle(\delta T)^2\rangle_{II}$  to the local fluctuations that is linear in  $k$ , with a purely geometrical coefficient given by the continued fraction representation of  $1/\tan \theta$ .

The linearity of  $\langle(\delta T)^2\rangle = \langle(\delta T)^2\rangle_I + \langle(\delta T)^2\rangle_{II}$  with  $k$  that we have demonstrated is consistent with the numerical results of Fig. 11 (right inset).

The conductance fluctuations of chaotic cavities are characterized by two  $k$ -independent parameters: the correlation length  $\gamma_{cl}$  and the variance  $\langle(\delta T)^2\rangle$ . In our integrable cavity we have seen that  $\langle(\delta T)^2\rangle$  is not universal, but energy dependent. Also, there does not exist a characteristic time for exiting the cavity. Therefore it is not obvious that a correlation function depending only on the energy (or momentum) increment can be defined. That is why we consider the normalized correlation function

$$(3.23) \quad C_k^N(\Delta k) = \frac{\langle\delta T(k+\Delta k)\delta T(k)\rangle}{\langle(\delta T)^2(k)\rangle},$$

where  $k$  varies on an interval much larger than  $\Delta k$ , but small enough to neglect secular variations.

From Eqs. (3.23) and (3.11) we obtain numerically the correlation functions shown in Fig. 11 for three  $N$ -intervals: 20-40 (dotted), 40-60 (solid), and 60-80 (dashed). A singularity for small  $\Delta k$  appears in all the  $N$ -intervals in the form of a cusp around the origin (inset). The linear behavior of  $C(\Delta k)$  is to be contrasted to the Lorentzian correlation function expected for a chaotic cavity. It agrees with the prediction of Ref. [68] and it is consistent with quantum calculations yielding decay of the power spectrum as  $x^{-2}$  at large  $x$  (see Fig. 6 and Ref. [10]).

We have seen an example of an open system with integrable dynamics exhibiting larger fluctuations than those of the chaotic case. The situation is analogous to the density of states of closed systems, which is characterized by stronger fluctuations in integrable than in chaotic geometries. The augmented fluctuations in *integrable closed and open* geometries can be traced to the same origin: *the bunching of trajectories into families* in the semiclassical expansions, the Berry-Tabor formula and Eq. (3.11) respectively.

The unbounded fluctuations we have found are unlikely to be experimentally detected in Mesoscopic Physics. It is a very small effect that necessitates a range of variation of  $N$  much larger than what is normally achieved [30, 37, 38]. Also, the cusp of the correlation function at the origin is related with very long trajectories, that may be longer than our physical cut offs. The case of the square is rather special among integrable systems since the conserved quantities of the cavity are the same as in the leads. Therefore, the geometry of the leads plays a very important role [34, 38] and renders the quantum signatures of integrability in open systems quite involved.

**3.6. Circular billiards, diffraction and tunneling.** – The circular billiard is particularly interesting because it has been realized experimentally [8, 9, 32, 35, 37], and it is an integrable geometry where the semiclassical transmission amplitude (2.16) is applicable since the contributing trajectories are isolated. Also, the proliferation of trajectories with the maximum number of bounces considered is much weaker than for the chaotic case, making the explicit summation of Eq. (2.16) much easier. Lin and Jensen [86] undertook such a calculation considering trajectories up to 100 bounces. As expected, going into



the semiclassical limit by increasing the number of modes  $N$  results in a better fulfillment of the unitarity condition  $T+R=N$  (only a 1% deviation for  $N=20$ ). Moreover, they demonstrated that the coherent backscattering is significantly reduced by off-diagonal contributions to the total reflection, and they obtained conductance fluctuations as a function of energy with high degree of regularity.

The signature of classical trajectories in the numerically obtained quantum transmission amplitudes has been established for circular billiards [87, 88, 50]. In particular, the Fourier transform of the transmission amplitudes shows strong peaks for lengths corresponding to the classical trajectories contributing in the semiclassical expansion (2.16). Since the injection angle depends on  $k$ , a given trajectory contributes only over a limited energy range. This is why in geometries with stable trajectories, like the circle, the Fourier peaks are more pronounced than for the stadium billiard. It has also been shown in Ref. [87] that  $\langle(\delta T)^2\rangle$  increases with  $k$ , consistently with the behavior found in the last chapter for another integrable case (the square).

Diffraction effects become important when the number of incoming modes  $N$  is small. The semiclassical approach we have presented can be generalized to include diffraction effects in the transmission and reflection amplitudes [89]. In the extreme limit of  $N=1$ , the wave-front impinging into the cavity is approximately circular and has the entering lead as the source. The semiclassical propagation of this wave-front can be built from classical trajectories launched from the center of the lead in all directions [88]. The resulting expansion reproduces, at the level of Fourier transforms, rather well the exact quantum mechanical data in the case of a circular billiard. Some of the harmonics of the quantum reflection amplitude do not correspond to classical trajectories, but to “ghost paths”, or diffractive trajectories (like reflections off the mouth of an exiting lead), that can be incorporated in an approximate way in this previous semiclassical formalism.

In Fig. 12 we present the correspondence between peaks in the squared modulus  $\mathcal{R}_{11}(L)$  of the Fourier transform of  $r_{11}(k)$  and the classical trajectories (including their repetitions) contributing to (2.16), established in Refs. [87, 88, 50], for the circular billiard of the inset. The first peak is not a classical trajectory contributing to reflection, but corresponds to diffraction off the lead mouths [87, 88]. This effect can be interpreted in terms of a trajectory that gets reflected back at the right lead (ghost path). For larger lengths  $L$ , we can identify a triangular path, a five-star path, a seven-star path, and so on. Since we are considering  $r_{11}$ , and since the angular momentum is conserved, the outgoing angle is opposite to the incoming one, and the transport trajectories tend to coincide with periodic orbits.

Placing a sufficiently high barrier into the cavity considerably changes the reflection amplitude and  $\mathcal{R}_{11}$  (panel b); some of the peaks are reduced, other augmented, and new length scales appear. Some of the new peaks are related with diffractions induced by the barrier. Interestingly enough, the dependence of the peak amplitudes is not monotonic with the strength of the barrier. This behavior is well described by a simple modification of Eq. (2.16) where each contribution is affected by the tunneling amplitude of a two-dimensional plane-wave encountering a barrier of infinite length [50].

It is important to note that the straightforward identification of classical trajectories in

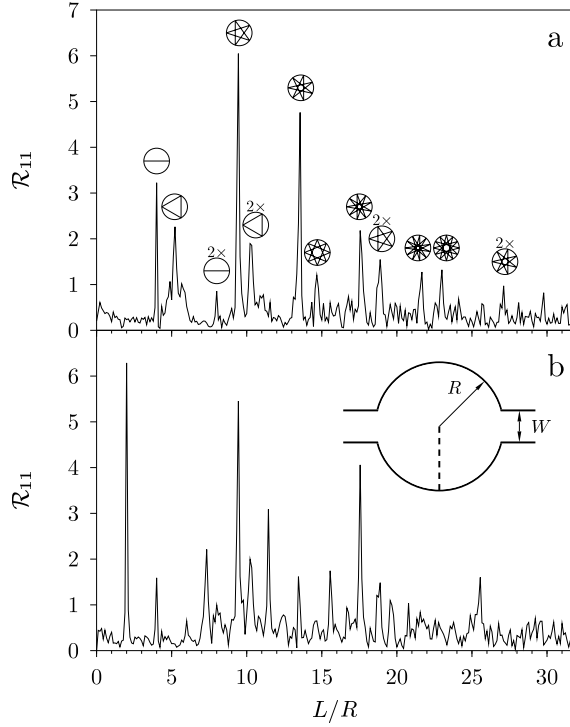


Fig. 12. – Length spectrum  $\mathcal{R}_{11}$  (magnitude squared of the Fourier transform of  $r_{11}(k)$ ) for the circular billiard of the inset. (a) the case without a barrier, (b) with a thin and infinitely high barrier (shown as the dashed line reaching from the edge to the center of the circle). Lengths are scaled to the radius  $R$  of the circle. In the absence of a barrier we identify the peaks in the length spectrum with periodic trajectories. (From Ref. [50].)

the quantum calculations is always at the level of transmission and reflection amplitudes. For the transmission and reflection coefficients, the identification is more problematic since we deal with pairs of trajectories, and the Fourier transforms yield differences of lengths.

#### 4. – Experiments on ballistic transport and other aspects of the theory

In the two previous sections we developed the semiclassical theory of ballistic transport, studying conductance fluctuations and weak localization in chaotic and integrable cavities. Our emphasis was set in the signatures of the underlying classical mechanics, but we did not discuss in detail the actual experimental work. We intend to provide here a brief description of the experimental results relevant in the development and testing of the theory. (For reviews on experiments in ballistic transport see Refs. [9, 13, 98].) The initial application of Quantum Chaos ideas in transport through ballistic cavities was followed by work in different regimes, other systems, and also the development of new theoretical tools. Without attempting to review such developments, we briefly discuss in this section the regime of mixed dynamics, the semiclassical approach of Kubo conductivity applied to the antidot lattice, and the connection between semiclassics and the random matrix theory of ballistic transport.

*4.1. Conductance fluctuations and weak localization in ballistic microstructures.* – The statistical analysis of the low-temperature magnetoconductance in ballistic *GaAs/AlGaAs* quantum dots was first performed by Marcus and collaborators [8, 9]. Different shapes (stadium and circle) with steep-walled confining potentials were achieved and the leads were oriented at right angles to reduce transmission via direct trajectories. The transport mean free path was estimated to be several times the size of the structures ( $a \simeq 0.5\mu\text{m}$ ) indicating that the ballistic regime was achieved, and the number of conducting channels was  $N = 3$  (that is, not quite in the semiclassical limit of the theory). Analyzing the magnetoconductance as we did in (2'6) gave for the stadium cavities a power spectrum in agreement with Eq. (2.40) over three orders of magnitude, and a deviation for large areas was observed (as in the inset of Fig. 13.b). The conductance fluctuations in the circular billiard were more structured (more weight in the high harmonics of the power spectrum) compared with the case of the stadium, demonstrating experimentally the possibility of distinguishing ballistic cavities according to their classical dynamics.

The magnetic field scale of the fluctuations was found to be consistent with the semiclassical prediction, and increasing with the mean conductance through the dot [29]. In the completely coherent picture of Sec. 2, the parameter  $\alpha_{cl}$  governing the area distribution in a chaotic cavity was given by the geometry and the escape rate. A phenomenological way of introducing decoherence [99] is by attaching a virtual lead that draws no current but provides a channel for phase breaking. Taking into account the virtual lead in our description will increase the escape rate (proportionally to  $L_\Phi$ ), and then  $\alpha_{cl}$ . The measurement of the conductance fluctuations allowed to estimate the temperature dependence of  $L_\Phi$ , thus providing an example where the theoretical ideas of Quantum Chaos were used to test fundamental properties of condensed matter systems.

The systematic study of conductance fluctuations, and the measurement of the ballistic weak localization, require a considerable amount of averaging. A given magnetoconductance curve offers only a limited interval for averaging since once the cyclotron radius becomes comparable to the size of the structure the nature of the classical dynamics

may change. In order to cope with this problem, alternative types of averages have been developed: by tuning the Fermi energy [30, 38], by thermal cycling the sample [31, 34], by different realizations of the residual disorder in an array of identical cavities [32], and by small distortions in the shape of the cavity [33, 37].

Keller *et al.* [30] fabricated microstructures where the electron density (and hence  $k_F$ ) was tunable while maintaining the geometry approximately fixed. Different shapes were considered: a stadium with displaced leads, the “stomach” and a polygonal shape with stoppers (the last two shapes are shown in the insets of Fig. 6). In the chaotic cavities a good quantitative agreement with the semiclassical theories is obtained, with the scale of the fluctuations depending on the cavity size. The polygonal geometry did not show qualitative differences with the chaotic case, illustrating the difficulties of observing experimentally the signatures of integrable dynamics. The energy average yielded a weak-localization peak, and the conductance of a given sample did not always show a minimum at  $B=0$ , consistent with the lack of self average of ballistic cavities.

The use of sub-micron stadium-shaped quantum dots (with  $N$  up to 7) cycled at room temperature allowed Berry and collaborators [31] to obtain average values and separate the weak localization peak from the conductance fluctuations. The line-shape of the peak was found to be Lorentzian, in agreement with the semiclassical prediction. Moreover, the field scales of the weak localization and conductance fluctuations were found to be related by the factor of 2 that we discussed in (27), giving strong support to the applicability of the semiclassical approach.

Chang and collaborators [32] fabricated arrays of microstructures connected in parallel and considered two shapes: stadium and circle. In each case, the 48 cavities were nominally identical but actually slightly different due to uncontrollable shape distortions and residual disorder. Thus, the conductance fluctuations were averaged out. The weak localization peak was found to be Lorentzian for the stadium cavities and triangular for the circular ones, in agreement with the semiclassical prediction and detailed numerical calculations [11]. Rectangular cavities, however, failed to yield a cusp of the magnetoresistance at  $B=0$ .

Microstructures admitting small shape distortions (less than 5 % in the area) by tuning the voltage of lateral gates (inset of Fig. 13.a) were developed by Chan, Marcus collaborators [33]. The lithographic shape of the cavity is clearly non-chaotic, however it is expected that dot-specific features tend to average away by the effect of the shape distortions. Also, these are relatively large structures, where disorder definitely affects the long trajectories.  $N$  was not in the semiclassical regime, as it was tuned to a value of 2. Conductance can be studied as a function of magnetic field and shape distortion, allowing to gather very good statistics. The fluctuations as a function of magnetic field show very good agreement with Eq. (2.40) (inset of Fig. 13.b). The shape distortion fluctuations yield an exponential power spectrum, in agreement with the calculations of Bruus and Stone showing that the semiclassical formalism of Sec. 2 can be extended to this case [100]. A Lorentzian shape for the weak localization peak was obtained, with a width related to the characteristic field of the conductance fluctuations, as predicted by semiclassical theory. The magnitude of the shape fluctuations at non-zero field had a

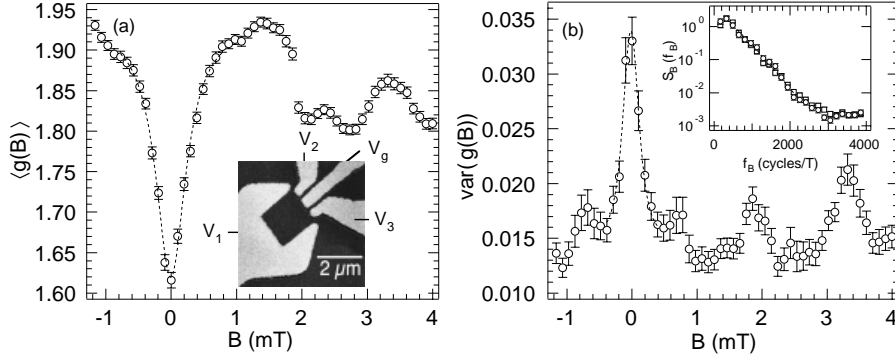


Fig. 13. – (a) Shape-averaged conductance showing a weak localization peak fitted to a Lorentzian (dashed). Inset: electron micrograph of device (the gate voltage  $V_g$  is used to produce shape distortion). (b) Variance of shape-distortion conductance fluctuations (in units of  $(e^2/h)^2$ ) Inset: power spectral density in magnetic field fitted by Eq.(2.40). (Adapted from Ref. [33].)

factor of 2 reduction with respect to the zero field value, and the line shape of  $\langle(\delta T)^2\rangle$  was found to be a Lorentzian squared [101]. The rich statistics that this type of structures allows to gather can be used to generate not only the moments of the conductance, but its whole distribution, and compare with the random matrix theory predictions [108, 109]. As we will see in the next chapter, the detailed study of the conductance distribution allows to estimate the coherence length [39]. Interestingly enough,  $L_\Phi$  seems to saturate below certain temperature (of the order of  $100 \text{ mK}$ ), in analogy with similar observations in disordered metals [102]

Bird and collaborators used thermal cycling on rectangular cavities to measure a weak localization peak that changes its shape from Lorentzian to triangular as the quantum point contacts at the entrance of the cavity are closed [34]. The transition occurs for  $N \simeq 2$  and demonstrates the non-trivial role played by the leads. Measurements and numerical analysis by Zozoulenko *et al.* [38] on square cavities suggested that, depending on the geometry of the leads, transport through the cavity is effectively mediated by just a few resonant levels, illustrating the importance of the injection conditions in the integrable case.

Lee, Faini and Mailly used shape and energy averages to extract the weak-localization peak of chaotic (stadia and stomach) and integrable (circles and rectangles) [37]. The former exhibited a Lorentzian line-shape, consistently with the theoretical predictions. However, among the integrable cavities, only the rectangle showed the expected triangular shape, while the circle yielded a Lorentzian. Chan has proposed [32] that this apparently discrepancy with his results is due to the shorter physical cut offs of Ref. [37], hindering long trajectories to exhibit the signatures of the integrable dynamics.

**4.2. Semiclassics vs. random matrix theory.** – In our discussion of ballistic weak localization (2.7) we stressed the fact that our semiclassical approach allows to calculate only one part of the effect, the elastic backscattering, corresponding to the interference of time-reversed trajectories in the diagonal reflection coefficients  $R_{aa}$ . Numerical calculations, as well as elementary considerations based on current conservation, show that the off-diagonal terms  $R_{ba}$  are also sensitive to a weak field. However, this  $B$ -dependence is not easily calculable within the diagonal semiclassical approximation of only keeping terms where we pair one trajectory with itself or with its time-symmetric. Moreover, the semiclassical results for the weak localization may depend on how we organize the sums. If instead of going through the approach developed in Sec. 2 of calculating transmission amplitudes and then the coherent backscattering, we calculate the average magnetoconductance effect directly from the real-space Green function, we obtain a vanishing result [103].

The problem that we face in calculating the magnitude of weak localization (or conductance fluctuations) arises from the fact that those are effects of order  $N^0$ , while semiclassics only assures the compliance of unitarity to leading order ( $N$ ). A complementary approach to semiclassics is that of random matrix theory (RMT), where we describe the ballistic transport through a chaotic cavity by its scattering matrix  $S$  (Eq. 2.6), and unitarity is automatically preserved by the condition  $SS^\dagger = I$ .

Random matrix approaches have been applied to a variety of physical problems, ranging from Nuclear Physics to level statistics in small quantum systems and conductance fluctuations in disordered mesoscopic conductors [42, 26, 16, 104, 105]. The basic assumption is that the relevant matrix is the most random among those verifying the required symmetries of the problem. The appropriate ensembles for unitary matrices are Dyson's COE and CUE (circular orthogonal and circular unitary) ensembles describing respectively the cases with ( $\beta = 1$ ) and without ( $\beta = 2$ ) time-reversal symmetry. For unitary matrices the eigenvalues are pure phases, and the random assumptions on the distribution of the matrices translate into the statistical properties of the eigenphases. Bümel and Smilansky proposed that chaotic scattering is represented by COE and CUE  $S$ -matrices, and derived statistical properties of the eigenphases from a semiclassical analysis [106].

Eigenphases are not directly related with transport properties, and therefore a parameterization of Dyson matrices in terms of conductance parameters needs to be established [107]. From that, the statistical properties of the conductance can be established. Without going through the derivations, we quote the results for the average conductance and the second moment [108, 109]

$$(4.1) \quad \langle T \rangle = \frac{1}{2}N + \langle \delta T \rangle \quad , \quad \langle \delta T \rangle = \frac{\beta - 2}{4\beta} \quad , \quad \langle (\delta T)^2 \rangle = \frac{1}{8\beta} .$$

The weak localization effect  $\Delta \langle T \rangle = \langle T \rangle_{\beta=1} - \langle T \rangle_{\beta=2} = -1/4$  can be shown to be the sum of a diagonal contribution ( $\sum_a \Delta \langle R_{aa} \rangle = 1/2$ ) and an off-diagonal contribution ( $\sum_{b \neq a} \Delta \langle R_{ba} \rangle = -1/4$ ), consistently with our results of (2.7).

RMT is able to predict not only the moments of the conductance, but the whole distribution in the case of small  $N$ . In particular, for  $N = 1$  the distribution is highly non-gaussian. The experimental quest for such peculiar distribution has led to the consideration of virtual leads, discussed in (4.1), and which can also be incorporated in a random matrix description [110, 111]. Determining experimentally the number of channels in the virtual leads has become a very useful way of estimating  $L_\Phi$  [39].

The random matrix hypothesis for the Hamiltonian of a chaotic dot (or the zero-dimensional non-linear sigma model) coupled to leads yields equivalent results to those of Eq. (4.1) [93, 94] and allows to calculate the crossover  $\beta = 1$  to  $\beta = 2$  as a function of magnetic field [101, 112, 105].

Unlike semiclassics, RMT is able to produce numerical values for the conductance fluctuations and weak localization. However, its applicability to ballistic cavities necessitates an ergodic behavior of classical trajectories. For instance, the existence of direct trajectories dramatically changes the previous values, and that is why the quantitative agreement of RMT and numerical simulations is only obtained in structures like the one at the bottom of Fig. 6, where the short-time scales were eliminated from the problem by introducing stoppers. Short-time process can be incorporated into the RMT approach [113, 114], but the formalism and its use becomes considerably less simple. Obviously, RMT is not of any help when dealing with cavities with integrable or mixed dynamics.

We therefore see that RMT and semiclassics are complementary techniques. The former immediately yields the universal behavior in the case of ergodic dynamics. The semiclassical diagonal approximation is applicable to a much wider range of classical behaviors, but it is not able to produce universal numbers. In addressing this failure we have to consider the possible breakdown of our two main assumptions: semiclassics and diagonal approximation. Similar questions arise in the study of the density-density correlator of closed systems, where standard semiclassics cannot recover the small energy (long time) quantum behavior. It has been suggested in this context that taking into account action correlations between very long trajectories may correct this failure of the diagonal semiclassical approximation [115]. In the context of ballistic transport, Argaman [116] pointed to the failure of the diagonal approximation for special pairs of long trajectories where the difference of actions does not vary enough in the integration interval. Similar arguments were presented by Aleiner and Larkin [117] separating the dynamics in scales shorter and longer than the Ehrenfest time. In the former the correlations of the disorder potential have to be taken into account, in the latter the classical diffusion equation can be used. Both approaches reproduce (under certain conditions of ergodicity and invoking the presence of a small amount of disorder) the universal values of Eq. (4.1), but they are not genuinely semiclassical in the sense of giving an operational prescription to handle a given geometry from the knowledge of the classical trajectories.

**4.3. Mixed dynamics.** – In our study of ballistic transport we have considered, so far, the extreme cases of hyperbolic and regular classical dynamics. Semiclassical theory predicts qualitative differences between these two cases, and the experiments seem to support these results. It is natural to ask about the behavior with a mixed phase space

containing both chaotic and regular regions. This is the most generic situation for a dynamical system, and since the microstructures do not have hard-walls potentials, it is experimentally relevant too.

Ketzmerick considered the problem of a dynamical system with mixed phase space [118], where the trapping generated by the infinite hierarchy of cantori leads to a power-law for the escape rate of the cavity  $P(\tau) \propto t^{-\beta}$ , with the exponent  $\beta > 1$ . From a semiclassical diagonal approximation to the conductance, Ketzmerick proposed that the graph of  $g$  vs.  $E$  has (in the case  $\beta < 2$ ) the statistical properties of fractional Brownian motion with fractal dimension  $D = 2 - \beta/2$ .

Numerical simulations by Huckestein and collaborators [119] in cavities with mixed dynamics connected to leads yielded the power-law distribution of the classical escape rate, but the quantum curve  $g(E)$  failed to exhibit fractal behavior. On the other hand, Casati and collaborators [120] obtained a fractal structure for the survival probability in an open quantum system classically described by a map with mixed phase space.

These unsettled theoretical issues illustrate the difficulties of describing generic Hamiltonian systems, and are particularly interesting given the recent experiments of Sachrajda *et al* [40]. The conductance fluctuations measured in soft-wall stadium and Sinai billiards exhibited fractal behavior in the curves  $g(B)$  over two orders of magnitude in magnetic field. Normally, we would have expected to be more difficult to observe the fractal behavior in experiment than in the simulations, since the physical cut-offs discussed in the introduction will limit the scale that can be resolved in phase space.

**4.4. Semiclassical approach to bulk conductivity.** – In Sec. 2 we mentioned that the Landauer formulation of the conductance could be obtained from linear response (Kubo formula) theory. The latter is given in terms of matrix elements of the current operator. The semiclassical approximation for matrix elements [121] and the consistent use of stationary-phase integrations can be then used to yield a semiclassical expression for the longitudinal conductivity as the sum over classical (Drude) component [122] and an oscillatory component [123, 124]. The latter is given by a periodic orbit expansion where the coefficients of the trace formula are affected by the classical correlator of the longitudinal component of the velocity along the trajectory. This approach has been very helpful to understand the classical and quantum oscillations of the magnetoconductivity in antidot lattices [125]. This formulation needs the incorporation of a small amount of disorder to produce a finite conductivity and has the drawback of not being able to yield a weak localization effect (since it is given as an expansion over *single* orbits). Even if the Kubo and Landauer approaches for the conductance give equivalent results at the quantum mechanically, such a connection has not been established at the semiclassical level. As discussed in (4.2) the difficulty arises from the lack of unitarity of the semiclassical approximations that we have described.



## 5. – Orbital magnetism in clean systems

The problem of orbital magnetism in an electron gas has a long history, going back to the pioneering work of Landau demonstrating the existence of a small diamagnetic response at weak fields  $H$  and low temperatures  $T$  (such that  $k_B T$  exceeds the typical spacing  $\hbar\omega$ ,  $\omega = eH/mc$ ) [126, 127]. The orbital response of a non-interacting 2DEG has a small diamagnetic value

$$(5.1) \quad -\chi_L = -\frac{g_s e^2}{24\pi m c^2}$$

( $g_s = 2$  is the spin degeneracy factor). The constriction of the electron gas (2D or 3D) to a finite region (area of volume) introduces a new energy scale in the problem (the typical level spacing  $\Delta$ ) leading to a modification of the Landau susceptibility. The finite-size corrections to the Landau susceptibility have received considerable attention; various geometries and physical regimes have been studied [14, 128]. We are interested in the orbital response of ballistic microstructures, as measured in the experiments of Refs. [27, 28]. We will show that semiclassical methods, similar to those used in the previous sections, allow us to undertake such studies [51, 52]. Moreover, the differences arising from the nature of the classical dynamics turn out to be more important than in the case of transport.

The magnetic susceptibility is a thermodynamical property and it is sensitive to the effect disorder and interactions. In this section we start with the simplest model of non-interacting electrons in a clean cavity. In the following sections we will incorporate the effect of residual disorder and electron-electron interaction.

**5.1. Thermodynamic Formalism.** – For a system of electrons in an area  $A$ , connected to a reservoir of chemical potential  $\mu$ , the magnetic susceptibility is defined by

$$(5.2) \quad \chi^{\text{GC}} = -\frac{1}{A} \left( \frac{\partial^2 \Omega}{\partial H^2} \right)_{T, \mu} .$$

The notation with the superscript GC is used in order to emphasize the fact that we are working in the grand canonical ensemble.

$$(5.3) \quad \Omega(T, H, \mu) = \Omega_0(T, H, \mu) + \Omega_i(T, H, \mu)$$

is the thermodynamic potential, decomposed in a non-interacting part

$$(5.4) \quad \Omega_0(T, H, \mu) = -\frac{1}{\beta} \int dE d(E) \ln[1 + \exp(\beta(\mu - E))]$$

depending on the one-particle density of states  $d(E)$  ( $\beta = 1/k_B T$ ) and the term  $\Omega_i$  arising from electron-electron interactions [129, 130]. We will not consider this last contribution until Sec. 7.

The choice of the ensemble in the macroscopic limit of the area  $A$  and the number of particles  $\mathbf{N}$  going to infinity is a matter of convenience. As it was recognized in the context of persistent currents in disordered rings [131, 19, 132], the equivalence between the ensembles may break down in the mesoscopic regime. Although the number of electrons can be large for a mesoscopic system, the fact that  $\mathbf{N}$  is fixed must be taken into account (by working in the canonical formalism) if a disorder or energy averaged susceptibility of an *ensemble* of isolated micro-systems is examined.

The magnetic susceptibility of a system of  $\mathbf{N}$  electrons is

$$(5.5) \quad \chi = -\frac{1}{A} \left( \frac{\partial^2 F}{\partial H^2} \right)_{T, \mathbf{N}} ,$$

with the free energy  $F$  and the thermodynamical potential  $\Omega$  are related by means of the Legendre transform

$$(5.6) \quad F(T, H, \mathbf{N}) = \mu \mathbf{N} + \Omega(T, H, \mu) .$$

In Condensed Matter Physics the simple dependence of the thermodynamical potential on the density of states in (5.4) makes the grand canonical ensemble the easiest to work with. In the case of disordered metals, in which the density of states (DOS) can be separated in a smooth and a (small) fluctuating part, Imry proposed convenient representation for the canonical free energy in terms of grand canonical quantities [19]. In our clean case we use the decomposition

$$(5.7) \quad d(E) = \bar{d}(E) + d^{\text{osc}}(E)$$

in the mean (or Weyl) part  $\bar{d}$  and the periodic orbit contribution  $d^{\text{osc}}$ . (Rigorously speaking,  $d^{\text{osc}}$  is not small since it is the sum of delta functions, therefore the expansion (5.7) has to be used after some thermal broadening [14].) We define a mean chemical potential  $\bar{\mu}$  as the one that accommodates the  $\mathbf{N}$  particles with the mean DOS  $\bar{d}$ .

$$(5.8) \quad \mathbf{N} = N(\mu) = \bar{N}(\bar{\mu}) .$$

Here

$$(5.9) \quad N(\mu) = \int_0^\infty dE d(E) f(E - \mu)$$

with the Fermi distribution function

$$(5.10) \quad f(E - \mu) = \frac{1}{1 + \exp[\beta(E - \mu)]} .$$

$\bar{N}$  is then obtained in Eq. (5.9) by replacing  $d(E)$  by  $\bar{d}(E)$ . Expanding (5.6) to second order in  $\mu - \bar{\mu}$  leads to an expansion of the free energy in terms of grand canonical quantities [132, 19]

$$(5.11) \quad F(\mathbf{N}) \simeq F^0 + \Delta F^{(1)} + \Delta F^{(2)} ,$$

with

$$(5.12a) \quad F^0 = \bar{\mu}\mathbf{N} + \bar{\Omega}(\bar{\mu}) ,$$

$$(5.12b) \quad \Delta F^{(1)} = \Omega^{\text{osc}}(\bar{\mu}) ,$$

$$(5.12c) \quad \Delta F^{(2)} = \frac{1}{2\bar{d}(\bar{\mu})} (N^{\text{osc}}(\bar{\mu}))^2 .$$

The functions  $\Omega^{\text{osc}}$  and  $N^{\text{osc}}$  are expressed by means of Eqs. (5.4) and (5.9), respectively, upon inserting the oscillating part  $d^{\text{osc}}$  of the density of states. The leading order contribution to  $F$  is given by the first two terms  $F^0 + \Delta F^{(1)}$  yielding the susceptibility calculated in the *grand* canonical case with the chemical potential  $\bar{\mu}$ .  $F^0$  gives rise to the diamagnetic Landau-susceptibility ( $-\chi_L$ ) independently of the confining geometry [133, 134, 14]. We will show that, as in the case of persistent currents, the average value of  $\Delta F^{(1)}$  vanishes and the additional term  $\Delta F^{(2)}$  becomes the dominant one.

**5.2. Semiclassical treatment of susceptibilities.** – For a semiclassical computation of  $\Delta F^{(1)}$  and  $\Delta F^{(2)}$  and their derivatives respect to  $H$  we calculate  $d^{\text{osc}}(E, H)$  from the trace

$$(5.13) \quad d(E, H) = -\frac{\mathbf{g}_s}{\pi} \text{Im} \int d\mathbf{r} G(\mathbf{r}, \mathbf{r}; E)$$

of the semiclassical one-particle Green function (Eq. (2.11)). Its contribution to  $d^{\text{osc}}(E)$  is given by all classical paths  $s$  (of non-zero length) joining  $\mathbf{r}$  to  $\mathbf{r}'$  at energy  $E$  [4, 43].

The evaluation of the trace integral (5.13) for chaotic and integrable systems leads to the Gutzwiller [4] and Berry-Tabor [85] periodic-orbit trace formulas, respectively. In order to calculate the magnetic susceptibility at small fields one has to carefully distinguish [14] between the three possibilities: a chaotic billiard, the special case of an integrable billiard remaining integrable upon inclusion of the  $H$ -field, and the more general case where the field acts as a perturbation breaking the integrability of a regular

structure. We start this section with the last situation, focusing on the experimentally relevant case of ballistic squares [27] and we later discuss chaotic and circular cavities.

For a generic integrable system (a *regular* geometry) any perturbation breaks the integrability of the dynamics. The Poincaré–Birkhoff theorem [57] states that as soon as the magnetic field is turned on, all resonant tori (*i.e.* all families of periodic orbits) are instantaneously broken, leaving only two isolated periodic orbits (one stable and one unstable). Therefore, neither Gutzwiller nor Berry–Tabor trace formulas are directly applicable and a uniform treatment of the perturbing  $H$ -field is necessary [3]. In the integrable zero-field limit each closed trajectory belongs to a torus  $I_{\mathbf{M}}$  and we can replace  $\mathbf{r}$  in the trace integral (5.13) by angle coordinates  $\Theta_1$  specifying the trajectory within the (one-parameter) family and by the position  $\Theta_2$  on the trajectory. For small magnetic field the classical orbits can be treated as essentially unaffected while the field acts merely on the phases in the Green function in terms of the magnetic flux through the area  $\mathcal{A}_{\mathbf{M}}(\Theta_1)$  enclosed by each orbit of family  $\mathbf{M}$ . Evaluating the trace integral along  $\Theta_2$  for the semiclassical Green function of an integrable system leads in this approximation to a factorization of the density of states

$$(5.14) \quad d^{\text{osc}}(E) = \sum_{\mathbf{M} \neq 0} \mathcal{C}_{\mathbf{M}}(H) d_{\mathbf{M}}^0(E)$$

into the contribution from the integrable zero-field limit

$$(5.15) \quad d_{\mathbf{M}}^0(E) = B_{\mathbf{M}} \cos \left( k_F L_{\mathbf{M}} - \nu_{\mathbf{M}} \frac{\pi}{2} - \frac{\pi}{4} \right)$$

( $L_{\mathbf{M}}$  and  $\nu_{\mathbf{M}}$  are respectively the length and Maslov index of the orbits of family  $\mathbf{M}$  and  $B_{\mathbf{M}}$  is the semiclassical weight [85]) and the function

$$(5.16) \quad \mathcal{C}_{\mathbf{M}}(H) = \frac{1}{2\pi} \int_0^{2\pi} d\Theta_1 \cos \left[ 2\pi \frac{H \mathcal{A}_{\mathbf{M}}(\Theta_1)}{\Phi_0} \right]$$

containing the  $H$ -field dependence ( $\Phi_0 = hc/e$ ). Calculating  $\Delta F^{(1)}$  from Eq. (5.12b) and taking the derivatives respect to  $H$  gives the grand canonical contribution to the susceptibility at small magnetic field

$$(5.17) \quad \frac{\chi^{(1)}}{\chi_L} = -\frac{24\pi}{\mathbf{g}_s} mA \left( \frac{\Phi_0}{2\pi A} \right)^2 \sum_{\mathbf{M}} \frac{R_T(\tau_{\mathbf{M}})}{\tau_{\mathbf{M}}^2} d_{\mathbf{M}}^0(\bar{\mu}) \frac{d^2 \mathcal{C}_{\mathbf{M}}}{dH^2}.$$

Here,  $\tau_{\mathbf{M}}$  is the period of a closed orbit of family  $\mathbf{M}$  and

$$(5.18) \quad R_T(\tau) = \frac{\tau/\tau_T}{\sinh(\tau/\tau_T)} \quad ; \quad \tau_T = \frac{\hbar\beta}{\pi} = \frac{L_T}{v_F}.$$

is a damping factor which arises from the convolution integral in Eq. (5.4) and gives an exponential suppression of long orbits according to the temperature dependent cut off  $\tau_T$  (or  $L_T$ ). As discussed in the introduction, this physical cutoff is important from a physical as well as computational point of view, as conceptual difficulties associated with the questions of absolute convergence of semiclassical expansions at zero temperature do not arise.

Eq. (5.17) is the basic equation for the susceptibility of an individual microstructure. When considering ensembles of ballistic microstructures however, an average ( $\overline{\quad}$ ) over Fermi energy ( $\mu = \hbar^2 k_F^2/2m$ ) or over the system size  $a$  has to be performed since there will usually be a dispersion of  $k_F$  and  $a$  among the members of the experimental ensemble. These averages lead to variations in the phases  $k_F L_{\mathbf{M}}$  of the DOS (5.15) which are much larger than  $2\pi$ . Therefore,  $\chi^{(1)}$  vanishes upon ensemble average. In order to characterize the orbital magnetism of ensembles we introduce the *typical* susceptibility  $\chi^{(t)} = (\overline{\chi^2})^{1/2}$  (the width of the distribution) and the ensemble averaged  $\overline{\chi}$  (its mean value, which is non-zero because of the *positive* term  $\Delta F^{(2)}$  in the expansion (5.11)).

If we assume that there are no degeneracies in the lengths of orbits from different families  $\mathbf{M}$  we obtain for  $\chi^{(t)}$

$$(5.19) \quad \left(\frac{\chi^{(t)}}{\chi_L}\right)^2 = \left(\frac{24\pi}{g_s} mA\right)^2 \left(\frac{\Phi_0}{2\pi A}\right)^4 \sum_{\mathbf{M}} \frac{R_T^2(\tau_{\mathbf{M}})}{\tau_{\mathbf{M}}^4} \overline{d_{\mathbf{M}}^0(\bar{\mu})^2} \left(\frac{d^2 C_{\mathbf{M}}}{dH^2}\right)^2.$$

In calculating  $\overline{\chi}$ , the grand canonical contribution  $\chi^{(1)}$  from  $\Delta F^{(1)}$  vanishes under energy average and the semiclassical approximation to the canonical correction  $\Delta F^{(2)}$  (Eq. (5.12c)) yields

$$(5.20) \quad \frac{\overline{\chi}}{\chi_L} \simeq \frac{\overline{\chi^{(2)}}}{\chi_L} = -\frac{24\pi^2}{g_s^2} \hbar^2 \left(\frac{\Phi_0}{2\pi A}\right)^2 \sum_{\mathbf{M}} \frac{R_T^2(\tau_{\mathbf{M}})}{\tau_{\mathbf{M}}^2} \overline{d_{\mathbf{M}}^0(\bar{\mu})^2} \frac{d^2 C_{\mathbf{M}}^2}{dH^2}.$$

Eqs. (5.17)–(5.20) provide the general starting point for a computation of the susceptibility of integrable billiards at small fields.

**5.3. Square billiards.** – In a square billiard each family of periodic orbits can be labeled by  $\mathbf{M} = (M_x, M_y)$  where  $M_x$  and  $M_y$  are the number of bounces occurring on the bottom and left side of the billiard. The length of the periodic orbits for all members of a family is  $L_{\mathbf{M}} = 2a(M_x^2 + M_y^2)^{1/2}$  and  $B_{\mathbf{M}} = m/\sqrt{\hbar k L_{\mathbf{M}}}$ . Since  $\nu_{\mathbf{M}} = 4(M_x + M_y)$  the Maslov index will be omitted from now on. The advantage of the square geometry, from the calculational point of view, is that as in (3.2), we can work in the extended space and use the free form of the Green function.

In the inset of Fig. 14 we represent a trajectory of the family  $\mathbf{M} = (1,1)$  of the shortest flux-enclosing periodic orbits. Instead of  $\Theta_1$  we use the lower reflection point  $x_0$  as orbit parameterization within the family. The orbits (1,1) have the unique length  $L_{11} = 2\sqrt{2}a$  and enclose a normalized area  $\mathcal{A}(x_0) = 4\pi\epsilon x_0(a-x_0)/a^2$ , where the index  $\epsilon = \pm 1$  specifies

the direction in which the trajectory is traversed. This set is particularly relevant in view of the cut off (5.18) discussed above, killing exponentially the long trajectories (for the usual experimental conditions  $L_T \simeq 2a$ ). The (small) contribution of the long trajectories can be calculated along the same lines that in the case of the family (1,1) [14].

The computation of  $d_{11}^0(\mu)$  for the square geometry gives for  $\chi^{(1)}$  (Eq. (5.17)) yields

$$(5.21) \quad \frac{\chi^{(1)}}{\chi^0} = \sin\left(k_F L_{11} + \frac{\pi}{4}\right) \int_0^a \frac{dx_0}{a} \mathcal{A}^2(x_0) \cos(\varphi \mathcal{A}(x_0))$$

as a function of the total flux  $\varphi = Ha^2/\Phi_0$ . The prefactor is defined by

$$(5.22) \quad \chi^0 = \chi_L \frac{3}{(\sqrt{2}\pi)^{5/2}} (k_F a)^{3/2} R_T(L_{11}) .$$

In the case of a square geometry, the integrals can be evaluated analytically,

$$(5.23) \quad \mathcal{C}_{11}(\varphi) = \frac{1}{\sqrt{2}\varphi} [\cos(\pi\varphi)C(\sqrt{\pi\varphi}) + \sin(\pi\varphi)S(\sqrt{\pi\varphi})] ,$$

where C and S respectively denote the cosine and sine Fresnel integrals, and the zero-field susceptibility of a clean cavity is [51, 52]

$$(5.24) \quad \chi^{(1)} = \chi_L \frac{4}{5(\sqrt{2}\pi)^{1/2}} (k_F a)^{3/2} \sin\left(k_F L_{11} + \frac{\pi}{4}\right) R_T(L_{11}) .$$

The results (5.21) and (5.24) show the  $(k_F a)^{3/2}$ -dependence typical for regular systems, with rapid oscillations as a function of  $k_F$  (that make  $\chi^{(1)}$  to vanish when averaged over variations of  $k_F$  or  $a$ ). In Fig 14 we see the good agreement between Eq. (5.24) (solid) and the numerically obtained quantum mechanical susceptibility (dotted). The small deviations between both traces is due to higher repetitions (trajectories  $\mathbf{M} = (M, M)$ ) that can easily be incorporated in our formalism [14]). The oscillations as a function of the flux at a given number of electrons in the square (solid) are in agreement with the numerical calculations (dashed).

The typical and average susceptibilities for a square geometry where only the dominant contributions of the family (1,1) are considered, can be written as

$$(5.25) \quad \frac{\chi^{(t)}}{\chi^0} \simeq \frac{\sqrt{\chi^{(1)2}}}{\chi^0} = \frac{1}{\sqrt{2}} \int_0^a \frac{dx_0}{a} \mathcal{A}^2(x_0) \cos(\varphi \mathcal{A}(x_0)) ,$$

$$(5.26) \quad \frac{\bar{\chi}}{\bar{\chi}^0} = \frac{1}{2} \int_0^a \frac{dx_0}{a} \int_0^a \frac{dx'_0}{a} [\mathcal{A}_-^2 \cos(\varphi \mathcal{A}_-) + \mathcal{A}_+^2 \cos(\varphi \mathcal{A}_+)] ,$$

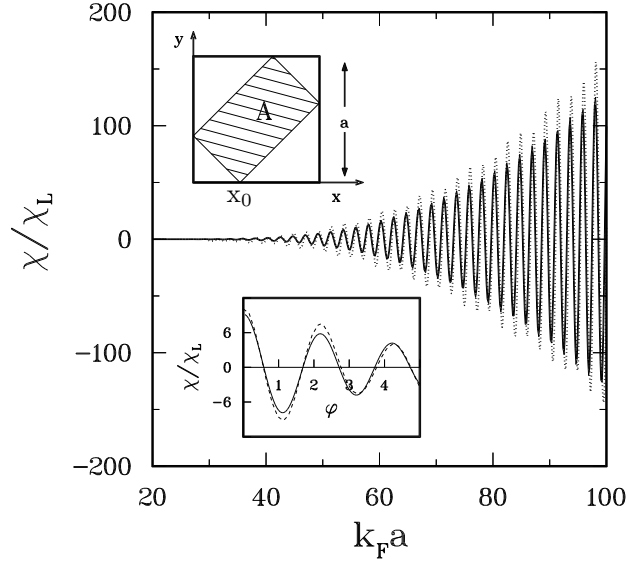


Fig. 14. – Magnetic susceptibility of a square as a function of  $k_F a$  from numerical calculations (dotted line) at zero field and at a temperature equal to 10 level-spacings. The solid line shows our semiclassical approximation (Eq. (5.24)) taking into account only the family (1,1) of shortest orbits. The period  $\pi/\sqrt{2}$  of the quantum result indicates the dominance of the shortest periodic orbits enclosing non-zero area with length  $L_{11} = 2\sqrt{2}a$  (upper inset). Lower inset: amplitude of the oscillations (in  $k_F L_{11}$ ) of  $\chi$  as a function of the flux through the sample from Eq. (5.22) (solid) and numerics (dashed). (From Ref. [52].)

with

$$(5.27) \quad \frac{\bar{\chi}^0}{\chi_L} = \frac{3}{(\sqrt{2}\pi)^3} (k_F a) R_T^2(L_{11})$$

and  $\mathcal{A}_{\pm} = \mathcal{A}(x_0) \pm \mathcal{A}(x'_0)$ . As in the previous case, the integrals (5.25) and (5.26) can be calculated in terms of Fresnel functions. In particular, the average zero-field susceptibility is paramagnetic and attains the value [51, 52]

$$(5.28) \quad \overline{\chi^{(2)}}(H=0) = \frac{4\sqrt{2}}{5\pi} k_F a \chi_L R_T^2(L_{11}) .$$

Since  $k_F a \gg 1$  we have that  $\chi^{(t)} \gg \bar{\chi} \gg \chi_L$ , and then we obtain a large enhancement of the Landau susceptibility by the effect of confinement in an integrable geometry.

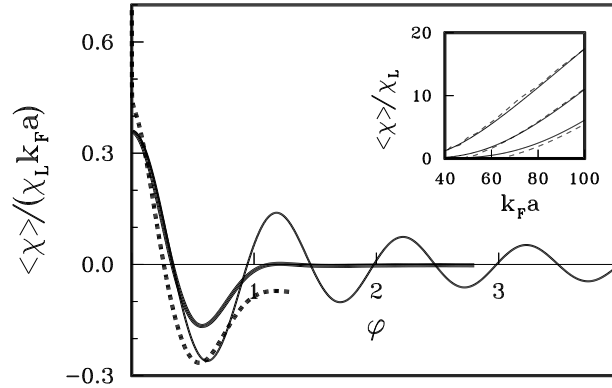


Fig. 15. – Thin solid curve: average magnetic susceptibility of an ensemble of squares from Eq. (5.26). Thick solid line: average over an ensemble with large dispersion of sizes. Thick dashed curve: average from numerics. The shift of the numerical with respect to the semiclassical results reflects the Landau susceptibility (due to  $F^0$  in Eq. (5.11)) not included in the latter. Inset: average susceptibility as a function of  $k_F a$  for various temperatures (8, 6 and 4 level spacings, from below) and a flux  $\varphi = 0.15$  and numerics (dashed). (From Ref. [52].)

The average susceptibility from (5.26) (thin solid line in Fig. 15) oscillates in the scale of one flux through the sample. For ensembles with a wide dispersion of lengths (like in the experiment of Ref. [27]) we have to also consider the effect on  $\mathcal{C}$  of the average over  $a$  (on a classical scale), which will suppresses the  $B$ -oscillations (thick solid line).

**5.4. Integrable versus chaotic behavior.** – Squares constitute a generic example of an integrable system perturbed by a magnetic field. It is interesting to compare our results with two extreme cases: circles (which remain integrable under the perturbation) and completely chaotic systems. The periodic orbits of the circular billiard are labeled by the topology  $\mathbf{M} = (M_1, M_2)$ , where  $M_1$  is the number of turns around the circle until coming to the initial point after  $M_2$  bounces. We can therefore write the field-dependent DOS as in (5.14), and we easily see that the susceptibility for circular billiard (of radius  $R$ ) has the same parametric dependence of the square:  $(k_F R)^{3/2}$  for  $\chi^{(1)}$  and  $\chi^{(t)}$ , and  $(k_F R)$  for  $\bar{\chi}$  [14]. The orbital response of small rings is usually expressed in terms of the persistent current  $I = -c(\partial F / \partial \Phi)_{T, \mathbf{N}}$  which can be calculated along the same lines than the susceptibility of the circle [135] and shows the previous parametric dependence on  $(k_F R)$ . The semiclassical results are in good agreement with the measurements of Ref. [28]. The generic behavior of integrable systems can be traced to the  $k_F^{-1/2}$  dependence of  $d^{\text{osc}}(E)$  in Eq. (5.14).

For chaotic systems (of typical length  $a$ ) with hyperbolic periodic orbits, the Gutzwiller



trace formula provides the appropriate path to calculate  $d^{\text{osc}}(E, H)$ . For temperatures at which only a few short periodic orbits are important,  $\chi$  can have any sign, and its magnitude is of the order of  $(k_F a)\chi_L$  [136, 137]. For an ensemble of chaotic billiards  $\chi \propto \chi_L$ . Therefore both susceptibilities are considerably reduced respect to the integrable case. The magnetization line-shape can be calculated along similar lines than those used in (2.7) for the coherent backscattering [14, 138].

## 6. – Semiclassical approach to weak disorder

In the previous section we described important differences in the orbital response of clean cavities according to their underlying classical mechanics. On the other hand, we know that any perturbing potential, such as the one provided by the disorder, immediately breaks the integrable character of the classical dynamics [57]. A natural question to pose is whether the difference chaotic versus integrable will survive when we go from the *clean* to the *ballistic* regimes and we consider the residual disorder that is always present in actual microstructures.

Disorder is usually studied in terms of the ensemble average over impurity realizations, since it is a perturbation of a electrostatic potential whose detailed nature is unknown. Typically, quantum perturbation theory is followed by the average over the strengths and positions of the impurities [129, 21]. This approach is suited for macroscopic metallic samples (which are self-averaging) or ensembles of mesoscopic samples (where different microstructures present different impurity configurations). The possibility of measuring a single disordered mesoscopic sample poses a conceptual difficulty since there is not an average process involved. In this section we first develop a general formalism of disordered Green functions for the ballistic regime, applicable to a wide range of physical problems, and then use this formalism to calculate the various averages of the susceptibility that we encounter in different experimental situations [53, 139].

**6.1. Disorder models.** – We assume that the disorder is generated by means of a given realization of a two-dimensional Gaussian potential of the form

$$(6.1) \quad V(\mathbf{r}) = \sum_j^{N_i} \frac{u_j}{2\pi\xi^2} \exp\left[-\frac{(\mathbf{r}-\mathbf{R}_j)^2}{2\xi^2}\right],$$

provided by  $N_i$  independent impurities located at points  $\mathbf{R}_j$  with uniform probability on an area  $V$  ( $n_i = N_i/V$ ). The strengths  $u_j$  obey  $\langle u_j u_{j'} \rangle = u^2 \delta_{jj'}$ . This model yields, in the limit  $\xi \rightarrow 0$ , the white noise disorder of  $\delta$ -function scatterers  $V(\mathbf{r}) = \sum_j^{N_i} u_j \delta(\mathbf{r}-\mathbf{R}_j)$ . The disorder potential  $V(\mathbf{r})$  is characterized by its correlation function

$$(6.2) \quad C(|\mathbf{r}-\mathbf{r}'|) = \langle V(\mathbf{r})V(\mathbf{r}') \rangle = \frac{u^2 n_i}{4\pi\xi^2} \exp\left[-\frac{(\mathbf{r}-\mathbf{r}')^2}{4\xi^2}\right].$$

Our model is quite simple, we do not aim to describe disorder within a microscopic model with realistic distributions of residual impurities in the semiconductor heterostructure, as done in Refs. [140, 141]. The model of Gaussian disorder is particularly appropriated for analytical calculations. On the other hand, many of the results that we will give only depend on the correlation function  $C(|\mathbf{r}-\mathbf{r}'|)$ , and are therefore valid for a wide class of disorder models.

Disorder effects depend on several length scales: the Fermi-wavelength  $\lambda_F$  of the electrons, the disorder correlation length  $\xi$  and the size  $a$  of the microstructure. In the

bulk case of an unconstrained (2DEG) we distinguish between *short range* (SR,  $\xi < \lambda_F$ ) and *finite range* (FR,  $\xi > \lambda_F$ ) disorder potentials. In the case of a microstructure a third, *long range* (LR) regime for  $\xi > a > \lambda_F$  has to be considered. The cleanest samples used in today experiments are in the finite range regime  $a > \xi > \lambda_F$ .

**6.2. Single-particle Green function.** – If we assume a microstructure with size  $a \gg \lambda_F$  and work in the FR or LR regimes, where the disorder potential is smooth on the scale of  $\lambda_F$ , the use of the semiclassical expression (2.11) for the single-particle Green function  $G(\mathbf{r}', \mathbf{r}; E)$  is well justified. The classical mechanics of trajectories with length  $L_s \ll l_T$  is essentially unaffected by disorder. Therefore the dominant effect on the Green function results from the shifts in the phases due to the modification of the actions (while the amplitudes  $D_s$  and topological indices  $\nu_s$  remain nearly unchanged). The first-order approximation to the action along a path  $\mathcal{C}_s$  in a system with weak disorder potential is

$$(6.3) \quad S_s^d \simeq S_s^c + \delta S_s,$$

here the clean action  $S_s^c$  is obtained by integrating along the *unperturbed* trajectory  $\mathcal{C}_s^c$  without disorder (*i.e.*  $S_s^c = k_F L_s$  in the case of billiards without magnetic field) instead of the actual path  $\mathcal{C}_s$ . The correction term  $\delta S_s$  is obtained, after expanding  $\mathbf{p} = \sqrt{2m[E - V(\mathbf{q})]}$  for small  $V/E$ , from the integral

$$(6.4) \quad \delta S_s = -\frac{1}{v_F} \int_{\mathcal{C}_s^c} V(\mathbf{q}) \, dq.$$

In this approximation an impurity average  $\langle \dots \rangle$  acts only on  $\delta S_s$  and the disorder averaged Green function reads

$$(6.5) \quad \langle G(\mathbf{r}', \mathbf{r}; E) \rangle = \sum_s G_s^c(\mathbf{r}', \mathbf{r}; E) \left\langle \exp \left[ \frac{i}{\hbar} \delta S_s \right] \right\rangle.$$

$G_s^c$  is the contribution of the trajectory  $s$  to the zero-disorder (clean) Green function  $G^c$ .

For trajectories of length  $L_s \gg \xi$ , the contributions to  $\delta S$  from segments of the trajectory separated more than  $\xi$ , are uncorrelated. The stochastic accumulation of action along the path can be therefore interpreted as determined by a random-walk process, resulting in a Gaussian distribution of  $\delta S_s(L_s)$ . For larger  $\xi$  or shorter trajectories ( $L_t \not\gg \xi$ ), one can still think of a Gaussian distribution of the de-phasing  $\delta S_s$  provided  $V(\mathbf{r})$  is generated by a sum of a large number of independent impurity potentials. As a consequence of the Gaussian character of the distribution of  $\delta S_s(L_s)$ , the characteristic function involved in Eq. (6.5) is given by

$$(6.6) \quad \left\langle \exp \left[ \frac{i}{\hbar} \delta S_s \right] \right\rangle = \exp \left[ -\frac{\langle \delta S_s^2 \rangle}{2\hbar^2} \right]$$

and therefore entirely specified by the variance

$$(6.7) \quad \langle \delta S_s^2 \rangle = \frac{1}{v_F^2} \int_{C_s^c} dq \int_{C_s^c} dq' \langle V(\mathbf{q}) V(\mathbf{q}') \rangle .$$

For an unconstrained 2DEG the sum in Eq. (6.5) is reduced to the direct trajectory joining  $\mathbf{r}$  and  $\mathbf{r}'$ . If  $L = |\mathbf{r} - \mathbf{r}'| \gg \xi$  the inner integral in Eq. (6.7) can be extended to infinity and we obtain

$$(6.8) \quad \langle \delta S^2 \rangle = \frac{L}{v_F^2} \int dq C(\mathbf{q}) .$$

The semiclassical average Green function for the bulk exhibits therefore an exponential behavior [53, 142] (on a length scale  $l_T > L \gg \xi$ )

$$(6.9) \quad \langle G(\mathbf{r}', \mathbf{r}; E) \rangle = G^c(\mathbf{r}', \mathbf{r}; E) \exp \left[ -\frac{L}{2l} \right] ,$$

with the damping governed by an inverse elastic mean free path

$$(6.10) \quad \frac{1}{l} = \frac{1}{\hbar^2 v_F^2} \int dq C(\mathbf{q}) = \frac{u^2 n_i}{4\sqrt{\pi} \hbar^2 v_F^2 \xi} ,$$

for the Gaussian potential (6.1).

Quantum diagrammatic perturbation theory for the potential (6.1) shows that the damping (6.9) of the one-particle Green function is also valid in the SR regime (where our semiclassical approach is no longer applicable). The quantum elastic MFP agrees with the semiclassical result (6.10) in the limit  $k_F \xi \gg 1$ , and it is equal to  $l_\delta = (v_F \hbar^3)/(m n_i u^2)$  for short range. The quantum results for the transport MFP [53] are  $l_T = l_\delta$  in the SR regime and  $l_T = 4(k_F \xi)^2 l$  for  $k_F \xi \gg 1$  (and therefore the transport MFP may be significantly larger than  $l$  [23]).

We now turn from the semiclassical treatment of the bulk to that of a confined system. We treat the ballistic regime  $l_T > a$  where both, the confinement *and* the impurities have to be considered. Confinement implies that the clean  $G^c(\mathbf{r}', \mathbf{r}; E)$  is given as a sum over all direct and multiply reflected paths connecting  $\mathbf{r}$  and  $\mathbf{r}'$ ; disorder modifies the corresponding actions according to Eq. (6.4).

In the SR and FR regimes the damping of each contribution  $\langle G_s \rangle$  to  $\langle G \rangle$  acquires a damping  $\exp(-L_s/2l)$  according to its length  $L_s$ ,

$$(6.11) \quad \langle G(\mathbf{r}', \mathbf{r}; E) \rangle = \sum_s G_s^c(\mathbf{r}', \mathbf{r}; E) \exp \left[ -\frac{L_s}{2l} \right] .$$

In the long range regime and for  $\xi \sim a$  the correlation integral (6.7) can no longer be approximated by  $L_s \int_{-\infty}^{+\infty} dq C(\mathbf{q})$  due to correlations across different sectors of an

orbit (with distance smaller  $\xi$ ). Therefore the orbit–geometry enters into the correlation integral. For  $\xi \gg a$  we can expand  $C(|\mathbf{r}-\mathbf{r}'|)$  (up to first order in  $(|\mathbf{r}'-\mathbf{r}|/\xi)^2$ ) and obtain a damping exponent that depends quadratically on  $L_s$  (in contrast to linear behavior in the finite range case), with a length scale given by the geometrical mean of the bulk MFP  $l$  and  $\xi$  [139].

**6.3. Two-particle Green function.** – The typical susceptibility (Eq. (5.19)), the ensemble averaged susceptibility (Eq. (5.20)), or in general a density-density correlation function, involve squares of the density of states. Writing the latter (Eq. (5.13)), in terms of the difference between advanced and retarded Green functions ( $G^{(+)} - G^{(-)}$ ) we are left with products of one-particle Green functions. The most interesting terms are the cross products  $G^{(+)}(\mathbf{r}', \mathbf{r}; E) G^{(-)}(\mathbf{r}, \mathbf{r}'; E) = G^{(+)}(\mathbf{r}', \mathbf{r}; E) G^{(+)*}(\mathbf{r}', \mathbf{r}; E^*)$ , because they survive the energy average and are sensitive to changes in the magnetic field.

In the non-interacting approach that we have used so far in this work, the two-particle Green function factorizes into a product of one-particle Green functions [130], therefore we will use in this section the former as a synonym for the latter. Unless specified, the Green functions will be retarded ones. Let us consider the product  $G(\mathbf{r}'_1, \mathbf{r}_1; E) G^*(\mathbf{r}'_2, \mathbf{r}_2; E)$ . The effect of the disorder potential can be taken into account perturbatively, for each realization of the disorder, in the same way as before by using Eqs. (6.3) and (6.4). We can therefore write the disorder average as a double sum over trajectories  $s$  and  $u$

$$(6.12) \quad \langle G G^* \rangle = \sum_s \sum_u \langle G_s G_u^* \rangle = \sum_s \sum_u G_s^c G_u^{c*} \langle \exp \left[ \frac{i}{\hbar} (\delta S_s - \delta S_u) \right] \rangle \\ = \sum_s \sum_u G_s^c G_u^{c*} \exp \left[ - \frac{\langle (\delta S_s - \delta S_u)^2 \rangle}{2\hbar^2} \right].$$

Here it is necessary to take into account the correlation of the disorder potential between points on trajectories  $s$  and  $u$ . One limiting case is that where  $s$  and  $u$  are, either the same trajectory, or the time reversal one of each other. In these cases their associated contribution acquires exactly the same phase shift and  $\langle G_s G_s^* \rangle = |G_s^c|^2$ . Within our approximation, the diagonal contributions  $s = u$ , which *e.g.* are responsible for the classical part of the conductivity, remain disorder-unaaffected, since we assume the trajectories have a length much smaller than  $l_T$ . (A semiclassical consideration of these effects for trajectories of length of the order of  $l_T$  or larger was performed in Ref. [142] for the bulk, giving a damping of the two–point Green function on the scale of  $l_T$ .) At the opposite extreme, if trajectories  $s$  and  $u$  are completely uncorrelated, *i.e.*, for long trajectories in classical chaotic systems or trajectories in integrable systems with a spatial distance larger than  $\xi$ , the average in Eq. (6.12) factorizes:  $\langle G_s G_u^* \rangle = \langle G_s \rangle \langle G_u^* \rangle$  and lead to single-particle damping behavior.

The double sum Eq. (6.12) may also involve pairs of trajectories which stay within a distance of the order of  $\xi$  (as for nearby paths on a torus of an integrable system). In

this case the behavior of  $\langle G_s G_u^* \rangle$  is more complicated and depends of the confinement geometry of the system under consideration. As a simple illustration of the interplay between disorder correlation and families of orbits, let us consider for the case of two trajectories  $s$  and  $u$  joining respectively the points  $\mathbf{r}_1 = (0, 0)$  with  $\mathbf{r}'_1 = (L, 0)$  and  $\mathbf{r}_2 = (0, y)$  with  $\mathbf{r}'_2 = (L, y)$ . We assume  $L \gg \xi$  and ignore the confinement effects. The separation  $y$  between the trajectories may be of the order of  $\xi$ . The variance of the relative phase between  $s$  and  $u$  is

$$(6.13) \quad \langle (\delta S_s - \delta S_u)^2 \rangle = 2L \frac{(K(0) - K(y))}{v_F^2}$$

with  $K(y) = \int_{-\infty}^{+\infty} C(x, y) dx = (\hbar^2 v_F^2 / l) \exp(-y^2 / (4\xi^2))$  for Gaussian potentials. Therefore  $\langle GG^* \rangle = G^c G^{c*} \tilde{f}(y)$  with

$$(6.14) \quad \tilde{f}(y) = \exp \left[ -\frac{L}{l} \left( 1 - \frac{K(y)}{K(0)} \right) \right].$$

This result is general for two trajectories of length  $L$  running parallel a distance  $y$  apart. The function  $\tilde{f}(y)$  expresses in a very simple way that as  $y \rightarrow 0$ , the effect of disorder disappears ( $\tilde{f}(0) = 1$ ) while for  $y \gg \xi$  the function  $\tilde{f}(y)$  behaves as the square of single particle Green function damping.

**6.4. Fixed-size impurity average of the magnetic susceptibility.** – We consider here a disorder average (which will henceforth be called a fixed-size impurity average) of an ensemble of structures for which the parameters of the corresponding clean system (geometry, size, and chemical potential) remain fixed under the change of impurity realizations. As shown in the previous section, averages over weak disorder exponentially damp, but do not completely suppress, oscillatory contributions (with phase  $k_F L_s$ ) to the single-particle Green function arising from the paths of a confined system.

We treat regular billiards at zero or small magnetic fields, where the density of states has the  $H$ -dependence of the formulae (5.14)–(5.16). The general result for  $\chi^{(1)}$ , Eq. (5.17), formally persists in the presence of smooth disorder with the replacement of  $\mathcal{C}_M$  by

$$(6.15) \quad \langle \mathcal{C}_M^d(H) \rangle = \frac{1}{2\pi} \int_0^{2\pi} d\Theta_1 \cos \left[ 2\pi \frac{H \mathcal{A}_M(\Theta_1)}{\Phi_0} \right] \exp \left[ -\frac{\langle (\delta S_M(\Theta_1))^2 \rangle}{2\hbar^2} \right],$$

where  $\langle \delta S_M^2(\Theta_1) \rangle$  is given by Eq. (6.7) with the integrals performed along the orbits of the family  $\mathbf{M}$  parameterized by  $\Theta_1$ .

In the case of square billiards, where the dominant contribution arises from the family  $(1, 1)$ ,  $\delta S(x_0)$  is independent of  $x_0$  and in the FR regime we have

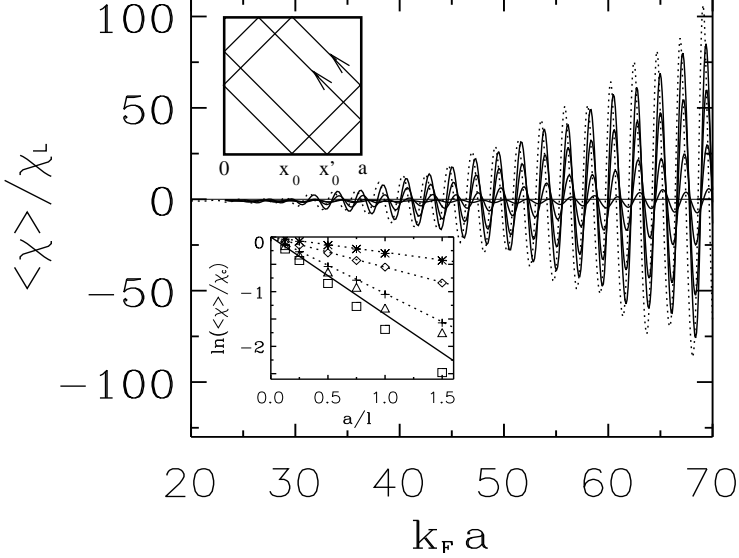


Fig. 16. – Susceptibility  $\langle \chi \rangle$  of a square billiard (at zero magnetic field and at a temperature equal to 6 level spacings) as a function of  $k_F a$  for the clean case (dotted) and for increasing Gaussian disorder ( $\xi/a = 0.1$ ) with elastic MFP  $l/a = 4, 2, 1, 0.5$  (solid lines in the order of decreasing amplitude). Upper inset: Two representative periodic orbits belonging to the family (1,1) of a square billiard. Lower inset: ratio  $\langle \chi \rangle / \chi_c$  as a function of the inverse elastic MFP  $a/l$  for  $\xi/a = 4, 2, 1, 0, 0.5$  (from the top). The symbols indicate the numerical quantum results for  $\xi = 0$  (triangles),  $\xi/a = 0.5$  (squares),  $\xi/a = 1$  (crosses),  $\xi/a = 2$  (diamonds),  $\xi/a = 4$  (stars). The solid line is the  $\xi = 0$  result. The dotted lines going through the different sets of symbols for show the semiclassical dampings in various regimes.

$$(6.16) \quad \langle \chi \rangle \simeq \langle \chi^{(1)} \rangle = \chi_c^{(1)} \exp \left[ -\frac{L_{11}}{2l} \right],$$

where  $\chi_c^{(1)}$  denotes the susceptibility of the system without disorder (Eq. (5.21)).

Fig. 14 shows results of the numerical quantum simulations for the average susceptibility  $\langle \chi \rangle$  of an ensemble of squares with fixed size but different disorder realizations at a temperature  $k_B T = 3g_s \Delta$ , where  $\Delta$  is the mean level spacing. The characteristic oscillations on a scale  $k_F L_{11}$  are the signature of the (1, 1) family and persist upon inclusion of disorder such that the elastic MFP  $l$  is of the order of the system size. The clean susceptibility (dotted line) is increasingly damped (solid lines) with decreasing elastic MFP ( $l/a = 4, 2, 1, 0.5$ ) for fixed  $\xi/a = 0.1$  (which represents a typical disorder corre-

lation length in experimental realizations). For details of the numerical simulations see Ref. [53]. The lower inset depicts the ratio  $\langle\chi\rangle/\chi_c$  for various correlation lengths  $\xi$  and  $l$ . The damping is exponential as predicted by Eq. (6.16) and the decays are well reproduced by the analytical expressions for the SR (solid line), FR and LR (dotted lines).

**6.5. Combined impurity and energy average of the susceptibility.** – The previously treated fixed-size impurity average is not realistic since in experimentally realizable structures disorder averages cannot be performed independently from size-averages. The detailed features of the confining potential do not remain unchanged for different impurity configurations. Therefore we have to consider *energy and disorder* averages. The typical susceptibility is now defined by  $\chi^{(t)} = \langle\chi^2\rangle^{1/2}$ . It applies to the case of repeated measurements on a given microstructure when different impurity realizations (and simultaneous changes in  $k_F$ ) are obtained by some kind of perturbation (*e.g.* cycling to room temperature). From now on we will reserve the term  $\chi_{\text{cl}}^{(t)}$  for the clean typical susceptibility  $(\overline{\chi^2})^{1/2}$ . The energy and impurity averaged susceptibility  $\langle\overline{\chi}\rangle$  describes the magnetic response of an ensemble of a large number of microstructures with different impurity realizations and variations in size. This is the relevant quantity for the interpretation of the experiment of Ref. [27].

The semiclassical results for  $\chi^{(t)}$  and  $\langle\overline{\chi}\rangle$  for a system of integrable geometry are obtained in an analogous way as we proceeded in the previous chapter. That is, by including in the integral (5.16) for  $\mathcal{C}_{\mathbf{M}}$  a  $\Theta_1$ -dependent disorder-induced phase  $\exp[i\delta S(\Theta_1)/\hbar]$ . However, now we have to take the square of  $\mathcal{C}_{\mathbf{M}}$  before the impurity average, and cross correlations between different paths on a torus  $\mathbf{M}$ , or between different tori, have to be considered. We discuss this effect, typical of integrable systems, for the case of a square billiard. For sake of clarity we moreover assume a temperature range such that only the contribution of the shortest closed orbit has to be taken into account. The contribution of orbits (1, 1) for the typical susceptibility reads:

$$(6.17) \quad \left(\frac{\chi^{(t)}}{\chi^0}\right)^2 = \frac{1}{2} \int_0^a \frac{dx_0}{a} \int_0^a \frac{dx'_0}{a} \mathcal{A}^2(x_0) \mathcal{A}^2(x'_0) \cos(\varphi\mathcal{A}(x_0)) \cos(\varphi\mathcal{A}(x'_0)) f(x_0, x'_0),$$

with  $\chi^0$  defined as in Eq. (5.22). The function

$$(6.18) \quad f(x_0, x'_0) = \left\langle \exp \left\{ \frac{i}{\hbar} (\delta S(x_0) - \delta S(x'_0)) \right\} \right\rangle \\ = \exp \left\{ -\frac{1}{2\hbar^2} [\langle\delta S^2(x_0)\rangle + \langle\delta S^2(x'_0)\rangle - 2\langle\delta S(x_0)\delta S(x'_0)\rangle] \right\}$$

accounts for the effect of disorder on pairs of orbits  $x_0$  and  $x'_0$ . For the magnetic response of an energy and disorder averaged ensemble we find correspondingly:



$$(6.19) \quad \frac{\langle \bar{\chi} \rangle}{\bar{\chi}^0} = \frac{1}{2} \int_0^a \frac{dx_0}{a} \int_0^a \frac{dx'_0}{a} [\mathcal{A}_-^2 \cos(\varphi \mathcal{A}_-) + \mathcal{A}_+^2 \cos(\varphi \mathcal{A}_+)] f(x_0, x'_0)$$

with  $\bar{\chi}^0$  and  $\mathcal{A}_\pm$  defined as in Eq. (5.27).

In the case of short range we reach the border of applicability of our semiclassical approximation. If we nevertheless take  $\xi \rightarrow 0$ , we see that orbits with  $x_0 \neq x'_0$  are disorder-uncorrelated and all such pair contributions are exponentially damped. Using exclusively the family (1,1), one obtains an overall suppression of the typical and average susceptibility

$$(6.20) \quad \lim_{\xi \rightarrow 0} \chi^{(t)} = \chi_{\text{cl}}^{(t)} e^{-L_{11}/2l\xi} \quad , \quad \lim_{\xi \rightarrow 0} \langle \bar{\chi} \rangle = \bar{\chi} e^{-L_{11}/l\xi} .$$

Note that the exponent for  $\langle \bar{\chi} \rangle$  differs by a factor 1/2 from that for  $\langle \chi \rangle$ .

In the finite range case of  $\lambda_F < \xi \ll a$ , the phase shifts  $\delta S(x_0)$  and  $\delta S(x'_0)$  in  $f(x_0, x'_0)$  are accumulated in a correlated way, if the spatial distance of two orbits  $x_0$  and  $x'_0$  is smaller than  $\xi$ . To evaluate the product term  $2\langle \delta S(x_0)\delta S(x'_0) \rangle$  in the exponent of  $f(x_0, x'_0)$  in this regime the integrations are performed as in Eq. (6.7) but with  $\mathbf{q}$  and  $\mathbf{q}'$  running along paths starting at  $x_0$ , respectively  $x'_0$ . Ignoring the additional correlations occurring near the bounces off the boundaries of the billiard, the trajectories  $x_0$  and  $x'_0$  (see inset Fig. 16) can be regarded as straight lines remaining at a constant distance  $y = |x_0 - x'_0|/\sqrt{2}$  from another. We can therefore approximate  $f(x_0, x'_0)$  by  $\tilde{f}(|x_0 - x'_0|/\sqrt{2})$  with the function  $\tilde{f}$  given by Eq. (6.14). For Gaussian correlation we thus have

$$(6.21) \quad f(x_0, x'_0) = \exp \left\{ -\frac{L_{11}}{l} \left[ 1 - \exp \left( -\frac{(x_0 - x'_0)^2}{8\xi^2} \right) \right] \right\} .$$

Orbits separated by  $|x_0 - x'_0| \gg \xi$  are disorder-uncorrelated and exponentially suppressed:  $f(x_0, x'_0) \simeq \exp(-L_{11}/l)$ . In contrast to that, disorder only weakly affects trajectories separated by  $|x_0 - x'_0| < \xi$ .

The disorder averages in the finite range regime lead, by means of the function  $f$ , to a non-exponential damping of the susceptibilities for systems with families of periodic orbits. This behavior becomes obvious for the case of square billiards where at  $H=0$  the integrals (6.17) and (6.19) can be evaluated analytically in the limits of  $L_{11} \ll l$  (extreme ballistic) and  $L_{11} \gg l$  (deep ballistic). We find for the typical and average susceptibility at  $H=0$  in the finite range case for  $L_{11} \ll l$  [53, 139]

$$(6.22) \quad \left( \frac{\chi^{(t)}}{\chi_c^{(t)}} \right)^2 \simeq 1 - \frac{L_{11}}{l} \left( 1 - c_t \frac{\xi}{a} \right) \quad , \quad \frac{\langle \bar{\chi} \rangle}{\bar{\chi}} \simeq 1 - \frac{L_{11}}{l} \left( 1 - c_a \frac{\xi}{a} \right) ,$$

and for  $L_{11} \gg l$  (by steepest descent):

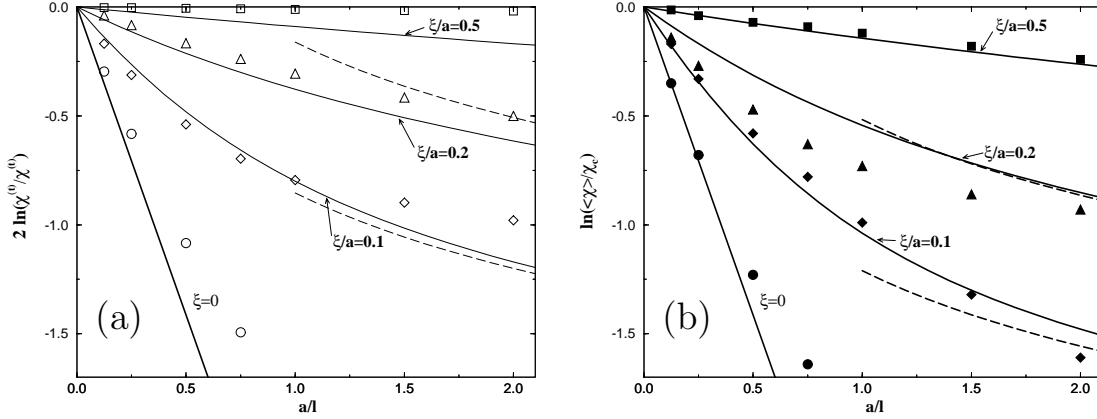


Fig. 17. – Ratio between disorder averaged and zero-disorder results for (a) the typical  $\chi^{(t)}$  (thin curves) and (b) the ensemble averaged  $\langle \bar{\chi} \rangle$  (thick curves) susceptibilities as a function of decreasing elastic MFP  $l$  for different values of  $\xi/a$ . The symbols denote the numerical quantum results, the solid lines (for  $\xi > 0$ ) the semiclassical integrals (6.17) (a) and (6.19) (b) and the dashed lines asymptotic expansions of the integrals for large  $a/l$ .

$$(6.23) \quad \left( \frac{\chi^{(t)}}{\chi_c^{(t)}} \right)^2 \simeq c_t \left( \frac{\xi}{a} \right) \left( \frac{l}{L_{11}} \right)^{1/2}, \quad \frac{\langle \bar{\chi} \rangle}{\bar{\chi}} \simeq c_a \left( \frac{\xi}{a} \right) \left( \frac{l}{L_{11}} \right)^{1/2}.$$

The constants in the above equations are  $c_t = (20/7)\sqrt{2\pi}$  and  $c_a = 2\sqrt{2\pi}$  [53]. Eq. (6.22) expresses the limit of very weak disorder, showing that the small disorder effect is further reduced due to the correlation of the disorder potential. The other limit, Eq. (6.23), is more interesting since it shows that disorder correlation effects lead to a replacement of the exponential disorder damping by a power law.

Fig. 17 depicts in logarithmic representation our collected results for the disorder averaged typical (a) and averaged (b) susceptibility for square billiards (at  $H = 0$  and  $k_B T = 2g_s \Delta$ ) as a function of the inverse elastic MFP for different disorder correlation lengths. The symbols denote results from numerical quantum simulations and the full curves semiclassical results from numerical integration of the Eqs. (6.17) and (6.19). For the short range case  $\xi = 0$  they reduce to Eq. (6.20) predicting an exponential decrease with exponent  $L_{11}/l_\delta$  which is in line with the quantum calculations (circles). The semiclassical results for the finite range are on the whole in agreement with the numerical results for  $\xi/a = 0.1$  (diamonds),  $\xi/a = 0.2$  (triangles) and  $\xi/a = 0.5$  (squares). The semiclassical curves seem to overestimate the damping of the typical susceptibility. The

dotted curves (shown for  $a/l \geq 1$ ) depict the limiting expressions (6.23) in the regime  $L_{11} > l$ .

**6.6. Relation to experiment and other theories.** – In the experiment of Lévy *et al.* [27], the magnetic susceptibility was measured for an array of about  $10^5$  ballistic square-like cavities. The size of the squares is on average  $a = 4.5 \mu m$ , with a large dispersion (estimated between 10 and 30%) along the array. Each individual square is a mesoscopic ballistic system since the phase-coherence length is estimated to be  $L_\Phi = 15\text{--}40 \mu m$  and the elastic MFP  $l = 4.5\text{--}10 \mu m$ . The potential correlation length can be estimated to be of the order of  $\xi/a \simeq 0.1$ . Taking the most unfavorable case of  $l \simeq a$  we obtain, with respect to the clean case, a disorder reduction for the averaged susceptibility of  $\langle \bar{\chi} \rangle / \bar{\chi} \simeq 0.37$ , showing that the features of the clean integrable systems (strong paramagnetic susceptibility at  $H = 0$ ) persist upon inclusion of disorder. Since  $\bar{\chi} \simeq 100 \chi_L$  [51, 52, 14], our calculations for the paramagnetic response of the ballistic squares agree quantitatively with the experimental findings (given the experimental uncertainties). However, the temperature dependence obtained in the experiment is much slower than the exponential suppression implied by Eqs. (6.23), (5.28) and (5.18). This is one of the motivations to consider the interaction effects that we discuss in the next section.

In a related theoretical work, Gefen and collaborators [143] followed a complementary approach to ours and calculated the disorder-averaged susceptibility for an ensemble of ballistic squares based on long trajectories [strongly] affected by scattering from  $\delta$ -like impurities. They found that the average susceptibility does not depend on the elastic MFP. At the temperatures of experimental relevance, these very long trajectories are irrelevant, and this is the reason why our numerical results do not present the proposed effect. McCann and Richter combined a diagrammatic approach with semiclassical techniques and studied the transition between the clean and diffusive regimes for  $\delta$ -like potentials [144]. They separated the contributions from trajectories persisting in the clean limit (as we have considered in this section) from scattered paths (as proposed in Ref. [143]), and demonstrated that the former are clearly dominant in the (temperature and disorder) regime of experimental relevance.

## 7. – Electron-electron interactions in the ballistic regime

As discussed in the introduction, in Mesoscopic Physics the electron-electron interactions are usually taken into account only by a renormalization of single-particle quantities (like the effective mass or the effective potential felt by individual electrons) and by the effect of the quasiparticle life-time as a limiting factor of the phase-coherence length  $L_\Phi$ . This is the approximation we have used so far in this work, which gives good account of transport experiments, dealing with open systems. On the other hand, when we go to dots weakly coupled to the electronic reservoirs, we enter in the regime of Coulomb blockade, where the effect of interactions becomes crucial for the conductance [145]. If we completely isolate the dots and measure thermodynamical properties, like the magnetic susceptibility, we expect important effects from the combined role of confinement and interactions. In the context of persistent currents in disordered metals, the effect of interactions was invoked [146, 147] as a possible source for the discrepancy found between the experimental results [148, 149, 150] and the non-interacting theories [132].

In Secs. 5 and 6 we concentrated ourselves on the effect of confinement in ballistic cavities and, working within a single-particle approach, we found a large orbital response which depends on the underlying classical mechanics. In this section we demonstrate that interactions also give rise to a large contribution, which has to be added to the non-interacting one. We show that the semiclassical approach can be extended to the interacting problem and that the new contribution to the susceptibility is also depending on the classical dynamics of non-interacting electrons [54].

**7.1. Screened Coulomb interaction in two dimensions.** – Interactions in a 2DEG formed at a semiconductor heterostructure have been thoroughly studied since the early eighties [151], by adopting the techniques used for the 3D electron gas, like Landau's Fermi liquid theory and Random Phase Approximation (RPA) [129, 130]. The latter approach yields an effective (momentum and frequency dependent) interaction potential

$$(7.1) \quad \mathcal{V}(\mathbf{q}; \omega_m) = \frac{\hat{V}(\mathbf{q})}{1 - \hat{V}(\mathbf{q})\Pi^0(\mathbf{q}; \omega_m)},$$

where  $\hat{V}(\mathbf{q}) = (2\pi e^2/\epsilon_\infty)(f_q/q)$  is the bare potential. The 2D Fourier transform of the standard 3D Coulomb interaction ( $2\pi e^2/q$ ) is reduced by two factors: the optical (high-frequency) dielectric constant  $\epsilon_\infty$  taking into account the screening by the valence electrons and the form-factor  $f_q$  arising from the finite extent of the electron wave-function in the direction perpendicular to the heterojunction [151]. The irreducible polarizability (particle-hole propagator) is given by

$$(7.2) \quad \Pi^0(\mathbf{q}; \omega_m) = -\frac{g_s}{\beta} \sum_{\epsilon_n} \int \frac{d\mathbf{p}}{(2\pi)^2} \mathcal{G}(\mathbf{p}; \omega_m) \mathcal{G}(\mathbf{p} + \mathbf{q}; \omega_m + \epsilon_n),$$

in terms of the non-interacting finite-temperature Green functions [129, 130] (for which we develop a semiclassical approximation latter in this section). The Matsubara frequencies associated with one-particle (two-particle) propagators are of fermionic (bosonic) kind:  $\epsilon_n = (2n + 1)\pi/\beta$  ( $\omega_m = 2m\pi/\beta$ ).

In two dimensions, the zero-temperature (time-ordered) irreducible polarizability admits the simple analytical form [151]

$$(7.3) \quad \Pi_T^0(\mathbf{q}; \omega) = -\frac{n}{E_F} \frac{k_F}{q} \left( \frac{q}{k_F} - \sqrt{a_+^2 - 1} + \sqrt{a_-^2 - 1} \right),$$

with  $n$  the 2D electron density,  $a_{\pm} = (\omega + i\eta)/(qv_F) \pm q/(2k_F)$ , and the complex square roots taken in the branch with positive imaginary part. RPA is a high-density expansion in the dimensionless parameter  $r_s = r_0/a_0$  ( $\pi r_0^2$  is the average area per electron, and  $a_0$  is the Bohr radius in the semiconductor). In *GaAs/AlGaAs* heterostructures we typically have  $r_s = 2$ , but as in standard metals, RPA gives good results beyond its regime of validity, and it has been extensively used in calculations of effective masses, inelastic scattering times, etc [151, 152].

The long wave-length limit of the static effective potential yields the Thomas-Fermi (or screened) 2D potential:

$$(7.4) \quad \hat{V}_{\text{TF}}(\mathbf{q}) = \frac{2\pi e^2/\epsilon_{\infty}}{q + q_s} \quad , \quad V_{\text{TF}}(\mathbf{r}) = \int \frac{d\mathbf{q}}{(2\pi)^2} \hat{V}_{\text{TF}}(\mathbf{q}) \exp[i\mathbf{q} \cdot \mathbf{r}] ,$$

where  $q_s = (g_s m e^2)/(\hbar^2 \epsilon_{\infty})$  is the screening wave-vector (we take  $f_q = 1$ ).  $V_{\text{TF}}(\mathbf{r})$  is the electrostatic potential created by a test charge at the origin, and given by the sum of the bare (long range) Coulomb potential and a term associated with the fact that electrons in the gas are pushed away from the [negative] external charge, resulting in the screening of the original potential. The screening properties of the 2DEG are poorer than in the three dimensional case. For instance, in the former the potential  $V_{\text{TF}}(\mathbf{r})$  decays for large distances as the third power of  $r$  while in the later the dependence is exponential. In RPA the difference in the decay of the effective potential is the factor  $r^{-d}$  of the Friedel oscillations. The poor screening in the 2DEG will then be a limitation to keep in mind when using local effective interactions.

When we consider the confinement into a quantum box, we will still keep the screened interaction of Eq. (7.4). This is a reasonable approximation since the size of the quantum boxes we want to describe ( $a = 4.5\mu m$ ) is much larger than the typical screening length ( $2\pi/q_s = 0.03\mu m$ ). We therefore expect the boundary effects on the screened interaction to be small.

Even if the semiclassical approach can be adapted to work with the potential  $V_{\text{TF}}(\mathbf{r})$  of Eq. (7.4) [155], we will make in this section a further (and strong) approximation and neglect the momentum dependence of  $\hat{V}_{\text{TF}}$ , which leads to the local potential

$$(7.5) \quad U(\mathbf{r}) = \lambda_0 N(0)^{-1} \delta(\mathbf{r}) ,$$

with  $N(0) = E_F/n = g_s m / (2\pi\hbar^2)$  the density of states and  $\lambda_0 = 1$  introduced to identify the order of perturbation.

**7.2. Thermodynamics and semiclassics of small interacting systems.** – The interaction induced thermodynamical properties are given by the contribution  $\Omega_i$  to the thermodynamical potential (Eq. (5.3)). The finite-temperature formalism for the grand-partition function yields a perturbative expansion for  $\Omega_i$  [129]. For local and spin independent interactions, the leading order (Cooper channel) contribution is represented diagrammatically in Fig. 7.2, and given by [154]

$$(7.6) \quad \begin{aligned} \Omega_i^C &= -\frac{1}{\beta} \sum_{k=1}^{\infty} \frac{(-\lambda_0)^k}{k} \sum_{\omega_m < E_F} \int d\mathbf{r}_1 \dots d\mathbf{r}_k \Sigma(\mathbf{r}_2, \mathbf{r}_1; \omega_m) \dots \Sigma(\mathbf{r}_1, \mathbf{r}_k; \omega_m) \\ &= \frac{1}{\beta} \sum_{\omega_m < E_F} \text{Tr} \{ \ln[1 + \lambda_0 \Sigma(\omega_m)] \} . \end{aligned}$$

The particle-particle propagator is given by [129]

$$(7.7) \quad \Sigma(\mathbf{r}', \mathbf{r}; \omega_m) = \frac{1}{\beta N(0)} \sum_{\epsilon_n < E_F} \mathcal{G}(\mathbf{r}', \mathbf{r}; \epsilon_n) \mathcal{G}(\mathbf{r}', \mathbf{r}; \omega_m - \epsilon_n) .$$

The trace over the space coordinates is a short way of expressing the expansion in all orders in  $\lambda_0 \Sigma$ . The short-length (high-frequency) behavior is incorporated in the screened interaction, thus requiring a cutoff of the frequency sums at  $E_F$  [154]. In Fig. 7.2 the wavy lines represent the local interaction and the solid lines the non-interacting Green function  $\mathcal{G}$  in the presence of the confining potential. The concept of particle-particle propagator, as well as the Cooperon contribution, come from the Cooper pairs in the theory of superconductivity. The main difference with our case is that here the interaction is repulsive (thus the plus sign in the trace) and that we have lost translational invariance (therefore we cannot trade the operators for ordinary functions by going to momentum representation). The factor  $k$  in each term of the expansion (7.6) is to be contrasted with the  $k!$  of the Feynman rules for the Green function, and it is responsible for the poor convergence properties of perturbative expansions for  $\Omega_i^C$  [129]. This is why higher-order diagrams are essential in the diagonal Cooper channel, as known from the theory of superconductivity [153] and persistent currents [146, 147].

The standard RPA contribution to  $\Omega_i^C$  [130] is obtained by reversing the direction of one of the loops in the diagrams of Fig. 7.2 (or by using similar expressions to those of Eq. (7.6) with the interchange of  $\lambda_0 \Sigma$  by  $U\Pi^0$ ). The first two diagrams of both series coincide, but semiclassical arguments indicate that the RPA expansion gives a much

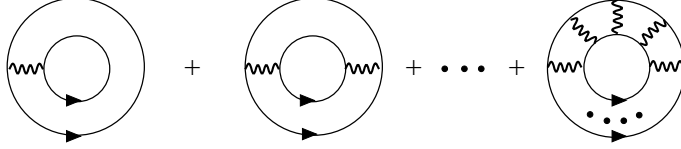


Fig. 18. – Leading Cooper-channel diagrams for the interaction contribution to the thermodynamic potential.

smaller contribution than that of the Cooper channel. The RPA susceptibility of a 3D electron gas has been calculated by Vignale as an expansion in  $r_s$  [156]. On the other hand, the Cooper channel gives for the 2DEG an interaction-induced susceptibility that overwhelms the Landau contribution and *increases* with  $k_F$  [153, 157].

We have seen in the previous sections that the non-interacting grand-canonical susceptibility averaged over the microstructures vanishes in leading order in  $\mathbf{N}$ , forcing us to make the distinction between the canonical and grand-canonical results. Conversely, we will see that the interacting contribution from  $\Omega_i$  does not vanish upon average, and that is why in this section we work in the grand-canonical ensemble.

The non-interacting finite-temperature Green functions appearing in the diagrams of Fig. 7.2 (and in Eqs. (7.2) and (7.7)) can be written in terms of retarded and advanced Green function as

$$(7.8) \quad \mathcal{G}(\mathbf{r}', \mathbf{r}; \epsilon_n) = \theta(\epsilon_n) G^{(+)}(\mathbf{r}', \mathbf{r}; E_F + i\epsilon_n) + \theta(-\epsilon_n) G^{(-)}(\mathbf{r}', \mathbf{r}; E_F + i\epsilon_n) .$$

The complex energy-arguments force us to go to the analytic continuation. However, if the Matsubara energies are much smaller than  $E_F$ , in a semiclassical expansion of  $G^{(+)}$  (Eq. (2.11)), we can expand the classical action around  $E_F$ . We can also include the effect of a weak magnetic field by a perturbation in the action (as we have consistently done in this work), and we arrive to the semiclassical approximation for the finite-temperature Green function

$$(7.9) \quad \mathcal{G}(\mathbf{r}', \mathbf{r}; \epsilon_n, B) = \frac{2\pi}{(2\pi i\hbar)^{3/2}} \left\{ \theta(\epsilon_n) \sum_{s(\mathbf{r}, \mathbf{r}')} \sqrt{D_s} \exp \left[ \frac{i}{\hbar} S_s - i \frac{\pi}{2} \nu_s \right] \exp \left[ -\frac{\epsilon_n \tau_s}{\hbar} \right] \exp \left[ i \frac{B \Theta_s}{\Phi_0} \right] \right. \\ \left. + \theta(-\epsilon_n) \sum_{s'(\mathbf{r}', \mathbf{r})} \sqrt{D_{s'}} \exp \left[ -\frac{i}{\hbar} S_{s'} + i \frac{\pi}{2} \nu_{s'} \right] \exp \left[ \frac{\epsilon_n \tau_{s'}}{\hbar} \right] \exp \left[ -i \frac{B \Theta_{s'}}{\Phi_0} \right] \right\}$$

where the unperturbed trajectories  $s$  and  $s'$  travel from  $\mathbf{r}$  to  $\mathbf{r}'$  in opposite directions, with the energy  $E_F$  and in the absence of magnetic field.  $\tau_s = \partial S_s / \partial E$  is the time associated with the trajectory  $s$ , and  $\Theta_s$  is the effective area (Eq. (2.1)). Long trajectories are exponentially suppressed in the expansion.

The usefulness of Eq. (7.9) goes far beyond the problem of orbital magnetism that we discuss in this work, as it provides a calculational approach to any perturbative problem where we have the knowledge of the single-particle classical dynamics. For instance, it has been used to calculate the interaction-induced renormalization of the density of states in open systems [158].

**7.3. First order perturbation, diagonal and non-diagonal contributions.** – The first-order (Hartree-Fock like) is obviously the simplest term to calculate in the diagrammatic expansion (7.6), and given by

$$(7.10) \quad \Omega_i^{(1)} = \frac{\lambda_0}{\beta} \sum_{\omega_m} \text{Tr} \{ \Sigma(\omega_m) \} .$$

Semiclassically,  $\Sigma(\mathbf{r}', \mathbf{r}; \omega_m)$  is a sum over pairs of trajectories joining  $\mathbf{r}$  to  $\mathbf{r}'$ . However, most pairs yield highly oscillating contributions which, after the spatial integrations, give higher order terms in  $1/k_F a$ . To leading order, the only pairs that contribute to the susceptibility are those whose dynamical phases  $\exp[iS_s(B=0)/\hbar]$  cancel while retaining a magnetic-field dependence. One way this can be achieved is by pairing each orbit  $s$  with its time reverse. The trace in Eq. (7.10) yields a sum over closed but not necessarily periodic trajectories (see Fig. 7.3 left, for a square). This *diagonal* contribution, is present independent of the nature of the classical dynamics.

In integrable systems, periodic orbits come in families within which the action integral is constant. If, as is generally the case, two orbits of the same family cross at a given point, it is possible to cancel the dynamical phases by pairing them (Fig. 7.3, right). This pair contributes to the trace in Eq. (7.10) because both orbits are continuously deformable so that the phase is canceled throughout an entire region of space. If we restrict ourselves to the family (1,1), this *non-diagonal* first-order contribution is given by [54]

$$(7.11) \quad \frac{\langle \chi_{i,11}^{(1)OD} \rangle}{\chi_L} = - \frac{3k_F a}{4\sqrt{2}\pi^3} \frac{d^2 \mathcal{C}_{11}^2(\varphi)}{d\varphi^2} R_T^2 \left( \frac{L_{11}}{L_T} \right)$$

The temperature dependence is governed by the function  $R_T$  of Eq. (5.18) and the field dependence by  $\mathcal{C}_{11}$  (Eq. (5.23)). The first-order contribution to  $\chi$  in the diagonal channel  $\langle \chi_i^{(1)D} \rangle$  has the same dependence on  $k_F a$  as in Eq. (7.11) and a similar  $T$  dependence; its magnitude is  $\sim 1.4$  times larger. Therefore, to first order in the interaction, the difference between chaotic systems (for which there is only the diagonal term) and regular ones (for which the non-diagonal term is also present) is numerical but not qualitative. Disorder



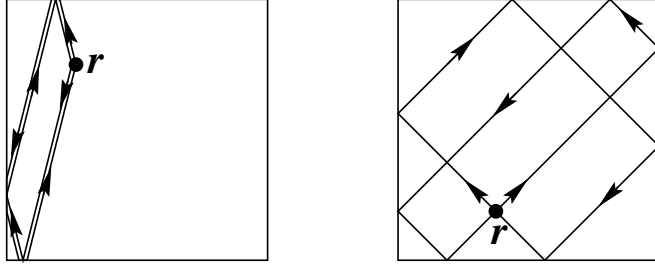


Fig. 19. – Typical pairs of real-space trajectories that contribute to the average susceptibility to first order in the interaction in the diagonal channel (left) and the non-diagonal channel (right).

will not affect the diagonal contributions since we have paired time-reversed trajectories. The suppression of  $\langle \chi_{i,11}^{(1)OD} \rangle$  by a smooth disorder potential will be, as in (6.5), a power law.

**7.4. Higher order terms.** – As mentioned before, we should consider all diagrams of the Cooper channel shown in Fig. 7.2. One should sum all terms which (i) do not vanish upon ensemble averaging, (ii) depend on  $B$ , and (iii) are of leading order in  $\hbar \sim 1/k_F a$ . For instance, (iii) is checked by  $\hbar$  power counting, since a pair of Green functions scales as  $N(0)/\hbar$ , interactions as  $[N(0)]^{-1}$ , and Matsubara sums as  $\hbar$ . Indeed, all terms in the series are of order  $\hbar$  despite the formal expansion in  $\lambda_0$ . Higher-order terms contain diagonal as well as non-diagonal contributions. However, in the latter terms the location of the additional interaction points is severely limited: they must lie on both periodic orbits to cancel the dynamical phases and so must be near the intersections of the two orbits. Further analysis [54, 155] shows that these contributions are smaller by a factor of  $1/k_F a$ . Therefore, it is only the diagonal contribution that is strongly renormalized by higher-order terms.

The diagonal contribution  $\Omega_i^D$  to  $\Omega_i$  is given by (7.6) with the substitution of  $\Sigma$  by its diagonal part

$$(7.12) \quad \Sigma^D(\mathbf{r}, \mathbf{r}'; \omega_m) = \frac{1}{(2\pi\hbar)^2 N(0)} \sum_{s(\mathbf{r}, \mathbf{r}')}^{L_s > \Lambda_0} D_s \frac{R(2\tau_s/\tau_T)}{\tau_s} \exp \left[ i \frac{2B}{\Phi_0} \Theta_s \right] \exp \left[ -\frac{\omega_m \tau_s}{\hbar} \right],$$

expressed as a *single* sum over trajectories  $s$  longer than the cutoff  $\Lambda_0 = \lambda_F/\pi$  (associated with the upper bound  $E_F$  on the Matsubara sum in Eq. (7.7)). While we cannot

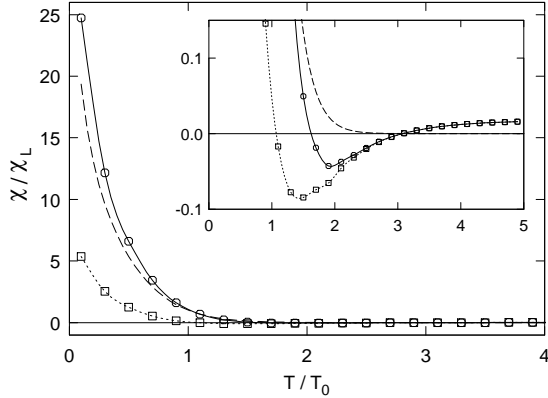


Fig. 20. – Temperature dependence of the zero-field susceptibility (solid line) for an ensemble of squares at  $k_F a = 50$ . The contribution of the non-diagonal channel (dashed, family (11) and repetitions) exceeds that of the diagonal Cooper channel (dotted) at low temperatures ( $k_B T_0 = \hbar v_F / 2\pi a$ ). Inset: expanded scale shows the change in sign as a function of  $T$  (From Ref. [54].)

diagonalize  $\Sigma^D$  analytically, it has the nice property that (except for  $\Lambda_0$ ) all variations occur on classical scales: rapid quantum oscillations on the scale of  $\lambda_F$  have been washed out, greatly simplifying the original quantum problem. In this sense,  $\Sigma^D$  is a “classical” operator. Hence, we can discretize  $\Sigma^D$  with mesh size larger than  $\lambda_F$ , sum over trajectories between cells, diagonalize, and so compute  $\Omega_i^D$  numerically.

In Fig. 74 we show the interaction contribution to the susceptibility of a square billiard (solid) as the sum of the the non-diagonal contribution of the family (11) (and its repetitions) (dashed) and the diagonal contribution  $\chi_i^D$  (dotted) from the numerical evaluation of  $\Omega_i^D$ . The non-diagonal contribution dominates  $\chi_i^D$ . Thus, *the existence of a family of periodic orbits— a characteristic of the non-interacting classical dynamics— has a crucial effect on the interaction contribution to the susceptibility.* We can distinguish three regimes for  $\chi^D$ . At low-temperature it is *paramagnetic* and decays on a scale similar to the non-diagonal contribution, but has a significantly smaller amplitude. In the intermediate range,  $\chi^D$  is small and *diamagnetic*. Finally, at high temperatures it is again *paramagnetic*, but very small. This is naturally understood by associating each regime with an order in the perturbation series. The low- $T$  part corresponds to the first-order term (orbits of the type in Fig. 73, left) which is exponentially suppressed by the temperature factor  $R$  when  $L_T$  becomes smaller than the shortest closed orbit. At this point the second-order term, due to closed paths of two trajectories connected by interactions, takes over. There is no minimum length of these paths, and hence the second-order term is less rapidly suppressed by  $T$ . For repulsive interactions, the sign is opposite of the first-order term, thus the sign change in  $\chi^D$ . At even higher temperatures

	$\chi^{(t)}/\chi_L$		$\langle\bar{\chi}\rangle/\chi_L$	
	regular	chaotic	regular	chaotic
non-interacting contribution	$(k_F a)^{3/2}$	$(k_F a)$	$(k_F a)$	$(k_F a)^0$
interacting contribution	$(k_F a)$	$(k_F a)/\ln(k_F a)$	$(k_F a)$	$(k_F a)/\ln(k_F a)$
smooth-disorder damping	$(\xi/a)^{1/2}(l/L)^{1/4}$	1	$(\xi/a)(l/L)^{1/2}$	1

TABLE I. –  $(k_F a)$  dependence of the non-interacting and interacting contributions to the magnetic response and the parametric dependence of their dampings due to the presence of smooth disorder for billiard-like microstructures in the presence (regular case) and absence (chaotic case) of families of periodic orbits.  $\chi^{(t)}$  and  $\langle\bar{\chi}\rangle$  are respectively the typical and energy-disorder averaged susceptibilities. We express them in units of the 2D Landau susceptibility  $\chi_L = e^2/(12\pi mc^2)$ .  $k_F$  is the Fermi wave-vector,  $a$  the typical size of the microstructure,  $l$  the elastic mean-free-path,  $\xi$  the correlation length of the disorder potential, and  $L$  is the length of the shortest flux-enclosing periodic trajectories.

once  $L_T \ll a$ , this term is a surface contribution and the third-order term takes over. The latter is a bulk contribution [153, 157] since with three interactions flux can be enclosed without bouncing off the boundary.

The previous interpretation of Fig. 7.4 should be reconsidered since, the final result for the diagonal channel at low  $T$  is much smaller than the first-order diagonal contribution. Moreover, we observe numerically that the terms in the perturbation series increase in magnitude with order and therefore we do not have a good convergence of the series. As often found with ill-convergent series, a renormalization mechanism contains the basic physical ingredients. The essential idea is to reorder the perturbation expansion (7.6) by gathering short paths as to produce effectively lower-order contributions [54, 155]. This analysis leads to a reduction of  $1/\ln(k_F a)$  of  $\langle\chi_i^{(1D)}\rangle$  and explains why the diagonal contribution is dominated by  $\langle\chi_{i,11}^{(1OD)}\rangle$ . The semiclassical ideas and the renormalization scheme can also be applied to the calculation of the orbital response of the 2DEG [157] and of disordered mesoscopic conductors [159, 155].

In table I we summarize the various contributions to the susceptibility for the cases of chaotic and regular geometries. As discussed in (6.6) the non-interacting theory is roughly in agreement with the experimental results (at the lowest temperatures). Incorporating the interaction-induced contribution, which is of the same order as the non-interacting one, still keeps us within the range of the measurements [27] (which have an uncertainty of a factor of 4). The disagreement on the temperature dependence of the susceptibility is reduced respect to that of the non-interacting case, but the temperature scale  $T_0$  in Fig. 7.4 is still significantly smaller than that in the experiment.

## 8. – Conclusions

The central line of this review has been the use of semiclassical methods in problems of Mesoscopic Physics. When applied to mesoscopic systems, the semiclassical analysis needs to be adapted according to physical considerations, often introducing cut off lengths (elastic mean-free-path, coherence length, etc). The ability of semiclassical methods to deal with problems that are not translational invariant gives them a very special place among the analytical tools used in the study of small systems.

In this article we have seen both the strength and weakness of the semiclassical tool. Semiclassics is able to yield the signatures of the underlying classical dynamics on quantum properties. It allows us to study important features of ballistic transport, like conductance fluctuations and weak localization, predicting the line-shape of the correlation function and the weak localization peak. Technically, only one part of these effects (the diagonal component) is easily obtained. For line-shapes in chaotic structures it is reasonable to expect that the diagonal part has the same information of the total effect, and we have verified this conjecture with numerical calculations. The magnitude of the conductance fluctuations and weak localization effects are not easily obtained from semiclassics. Random matrix theory, whenever it is applicable, presents a better route to extract universal values.

Each integrable system has its own specificity, but semiclassics can be applied to all cases and therefore remains the only analytical tool in dealing with transport through integrable cavities. The semiclassical analysis predicts important differences between the quantum interference phenomena in transport through integrable and chaotic cavities. Such a distinction is supported by many numerical calculations.

The experimental developments in quantum transport have been largely motivated by the theoretical results. In the case of chaotic cavities, good agreement is obtained between the measurements and the theoretical predictions. Signatures of integrable dynamics have been obtained experimentally in the power spectrum of the conductance fluctuations and in the (non-Lorentzian) weak localization peak. But the integrable behavior is much more fragile than in the chaotic case and it does not show up in some of the experiments on cavities with regular geometry. The experimental attention has somehow shifted to the chaotic case, where the semiclassical and random matrix theory predictions have been tested and used as a way of extracting information on the phase coherence length. However, we feel that regular microstructures deserve more attention if we want to achieve a thorough understanding of their physics.

There has been a growing interest in the transport through cavities with mixed dynamics lately. Further theoretical and experimental work seems necessary to make progress in our understanding of this generic case.

The semiclassical tool is also helpful to study thermodynamical properties of microstructures, like the magnetic susceptibility. The orbital response is a direct consequence of the magnetic field dependence of the density of states. The latter is known to be very sensitive to the underlying classical dynamics, exhibiting larger fluctuations in the integrable case than in the chaotic one. This behavior translates into an enhanced

susceptibility for integrable cavities (which is mainly given by the effect of short orbits).

We have presented a formalism capable of incorporating weak-disorder effects arising from smooth potentials (slowly varying on the scale of the Fermi wave-length). Such a formalism is expressed in terms of one and two-particle Green functions and can be applied to transport and thermodynamical quantities. For the magnetic susceptibility it predicts a weak (power-law) suppression of the clean values.

It might have not been evident to foresee, but the semiclassical tool can also be adapted to treat problems of electron-electron interaction, and the resulting contribution to the magnetic susceptibility turns out to depend on the classical dynamics of non-interacting electrons. The agreement between theory and experiment concerning the magnetic response of ballistic microstructures is only qualitative (and at the lowest temperatures), and much less satisfactory than in the case of transport. The difficulties from the theoretical side are probably related to the approximated way in which we are able to take interactions into account. We expect that the few available experimental results of orbital magnetism in the ballistic regime will soon be complemented by detailed studies.

In this work we have presented a few examples illustrating the link between Mesoscopic Physics and semiclassical theories, and we have left aside other problems of sustained interest at present, like the Coulomb blockade in quantum dots [145], the tunneling through quantum wells with tilted magnetic fields [160], and the electron transport with inhomogeneous magnetic fields [161], where semiclassics is also a very helpful approach.

### Acknowledgements

The work described in these lectures is mainly the result of long and enjoyable collaborations with H.U. Baranger, K. Richter, A.D. Stone and D. Ullmo. I further acknowledge fruitful collaborations in other aspects of Mesoscopic Physics (covered or not in this article) with Y. Alhassid, C.W.J. Beenakker, D.P. DiVincenzo, G.-L. Ingold, I.K. Marmorkos, E.R. Mucciolo, F. von Oppen, J. Petitjean, J.-L. Pichard, P. Pichaureau, P. Schmitteckert, M. Schreier, and D. Weinmann.

Support from the CNRS (Coopération CNRS/DFG), the French-German program PROCOPE, and the “Institut Universitaire de France” are gratefully acknowledged.

## REFERENCES

- [1] Proceedings of the 1989 Les Houches Summer School on *Chaos and Quantum Physics*, edited by M.-J. Giannoni, A. Voros, and J. Zinn-Justin (North-Holland, Amsterdam, 1991).
- [2] Proceedings of the 1991 Enrico Fermi International School of Physics on *Quantum Chaos*, edited by G. Casati, I. Guarneri and U. Smilansky (North-Holland, Amsterdam, 1993).
- [3] A.M. Ozorio de Almeida, *Hamiltonian Systems: Chaos and Quantization* (Cambridge University Press, 1988).
- [4] M.C. Gutzwiller, *Chaos in Classical and Quantum Mechanics* (Springer-Verlag, Berlin, 1990).
- [5] H. Friedrich and D. Wintgen, Phys. Rep. **183**, 37 (1989).
- [6] H.-J. Stöckmann, J. Stein, and M. Kollmann, in *Quantum Chaos*, edited by G. Casati and B. Chirikov (Cambridge University Press, Cambridge, 1995).
- [7] R.A. Jalabert, H.U. Baranger and A.D. Stone, Phys. Rev. Lett. **65**, 2442 (1990).
- [8] C.M. Marcus, A.J. Rimberg, R.M. Westervelt, P.F. Hopkins and A.C. Gossard, Phys. Rev. Lett. **69**, 506 (1992).
- [9] C.M. Marcus, R.M. Westervelt, P.F. Hopkins, and A.C. Gossard, Chaos, **3**, 643 (1993).
- [10] H.U. Baranger, R.A. Jalabert, and A.D. Stone, Chaos, **3**, 665 (1993).
- [11] H.U. Baranger in *Nanotechnology*, edited by G. Timp (AIP Press, 1995).
- [12] A.D. Stone, in Ref. [17], p. 325.
- [13] *Chaos and Quantum Transport in Mesoscopic Cosmos*, special issue, Chaos, Solitons&Fractals, edited by K. Nakamura **8**, 971-1412 (1997).
- [14] K. Richter, D. Ullmo and R.A. Jalabert, Phys. Rep. **276**, 1 (1996).
- [15] K. Richter, *Semiclassical Theory of Mesoscopic Quantum Systems*, Springer Tracts in Modern Physics (Springer-Verlag, in press).
- [16] *Mesoscopic Phenomena in Solids*, edited by B.L. Altshuler, P.A. Lee, and R.A. Webb, (North-Holland, Amsterdam, 1991).
- [17] Proceedings of the 1994 Les Houches Summer School on *Mesoscopic Quantum Physics*, edited by E. Akkermans, G. Montambaux, J.-L. Pichard, and J. Zinn-Justin (North-Holland, Amsterdam, 1995).
- [18] S. Datta, *Electronic Transport in Mesoscopic Systems* (Cambridge University Press, Cambridge, 1995).
- [19] Y. Imry, *Introduction to Mesoscopic Physics* (Oxford University Press, Oxford, 1997).
- [20] S. Washburn and R.A. Webb, Adv. Phys. **35**, 375 (1986); Rep. Prog. Phys. **55**, 1311 (1992).
- [21] P.A. Lee and T.V. Ramakrishnan, Rev. Mod. Phys. **57**, 287 (1985).
- [22] C.W.J. Beenakker and H. van Houten in *Solid State Physics*, Vol. 44, edited by H. Ehrenreich and D. Turnbull (Academic Press, New York, 1991).
- [23] S. Das Sarma and F. Stern, Phys. Rev. B **32**, 8442 (1988).
- [24] M.L. Roukes *et al.*, Phys. Rev. Lett. **59**, 3011 (1987).
- [25] C.J.B. Ford *et al.*, J. Phys. C **21**, L325 (1988); C.J.B. Ford, S. Washburn, M. Büttiker, C.M. Knoedler, and J.M. Hong, Phys. Rev. Lett. **62**, 2724 (1989).
- [26] O. Bohigas, M.-J. Giannoni, and C. Schmit, Phys. Rev. Lett. **52**, 1 (1984); O. Bohigas, in Ref. [1], p. 87.
- [27] L.P. Lévy, D.H. Reich, L. Pfeiffer, and K. West, Physica B **189**, 204 (1993).
- [28] D. Mailly, C. Chapelier, and A. Benoit, Phys. Rev. Lett. **70**, 2020 (1993).
- [29] C.M. Marcus, R.M. Westervelt, P.F. Hopkins and A.C. Gossard, Phys. Rev. B **48**, 2460 (1993); R.M. Clarke *et al.*, Phys. Rev. B **52**, 2656 (1995).
- [30] M.W. Keller, O. Millo, A. Mittal, D.E. Prober, and R. N. Sacks, Surf. Sci., **305**, 501 (1994); M.W. Keller *et al.*, Phys. Rev. B **53**, R1693 (1996).

- [31] M.J. Berry, J.H. Baskey, R.M. Westervelt, and A.C. Gossard, Phys. Rev. B **50**, 8857 (1994); M.J. Berry, J.A. Katine, R.M. Westervelt, and A.C. Gossard, Phys. Rev. B **50**, 17721 (1994).
- [32] A.M. Chang, H.U. Baranger, L.N. Pfeiffer, and K.W. West, Phys. Rev. Lett. **73**, 2111 (1994); A.M. Chang, in Ref. [13], p. 1281.
- [33] I.H. Chan, R.M. Clarke, C.M. Marcus, K. Campman, and A.C. Gossard, Phys. Rev. Lett. **74**, 3876 (1995); C.M. Marcus *et al.*, in Ref. [13], p. 1261.
- [34] J.P. Bird *et al.*, Phys. Rev. B **52**, R14336 (1995); and in Ref. [13], p. 1299.
- [35] M. Persson *et al.*, Phys. Rev. B **52**, 8921 (1995).
- [36] G. Lütjering *et al.* Surf. Sci. **361/362**, 709 (1996).
- [37] Y. Lee, G. Faini, and D. Mailly, Phys. Rev. B, **56**, 9805 (1997); and in Ref. [13], p. 1325.
- [38] I.V. Zozoulenko, R. Schuster, K.-F. Berggren, and K. Ensslin, Phys. Rev. B **55**, R10209 (1997).
- [39] A.G. Huibers *et al.* Phys. Rev. Lett. **81**, 1917 (1998); cond-mat/9904274.
- [40] R.P. Taylor *at al.*, Phys. Rev. Lett. **78**, 1952 (1997); A.S. Sachrajda *at al.*, Phys. Rev. Lett. **80**, 1948 (1998).
- [41] A. Mirlin, in this issue.
- [42] F. Haake, in this issue.
- [43] M. Brack and R.K. Bhaduri, *Semiclassical Physics* (Addison-Wesley, Reading, 1997).
- [44] D.E. Khmelnitskii and A.I. Larkin, Ups. Fiz. Nauk. **136**, 533 (1982) [Sov. Phys. Usp. **25**, 185 (1982)].
- [45] S. Chakravarty and A. Schmid, Phys. Rep. **140**, 195 (1986).
- [46] N. W. Ashcroft and N. D. Mermin, *Solid State Physics* (Holt, Rhinehart, and Winston, New York, 1976).
- [47] R. Blümel and U. Smilansky, Phys. Rev. Lett. **60**, 477 (1988); Physica D **36**, 111 (1989).
- [48] H.U. Baranger, R.A. Jalabert, and A.D. Stone, Phys. Rev. Lett. **70**, 3876 (1993).
- [49] P. Pichaireau and R.A. Jalabert, Eur. Phys. J. B **9**, 299 (1999).
- [50] M. Schreier, K. Richter, G.-L. Ingold, and R.A. Jalabert, Eur. Phys. J. B **3**, 387 (1998).
- [51] F. von Oppen, Phys. Rev. B **50**, 17151 (1994).
- [52] D. Ullmo, K. Richter, and R.A. Jalabert, Phys. Rev. Lett. **74**, 383 (1995).
- [53] K. Richter, D. Ullmo, and R.A. Jalabert, Phys. Rev. B, **56**, R5619 (1996).
- [54] D. Ullmo, H.U. Baranger, K. Richter, F. von Oppen, and R.A. Jalabert, Phys. Rev. Lett. **80**, 895 (1998).
- [55] R. Landauer, Phil. Mag. **21**, 863 (1970).
- [56] M. Büttiker, Phys. Rev. Lett. **57**, 1761 (1986).
- [57] V.I. Arnold, *Mathematical Methods of Classical Mechanics* (Springer-Verlag, New York, 1984).
- [58] C. Jung and H.-J. Scholz, J. Phys. A **21**, 2301 (1988).
- [59] T. Tél in *Direction in Chaos, Vol. 3*, edited by Hao Bai Lin (World Scientific, Singapore, 1990) p. 149.
- [60] U. Smilansky in Ref. [1], p. 371.
- [61] P. Gaspard and S.A. Rice, J. Chem. Phys. **90**, 2225; 2242; 2255 (1989).
- [62] R.V. Jensen, Chaos **1**, 101 (1991).
- [63] R.B.S. Oakeshott and A. MacKinnon, Superlat. and Microstruc. **11**, 145 (1992).
- [64] P. Lecheminant, J. Phys. I France **3**, 299 (1993).
- [65] M.V. Berry and M. Robnik, J. Phys. A **19**, 649 (1986).
- [66] E. Doron, U. Smilansky, and A. Frenkel, Phys. Rev. Lett. **65**, 3072 (1990); Physica D **50**, 367 (1991); in Ref. [2].
- [67] W. Bauer and G. F. Bertsch, Phys. Rev. Lett. **65**, 2213 (1990).
- [68] Y.-C. Lai, R. Blümel, E. Ott, and C. Grebogi, Phys. Rev. Lett. **68**, 3491 (1992).

- [69] W.A. Lin, J.B. Delos and R.V. Jensen, *Chaos* **3**, 665 (1993).
- [70] O. Legrand and D. Sornette, *Physica D* **44**, 229 (1990); *Phys. Rev. Lett.* **66**, 2172 (1991).
- [71] C.W.J. Beenakker and H. van Houten, *Phys. Rev. B* **37**, 6544 (1988).
- [72] H.U. Baranger, D.P. DiVincenzo, R.A. Jalabert, and A.D. Stone, *Phys. Rev. B* **44**, 10637 (1991).
- [73] H.U. Baranger and P.A. Mello, *Phys. Rev. B* **54**, R14297 (1996).
- [74] D.C. Langreth and E. Abrahams, *Phys. Rev. B* **24**, 2978 (1981).
- [75] H.U. Baranger and A.D. Stone, *Phys. Rev. B* **40**, 8169 (1989).
- [76] D.S. Fisher and P.A. Lee, *Phys. Rev. B* **23**, 6851 (1981).
- [77] A.D. Stone and A. Szafer, *IBM J. Res. Dev.* **32**, 384 (1988).
- [78] P.A. Lee and D.S. Fisher, *Phys. Rev. Lett.* **47**, 882 (1981).
- [79] A. MacKinnon, *Z. Phys. B* **59**, 385 (1985).
- [80] K. Shepard, *Phys. Rev. B* **43**, 11623 (1991).
- [81] J.U. Nöckel, A.D. Stone, and H.U. Baranger, *Phys. Rev. B* **48**, 17569 (1993).
- [82] Note a sign mistake in the original work of Ref. [7] and in Eq. (9) of Ref. [10]. This point was noticed and corrected by W.A. Lin, see Ref. [86].
- [83] J.H. Jensen, *Phys. Rev. Lett.* **73**, 244 (1994).
- [84] W.H. Miller, *Adv. Chem. Phys.* **25**, 69 (1974).
- [85] M.V. Berry, M. Tabor, *Proc. R. Soc. Lond. A.* **349**, 101 (1976).
- [86] W.A. Lin and R.V. Jensen, *Phys. Rev. B* **53**, 3638 (1996); W.A. Lin, in Ref. [13], p. 995.
- [87] H. Ishio and J. Burgdörfer, *Phys. Rev. B* **51**, 2013 (1995).
- [88] C. D. Schwieters, J. A. Alford, and J. B. Delos, *Phys. Rev. B* **54**, 10652 (1996).
- [89] G. Vattay, J. Cserti, G. Palla, and G. Szálka, in Ref. [13], p. 1031.
- [90] M. C. Gutzwiller, *Physica D* **7**, 341 (1983).
- [91] T. Ericson, *Phys. Rev. Lett.* **5**, 430 (1960).
- [92] F. Borgonovi and I. Guarneri, *J. Phys. A* **25**, 3239 (1992); *Phys. Rev. E* **48**, R2347 (1993).
- [93] S. Iida, H.A. Weidenmüller, and J.A. Zuk, *Annals of Phys.* **200**, 219 (1990).
- [94] C.H. Lewenkopf and H.A. Weidenmüller, *Annals of Phys.* **212**, 53 (1991).
- [95] L. Wirtz, J.-Z. Tang, and J. Burgdörfer, *Phys. Rev. B* **56**, 7589 (1997).
- [96] A.Ya. Khinchin, *Continued Fractions* (University of Chicago Press, Chicago, 1964).
- [97] Notice the missing  $\varepsilon'_n$  in the exponent of Eq. (19) of Ref. [49].
- [98] R.M. Westervelt, in Ref. [11].
- [99] M. Büttiker, *Phys. Rev. B* **33**, 3020 (1986); *IBM J. Res. Dev.* **32**, 63 (1988).
- [100] H. Bruus and A.D. Stone *Phys. Rev. B* **50**, 18275 (1994).
- [101] K.B.Efetov, *Phys. Rev. Lett.* **74**, 2299 (1995).
- [102] P. Mohanty, E.M.Q. Jariwala, and R.A. Webb, *Phys. Rev. Lett.* **78**, 3366 (1997).
- [103] D. Ullmo, unpublished.
- [104] C.W.J. Beenakker, *Rev. Mod. Phys.* **69**, 731 (1997).
- [105] T. Guhr, A.M. Müller-Groeling, and H. A. Weidenmüller, *Phys. Rep.* **283**, 37 (1998).
- [106] R. Blümel and U. Smilansky, *Phys. Rev. Lett.* **64**, 241 (1990).
- [107] R. A. Jalabert and J.-L. Pichard, *J. Phys. (France)* **5**, 287 (1995).
- [108] H.U. Baranger and P.A. Mello, *Phys. Rev. Lett.* **73**, 142 (1994).
- [109] R.A. Jalabert, J.-L. Pichard, and C.W.J. Beenakker, *Europhys. Lett.* **27**, 255 (1994).
- [110] H.U. Baranger and P.A. Mello, *Phys. Rev. B* **51**, 4703 (1995).
- [111] P.W. Brouwer and C.W.J. Beenakker, *Phys. Rev. B* **51**, 7739 (1995); **55**, 4695 (1997).
- [112] Z. Pluháň, H.A. Weidenmüller, J.A. Zuk, and C.H. Lewenkopf, *Phys. Rev. Lett.* **73**, 2115 (1994).
- [113] E. Doron and U. Smilansky, *Nucl. Phys. A* **545**, 455c (1992).
- [114] P.A. Mello and H.U. Baranger, *Europhys. Lett.* **33**, 465 (1996).
- [115] N. Argaman *et al.*, *Phys. Rev. Lett.* **71**, 4326 (1993).



- [116] N. Argaman, Phys. Rev. Lett. **75**, 2750 (1995); Phys. Rev. B **53**, 7035 (1996).
- [117] I.A. Aleiner and A.I. Larkin, Phys. Rev. B **54**, 14423 (1996).
- [118] R. Ketzmerick, Phys. Rev. B **54**, 10841 (1996).
- [119] B. Huckestein, R. Ketzmerick, and C.H. Lewenkopf cond-mat/9908090.
- [120] G. Casati, I. Guarneri, and G. Maspero, unpublished 1999.
- [121] M. Wilkinson, J. Phys. A **20** 2415 (1987).
- [122] R. Fleischmann, T. Geisel and R. Ketzmerick, Phys. Rev. Lett. **68**, 1367 (1992).
- [123] K. Richter, Europhys. Lett. **29**, 7 (1995).
- [124] G. Hackenbroich and F. von Oppen, Europhys. Lett. **29**, 151 (1995); Z. Phys. B **97** 157 (1995).
- [125] D. Weiss *et al.*, Phys. Rev. Lett., **70**, 4118 (1993).
- [126] L.D. Landau, Z. Phys. **64**, 629 (1930).
- [127] R.E. Peierls, *Surprises in Theoretical Physics* (Princeton University Press, Princeton NJ, 1979).
- [128] Yu.N Ovchinnikov, W. Lehle, and A. Schmid, Ann. Physik **6**, 487 (1997).
- [129] A.A. Abrikosov, L.P. Gorkov, and I.E. Dzyaloshinski, *Methods of Quantum Field Theory in Statistical Physics* (Prentice-Hall, Englewood Cliffs, 1963).
- [130] A.L. Fetter and J.D. Waleka, *Quantum Theory of Many-Particle Systems* (McGraw-Hill, New York, 1971).
- [131] H. Bouchiat and G. Montambaux, J. Phys. (Paris) **50**, 2695 (1989).
- [132] A. Schmid, Phys. Rev. Lett. **66**, 80 (1991); F. von Oppen and E.K. Riedel, *ibid* 84; B.L. Altshuler, Y. Gefen, and Y. Imry, *ibid* 88.
- [133] R. Kubo, J. Phys. Soc. Japan **19**, 2127 (1964).
- [134] S.D. Prado, M.A. M. de Aguiar, J.P. Keating and R. Eglydio de Carvalho, J. Phys. A **27**, 6091 (1994).
- [135] R.A. Jalabert, K. Richter, and D. Ullmo, Surf. Sci., **361/362**, 700 (1996).
- [136] B. Shapiro, Physica A, **200**, 498 (1993).
- [137] O. Agam, J. Phys. I (France) **4** 694 (1994).
- [138] K. Richter and B. Mehlige, Europhys. Lett. **41**, 587 (1998).
- [139] K. Richter, D. Ullmo, and R.A. Jalabert, J. Math. Phys. **37**, 5087 (1996).
- [140] J.A. Nixon and J.H. Davies, Phys. Rev. B **41**, 7929 (1990).
- [141] M. Stopa, Phys. Rev. B **53**, 9595 (1996).
- [142] A. D. Mirlin, E. Altshuler, and P. Wölfle, Ann. Physik **5**, 281 (1996).
- [143] Y. Gefen, D. Braun, and G. Montambaux, Phys. Rev. Lett. **73**, 154 (1994).
- [144] E. McCann and K. Richter, Europhys. Lett. **43**, 241 (199), Phys. Rev. B **59**, 13026 (1999).
- [145] M. Kastner, Rev. Mod. Phys. **64**, 849 (1992).
- [146] V. Ambegaokar and U. Eckern, Phys. Rev. Lett. **65**, 381 (1990); U. Eckern, Z. Phys. B **42**, 389 (1991).
- [147] U. Eckern and P. Schwab, Adv. Phys. **44**, 387 (1995).
- [148] L.P. Lévy, G. Dolan, J. Dunsmuir, and H. Bouchiat, Phys. Rev. Lett. **64**, 2074 (1990).
- [149] V. Chandrasekhar, R.A. Webb, M.J. Brady, M.B. Ketchen, W.J. Gallagher, and A. Kleinsasser, Phys. Rev. Lett. **67**, 3578 (1991).
- [150] P. Mohanty, E.M.Q. Jariwala, M.B. Ketchen, and R.A. Webb, in *Quantum Coherence and Decoherence*, edited by K. Fujikawa and Y.A. Ono (Elsevier, 1996).
- [151] T. Ando, A.B Fowler, and F. Stern, Rev. Mod. Phys. **54**, 437 (1982).
- [152] R. Jalabert and S. Das Sarma Phys. Rev. B **40**, 9723 (1989).
- [153] L.G. Aslamazov and A.I. Larkin, Sov. Phys.-JETP **40**, 321 (1975).
- [154] B.L. Altshuler and A.G. Aronov, in *Electron-electron interactions in Disordered systems*, edited by A.L. Efros and M. Pollak (North-Holland, Amsterdam, 1985).
- [155] D. Ullmo, H.U. Baranger, K. Richter, F. von Oppen, and R.A. Jalabert, unpublished.

- [156] G. Vignale, Phys. Rev. B **50**, 7668 (1994).
- [157] K. Richter, H.U. Baranger, F. von Oppen, and D. Ullmo, unpublished.
- [158] Y. Takane, J. Phys. Soc. Japan **67**, 3003 (1998).
- [159] D. Ullmo, K. Richter, H.U. Baranger, F. von Oppen, and R.A. Jalabert, Physica E **1**, 268 (1997).
- [160] T.M. Fromhold *et al.*, Phys. Rev. Lett. **72**, 2608 (1994).
- [161] P.D. Ye *et al.*, Phys. Rev. Lett. **74**, 3013 (1995).